liten
cea tech

SCIENTIFIC REPORT 2018

EDITO

L'institut CEA-LITEN au cœur du développement des systèmes énergétiques renouvelables à faible empreinte carbone

Les activités de recherches, développements et innovations conduites par l'institut CEA-Liten adressent le domaine des technologies de l'énergie à faible empreinte carbone avec un impact environnemental maitrisé. En adéquation avec la stratégie nationale « bas carbone » et les objectifs de la loi de programmation pluriannuelle de l'énergie de 2018, elles portent notamment sur le développement de nouveaux concepts scientifiques, technologiques ou numériques pour intégrer une part croissante d'énergies renouvelables dans le mix national et pour augmenter l'efficacité énergétique dans de nombreux domaines tels que le transport, l'industrie ou l'habitat. Couvrant toute la chaine de valeur, de la synthèse des matériaux au test en vraie grandeur de composants et systèmes prototypes, elles sont orientées vers un objectif de transfert industriel.

Le CEA-Liten, fort de 975 collaborateurs, dont 57 Experts Seniors, 12 Directeurs de Recherches ou Experts Internationaux et 120 doctorants ou post-doctorants, adosse ses activités de recherche sur une dizaine de plateformes expérimentales et numériques et cultive des collaborations renforcées et fructueuses avec une vingtaine de laboratoires académiques nationaux et européens.

En 2018 le CEA-Liten a publié 202 articles dans des journaux à comité de lecture, a déposé 192 brevets, a créé 1 startup et a conclu près de 300 nouveaux contrats de recherche partenariale. 36 thèses ont été soutenues et 32 nouvelles ont été engagées. 3 nouvelles habilitations à diriger les recherches ont été obtenues portant à 33 le nombre de nos chercheurs HDR.

Vous trouverez dans ce Rapport Scientifique 2018 quelques exemples des avancées scientifiques de l'année qui, nous l'espérons, vous donnera l'envie de mieux nous connaitre et de collaborer avec nous.

Florence Lambert,
LITEN CEO

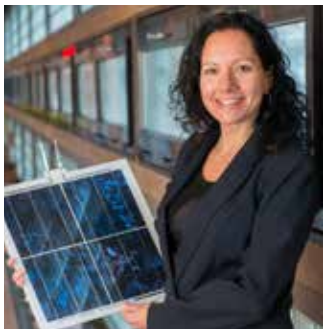

The CEA-LITEN Institute committed in the development of renewable and sustainable energy systems

The research, development and innovation activities conducted by the CEA-Liten Institute address the field of low-carbon energy technologies with a controlled environmental impact. In line with the national «low-carbon» strategy and the objectives of the 2018 multi-annual French energy road-map, the CEA-Liten's activities include the development of new scientific, technological or numerical concepts for integrating a growing share of renewable energies into the national mix and for increasing energy efficiency in many areas such as transport, industry or housing. These activities–covering the entire value chain, from material synthesis to full-scale testing of prototype components and systems–are oriented towards an industrial transfer objective.

CEA-Liten, with 975 employees, including 57 Senior Experts, 12 Research Directors or International Experts and 120 PhD students or postdocs, supports its research activities on about ten experimental and digital platforms and cultivates strengthened and fruitful collaborations with about twenty national and European academic laboratories.

In 2018 CEA-Liten published 202 articles in peer-reviewed journals, filed 192 patents, created 1 startup and has signed nearly 300 new partnership research contracts. 36 theses were defended and 32 new ones were launched. The 3 new habilitated scientists to PhD student supervision bring the number of our HDR researchers to 33.

In this 2018 edition of CEA-Liten's Scientific Report, you will find some examples of this year's scientific advances, wishing they will hopefully make you want know more about us. We are looking forward to collaborating with you soon.

Florence Lefebvre-Joud,
Deputy Director for Science

CONTENTS

www.liten.cea.fr

KEY FIGURES

MATTER & MATERIALS | RENEWABLE ENERGIES | ENERGY STORAGE AND CONVERSION | ENERGY EFFICIENCY

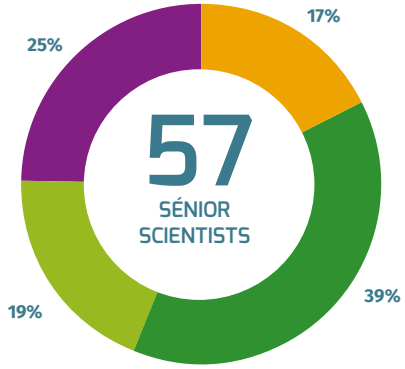

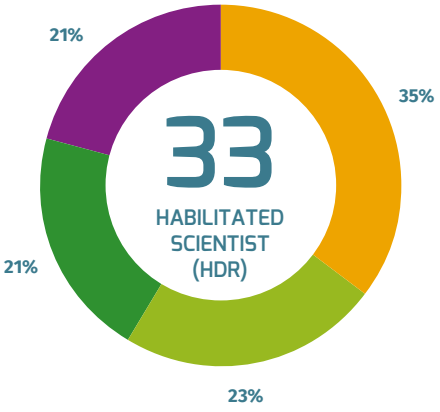

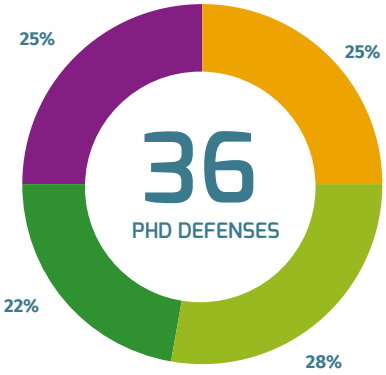

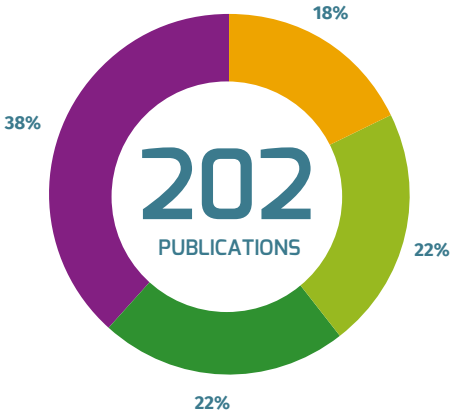

SUSTAINABLE TECHNOLOGIES FOR CIRCULAR ECONOMY AND ENERGY TRANSITIONS: ECO-INNOVATION APPROACHES SUPPORTING OUR DEVELOPMENTS

Élise MONNIER, Nouha GAZBOUR, Marilyne JOANNY, Stéphanie DESROUSSEAUX and Emmanuelle COR

CONTACT elise.monnier@cea.fr

1. Introduction

Liten is creating solutions to support transitions towards sustainable efficient energy systems and circular economy. The institute is spearheading the EU's efforts to limit dependency on fossil fuels and reduce greenhouse gas emissions in three key areas: renewable energy, energy efficiency/storage and development of materials. We are committed to ensuring that the technology we develop addresses today's environmental challenges like climate change and energy efficiency but also anticipates tomorrow's ones such as resource scarcity, land use change and biodiversity. Our eco-innovation program, launched in 2010, tackles this issue.

It aims at developing and implementing proactive solutions to drive technological innovation forward while taking into account environmental considerations and product lifecycle concerns. The goal is to combine value creation—in the form of products and services—with the reduction of environmental impacts throughout the lifecycle of the products and services developed. Many different techniques have been adapted by our research teams to eco-innovate such as guided creativity, eco-design methodologies, life cycle assessment (LCA)... Original methods using eco-innovation and eco-design approaches appeared very powerful to allow a broad range of our technologies to enhance effectively their environmental performance while developing new concepts.

2. Eco-innovation and eco-design approaches supporting technological research

This activity was born in 2010 in Liten in order to understand and communicate on the environmental performance of our technological solutions. We use a wide range of techniques, drawing on opportunity analysis, environmental impact assessment (like Life Cycle Assessment or LCA...), eco-design expertise, creativity and innovation, development of adjusted tools or methodology, training courses or coaching. These approaches aim to develop responsive processes, adapted to technological research programs regarding development speed, in order to achieve better environmental performances. These services are provided to internal and external partners alongside Liten's technological developments.

We leverage LCA methods like those in the ISO 14040 [1] and ISO 14044 [2] standards and the ILCD Handbook [3] to perform a quantitative analysis of the environmental benefits and impacts of innovative technologies. We also use a holistic approach to eco-design to ensure that environmental performance is used as a starting point for the development of a new technology and considered at every step in the design and development process. Finally, we can measure the environmental benefits and impacts of a product at all stages in its lifecycle, from manufacturing to use and, ultimately, recycling. We start by selecting relevant indicators from the European Commission's list of eleven impact categories [4]. For example, a technology impact on climate change will be measured according to greenhouse gas emissions in CO_2 equivalent throughout the technology lifecycle. Factoring in these impacts from the early stages of technology development is crucial to making the most environmentally-responsible choices at subsequent stages in the development process.

2.1 The example of the use of Life Cycle Assessment for eco-design and eco-innovation

Life cycle assessment is a multistage (lifecycle stages) and a multicriteria (environmental impact categories) analysis based on a 4-step method, illustrated in Figure 1, and providing a quantification of environmental impacts of a product or a service throughout their lifecycle. The method is standardized, providing a reliable tool and trustable results thanks to a commitment to the guarantee of transparency of the study. The first step aims at framing the studied system (product, process or service) with the definition of its boundaries and of a functional unit describing the service delivered. In this step, the environmental categories of interest for the study are identified. In the second step of the assessment, input and output flows involved in the system life cycle (such as energy, material, wastes, emissions in air, or water...) are qualified and quantified, providing the so-called Life

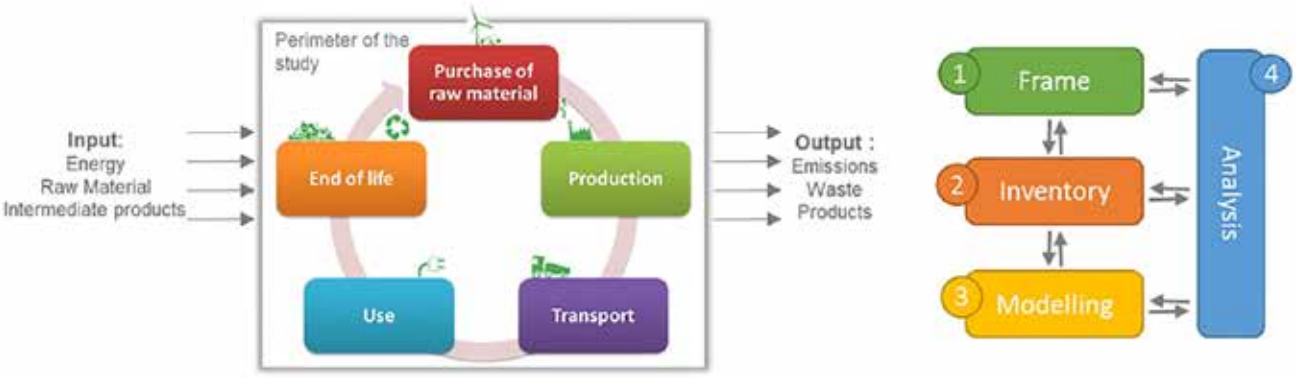

Fig. 1: Boundaries for the Life Cycle Inventory of an LCA (left) and diagram of the 4-steps iterative method as described in ISO14040 and ISO14044 standards (right).

Cycle Inventory (LCI) on Figure 1. The data are collected from actors (e.g. industrial partners) involved at every stage of the product or service life cycle, providing primary data. However, some data may not be available and secondary data are then used, collected from databases or from literature surveys. Secondary data relies on assumptions that have to be duly documented. The following third step is dedicated to the modeling of the system and enables the conversion of the data from the LCI of the studied system, into quantified environmental impacts, using characterization factors. There are various acknowledged characterization methods available and they are the results of a thorough research work by the international community in the field of environmental science. The last step of the assessment is the analysis of the quantified impacts obtained through the modelling. In order to identify environmental hotspots of the studied process, product or service, the investigation can be made according to three dimensions: impact categories, life cycle stages, input or output flows. These results can offer a starting point for eco-designing and eco-innovation lines. The last step also includes various studies which aim at consolidating the LCA results: a sensitivity analysis to assess the reliability of inventory and modelling assumptions, a coherence study with the initial frame, data quality assessment and uncertainty analysis, involving for instance a Monte Carlo method. These verifications can be made at each step of the method, as it is an iterative approach, each step being regularly reassessed in view of data, frame, assumptions and results from other steps.

In the last 5 years, LCA method has been used by CEA-Liten in several European programs, jointly with economical assessment in support of technology development, in order to evaluate the environmental benefit of the technological developments performed in comparison to state of the art solutions. For example, in the field of high temperature electrolysis and fuel cells (SOEC/SOFC), the oxidation of the metallic interconnects is responsible of an important part of the degradation. That is why it is needed to protect them against oxidation. In the frame of the H2020 AGRAL project, a breakthrough coating has been considered, with the aim to extend the lifetime of those technologies. It is made of a metal/ceramic composite, combining the high electrical conductivity of the metal, and the high corrosion resistance of the oxide and has been deposited on the interconnections as a thin coating [5]. According to the life cycle impact assessment, it appeared that the addition of this specific material and the associated process step to the overall manufacturing process, has only a minor contribution to the environmental impact on a set of 11 impact categories (Fig. 2). This observation allowed to consider the opportunity to add this kind of material as thin layer in order to increase the lifespan of metallic interconnects, without significant increase of burden for the environment. As a consequence, the lifespan of the system would be increased, avoiding the production environmental impact for its replacement at a too early life stage.

Life cycle assessment is part of a toolbox for eco-design and eco-innovation in Liten. However, these tools commonly used for mature products and services can show their limitations in a technological research context. As a consequence, the lack of maturity for technologies, or even the discrepancy in maturity for various components of a system, is a driver to develop appropriate new tools. In addition, some tools assessing technologies and costs performances but not taking into account the environmental aspect, they are to be adapted to offer a comprehensive solution. The next paragraph illustrates the work realized in Liten on these aspects.

2.2 Other approaches for the integration of environmental aspects in research & development

The implementation and the validation of other methods than LCA for environmental impact improvements are developed in our institute. For instance, the concept of Design-to-Life (D2L) described by Bauer in [6] and [7] is a new alternative end-of-life approach compared to reuse or remanufacturing. It enables to increase the lifespan of products, when performances have decreased, by offering a new usage and thus decreasing end of life impacts on the environment. In the specific case of batteries for electrical vehicles, this second life can be in stationary storage which requires lower performances. This scenario is also named repurposing. The use of LCA will help to comfort the choice of this scenario by proving that it is less environmentally impacting than the reuse, remanufacturing or disposal options. For repurposing, there is a need to define the different possible uses from the design phase, in order to propose solutions accepting, for instance, modularity or enabling easy disassembling and reassembling steps (Fig. 3). Reverse logistic also needs to be assessed in the early stage of designing.

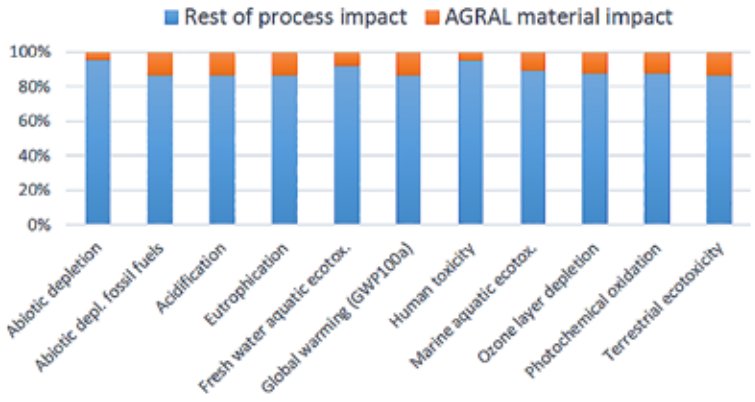

Fig. 2: Interconnectors environmental impacts assessment for a scenario involving the highest AGRAL material amount studied.

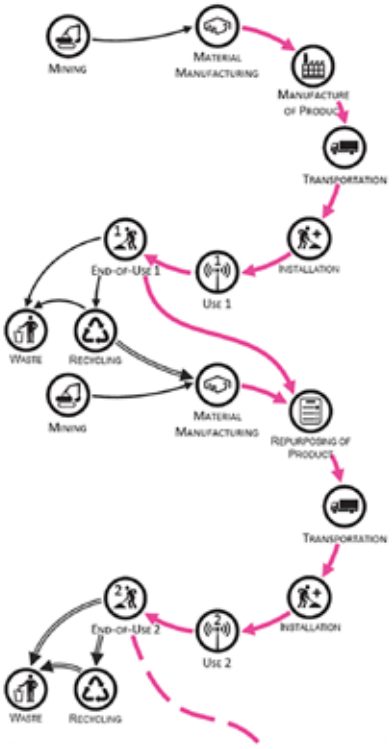

Fig. 3: Diagram for the D2L concept, developed by Bauer [6].

Ecodesign approaches aim at designing products, processes or services with special consideration regarding environmental impacts of the product, process or service during its whole lifecycle. Other specifications such as technical, economic or safety considerations must always be in line with environmental performances when developing eco-designed systems [8]. For example, in the context of urban energy supply, numerous technical constraints are existing when designing optimized energy systems. A current doctoral work in our institute focuses on the integration of environmental dimension in an energy simulation software, initially based on economic and technical optimisation dimensions. In the context of this work, a recent review on simulation softwares [9] showed that too little impact categories are analysed in the specific case of hybrid energy systems and that in most cases, only the use phase of the life cycle is considered. Upstream and downstream contributions are neglected. As the energy systems are becoming increasingly complex, the impacts may shift away from the operating stage, for instance to the manufacturing stage of devices or to their end-of-life options. In terms of impact shift, it is also necessary to look further than global warming potential and take into account other impacts such as depletion of critical materials, acidification, eco-toxicity. Only then, the simulation tool will provide an optimisation of the hybrid energy system, including the environment dimension on top of techno-economic capabilities, to the designers and to decision-makers.

With the example of these activities, we aimed at developing the four different levels of eco-design of our technologies, presented by Teulon in [10] and illustrated in Figure 4 to go towards innovation, driven by environmental performances.

Regarding application fields, our eco-design and eco-innovation methods apply to our emerging technologies, such as:

- The development of materials and processes for the energy transition and for the circular economy (additive manufacturing, magnets value chain, chemistry and green processes: catalysis, supercritical fluids, recycling, etc.);
- Energy efficiency, applied to low carbon mobility, building sector or industry;
- Renewable energy production (biomass energy or solar energy).

3. Eco-design: a tool to design and develop more eco-friendly photovoltaic technologies

Among the various renewable energies, photovoltaic (PV) solar energy, which directly converts sunlight into electricity, has experienced a big growth during the last ten years; global PV module production capacity at the end of 2015 was estimated to be about 60 GW_p [11]. In this context, it is therefore necessary to ensure that new PV technologies, which are complex and the result of several manufacturing stages, meet the criteria of a product with low environmental impact, referred here as eco-designed. The state of the art on eco-design shows that the consideration of environmental constraints in R&D projects with low "Technology Readiness Level" (TRL) is still an emerging phenomenon [12], for two main reasons. On the one hand, environmental impact assessment is relatively complex for a non-mature technology under development (low TRL) because its characteristics and manufacturing processes are not yet fully defined. On the other hand, the identified tools in the literature have several limitations that impede their appropriation in R&D organizations [13].

CEA-Liten led research work since 2015 to develop a methodology to enable the sustainable integration of eco-design into R&D organizations to support the PV industry in innovation and competitiveness. The developed method is thus based on the estimation of the evolution rate of technical, economic and environmental criteria of a new technology (low TRL) compared to a technology of reference [14]. The construction of the database associated relies on Life Cycle Assessment (LCA), used as a management tool to provide reliable results, despite the low TRL level. To this end, three lines of research have been addressed.

The first axis concerned the development of an approach taking into account the complexity of the environmental analysis of a technology under development (or "immature technology" with low TRL), while ensuring the reliability of the results. The proposed approach consisted of the establishment of a detailed reference database on the silicon technology, capturing over 90 % of the world's annual PV production [15]. The critical dynamic parameters were at first identified, such as the PV module efficiency, the solar irradiance, the performance ratio, the technology lifetime and associated degradation rate. In addition, all the data covering the entire value chain (from feedstock, ingots, wafers, cells, modules, to system) were capitalized and, through the LCA baseline, environmental results were stored.

The second axis concerned the development of an approach specific to the photovoltaic field and able to take into account not only the environmental impacts, but also the industrial needs through the technical and economic performances of the technology under development. Thus, this approach aims to assess the evolution rate of a new technology from technical, economic and environmental points of view, compared to the reference technology (Fig. 5). The originality of the approach is based on the use of the LCA as a steering tool for the estimation of the environmental evolution, thus satisfying the criteria of reliability and transparency of results even from the R&D phase.

Finally, to integrate this approach into R&D organizations in a sustainable way, the method developed was implemented in a software "ECO PV", a computer tool

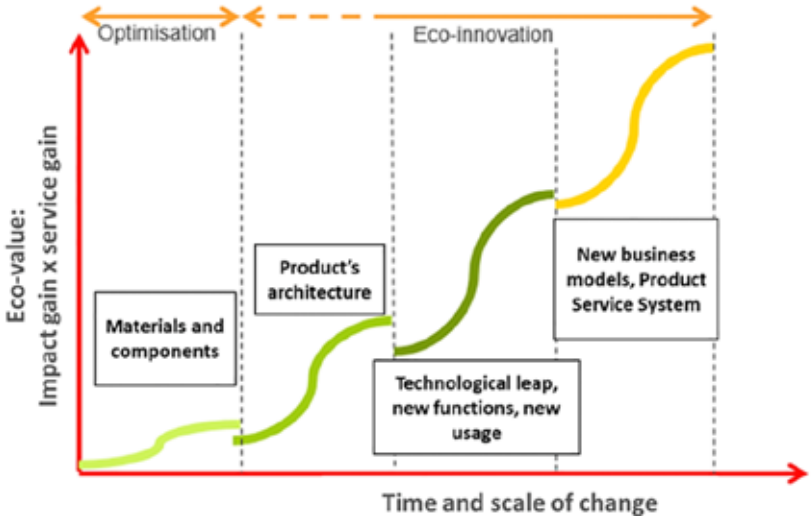

Fig. 4: The four levels of eco-design, from [10]

with an ergonomic "user" interface, in order to satisfy the double ambition of this research work:

- On the one hand, the democratization and capitalization of environmental knowledge within the R&D organization, accessible not only to environmental experts, but also to R&D engineers in PV
- On the other hand, a continuation of the integration of the approach developed within this same organization.

The feedback from the "beta-tests" within CEA-Liten confirmed the ease of use of the tool by all the R&D engineers involved, from PV material to PV system expertise. The integration of the tool into several R&D projects within the CEA-Liten at INES also confirmed the functionality of the tool. The results obtained showed its relevance versus the expectation of the R&D engineers and industrial partners, who were guided towards more eco-friendly choices during the development phase of innovative technologies (Fig. 6).

Moreover, the automation of the environmental analysis, by highlighting the dynamic parameters of the system, confirmed the sustainability of the methodology. This has made it possible to transfer knowledge between the various value chain experts, initiating a process of systematic integration of eco-design within the organization's activity.

Finally, this research work enabled to generate reliable, simple and quantified results and to develop an eco-design methodology to guide the technological choices of projects in the upstream phases of R&D, in order to design and develop more eco-friendly photovoltaic technologies.

4. Eco-innovation: enabling promising and eco-friendly research programs to emerge

Approaches like Life Cycle Assessment (LCA) or Eco-design have proven their interest for the development of Liten's solutions in the last 10 years. They allow the production of sound knowledge about quantitative environmental performance of our technologies and their incremental enhancement. Apart from dedicated tool development, their implementation happens sometimes within the duration of research project but most of the time from one project to another. For these reasons, a reflection has been conducted to increase these approaches added value to target the innovation generation, in addition to the knowledge generation and optimization pathways in a more reactive and less constraining way for research activities.

At the end of 2016, a dedicated eco-innovation program has been launched to incubate and experiment an adjusted method to the context of research in new energy technologies. The aim of this eco-innovation method is to reduce the amount of environmental impacts

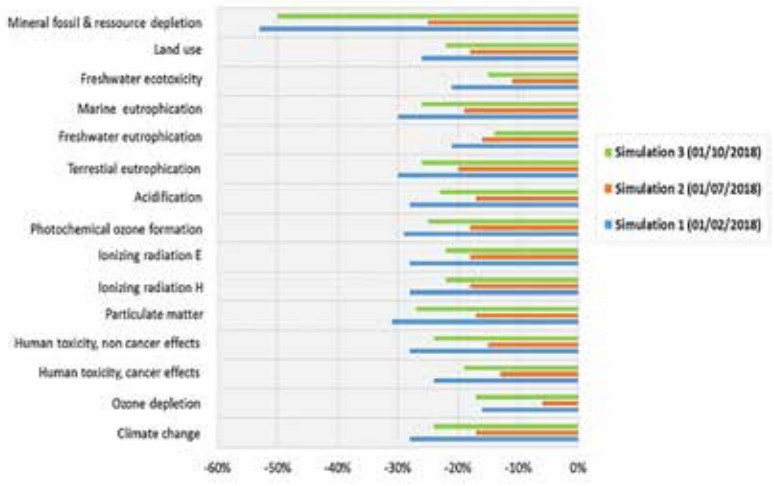

Fig. 6: Example of the results of eco-design obtained during several phases of one project, to estimate the environmental gain of the technology under development within such project.

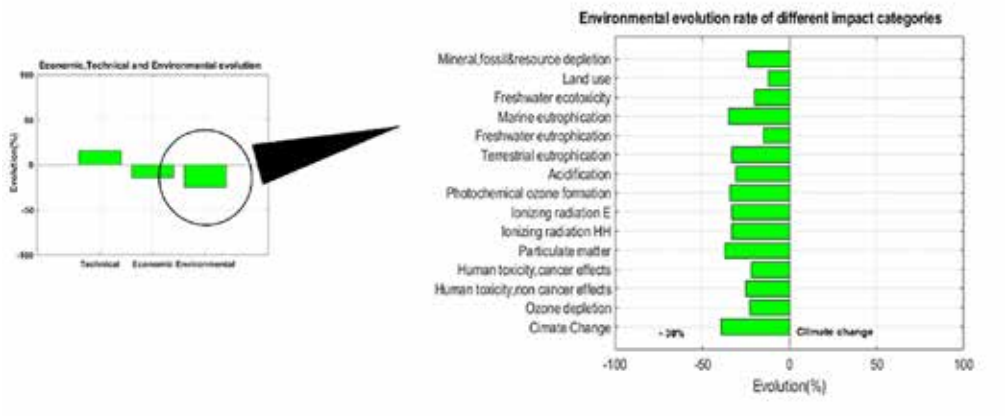

Fig. 5: Evolution rate of a new technology under development compared to the reference technology, from technical, economic and environmental points of view.

of developed technologies per unit of delivered service. The methodology had to be used at the beginning of the R&D projects and be seen as an opportunity by research teams. Based on these specifications, and on innovation, eco-design and change management techniques, a four steps innovative approach, illustrated in Figure 7,has been proposed and tested by the Liten R&D teams.

With the use of this approach, more than 300 eco-ideas have been generated in two years on the following topics: smart thermal energy storage, sodium-ion batteries and innovation for renovation and construction sector. Then, 56 of those ideas were selected by our research teams to be valorized among existing or new private and public research programs. Four promising ideas in particular will be soon patented and four disruptive ones are under exploration through doctoral work. Based on these results, the generic eco-innovation method with a handful of relevant tools has been improved and formalized to be applied on any topic of our technological context. In the following paragraphs, we demonstrate practically the obtained results of this methodology on the three cited topics.

4.1 Eco-innovation for smart thermal energy storage

The first case study on which the eco-innovation method has been tested, is related to a thermal energy storage concept, using a phase change material and smart management technologies. This system allows the delay of thermal energy production during its use. This kind of system presents environmental advantages at urban scale because it contributes to the reduction of fossil energy use when energy consumption peaks are occurring all along the day. However, from a life cycle point of view, this kind of system presents some disadvantages and strong environmental burden during manufacturing, installation, maintenance and end of life phases.

The eco-innovation method has been applied on this case study to design more sustainable solutions for thermal energy storage technology, and to keep its performance during use phase. The research team motivation for working on this subject was to enable a concept at medium maturity level to meet faster its market by increasing its attractiveness with environmental aspects. The innovation question on which the research team worked on was: "How this system could be simple to use throughout its whole life cycle while being efficient?"

A mental map has been built based on the results of the 4 steps of the eco-innovation methodology:

1- Define opportunities on the system development, based on the motivations of the team to perform innovation on this system;
2- Analyze the eco-innovation question with the support of several tools, such as Simplified LCA, functional analysis, usage scenarios...;
3- Find ideas to answer the question, in a creative context to empower breakthrough ideas ;
4- Select the ideas using evaluation tools and communication.

The concepts proposed at the end of the experimentation maximize environmental benefits during the use phase without increasing other life-cycle-phase environmental impacts. Main innovations consist in the improvement of system intelligence and its interface with grid operators' tools. The physical form of the technology, as well as a smart self-managed maintenance, have been proposed during the ideation process.

To conclude on this case study, 17 new concepts of thermal storage technologies have been imagined by research teams at the CEA and for two of them, a patent has been submitted.

4.2 Eco-innovation for construction and renovation sector

Since several years, research in the building sectors has been focused on the improvement of environmental impacts of the materials and products used in construction. This has been impulsed by a demanding regulatory context towards construction sector (RT 2012, Energy Carbone experimentation...). At CEA-Liten, research teams working on technologies implemented in buildings want to address in their research programs the future greenhouse gas and energy efficiency requirements defined by policies.

The application of the eco-innovation methodology aimed at supporting a team of researchers in the integration of an additional environmental aspect within their research framework and strategy. The intern crowdsourcing tool "Idée-Clic" has been used to launch a call for ideas on this topic. The innovation question asked on our internal website was "How to modify construction and renovation of buildings to enable sustainable cities (air quality, resource efficiency, low carbon)?". In 4 weeks, 159 ideas have been proposed by the different CEA institutes and services. 72% of them are today supported by our transversal evaluation committee (Fig. 8).

Ideas generated were about the development or the improvement of building components or the building itself. Other ideas related to the usage of building or

Fig. 7: Eco-innovation methodology developed for CEA-Liten activities.

neighborhoods interconnect were also proposed. Some of them are already in development. For example, a PhD project focuses on the development of photonic walls for thermal infrared emission to improve thermal comfort in buildings.

During this experimentation, the active users of the crowdsourcing tool have estimated the environmental benefits and impacts of their idea with a life cycle perspective of the building. 82% of the proposed ideas have been identified as proposition for reducing greenhouse gases emissions during the building's life cycle. 24% of them have been also identified as interesting for the reduction of the three environmental indicators aimed in the campaign, simultaneously: greenhouse gases emissions, air quality and use of material reduction.
In the context of this specific experimentation, the use of open innovation tools allowed the generation of breakthrough innovation ideas, due to its capacity to simultaneously gather ideas from hundreds of persons.

4.3 Eco-innovation for sodium-ion batteries

Materials with high grey energy have specificities that are interesting for developing new technologies related to energy. In the development of sodium-ion batteries, vanadium is highly used to obtain the performances expected (power and cyclability for charge). However, vanadium increases consequently the environmental impacts of the synthesis of active material used for the manufacture of sodium-ion batteries. It has also been added by the European Union in 2017, on the list of critical Raw Materials (CRM) [16]. Therefore, designing a Na-ion battery with low impacts materials is a challenge that needs to be addressed to anticipate a technological and environmental lock that could question, in the future, the relevance of a technology which is today at low maturity level. The eco-innovation methodology developed in CEA-Liten was therefore applied to find a way to create high-power active materials with high cyclability and without critical materials for sodium-ion batteries. Several criteria were used to select the most innovative materials to replace vanadium. New ideas were generated at the end of the experimentation including:

- The development of lamellar material for Na-ion: this idea aimed at replacing $Na_3V_2(PO_4)_2F_3$ material by a lamellar oxide as a positive electrode which will aim at boosting the electromechanical performances of the cells in the Na-ion battery and avoid the use of vanadium.
- The use of sulfates in the positive electrode: this second innovative idea has strong potential in terms of electrical energy discharge.

These two ideas were selected among 43 innovative ideas imagined by Liten's research teams, working on batteries technologies. The use of creativity methods for a constraint technological topic was a success, and these two ideas are two key subjects that the research team will develop in the context of a PhD student work and a collaborative research project.
Moreover, after the experimentation other eco-innovation tracks have been identified on the Na-ion technologies, such as the use of biomass-based and bio-polymer hard carbons as advanced materials for the anode manufacturing. This experimentation has highlighted the importance of setting ideas selection criteria before the innovation ideation. The implication of the people in the idea selection was a key aspect of the approach, for the maturation of the generated ideas.

5. Conclusion and perspectives

Life Cycle Analysis and eco-design approaches performed in Liten's research activities are tools allowing our institute to identify future environmental locks for our technologies. It brings incremental innovations in our research programs without necessarily bringing the emergence of breakthrough ideas. For 10 years, several collaborative research projects or doctoral works made it possible to diversify the offer of dedicated eco-design tools for technologies developed by the Liten: photovoltaic sector, energy optimization, recycling activities...
The work realized in 2017-2018 by the LCA and eco-innovation team at CEA-Liten showed the importance of adapting eco-design tools to RTO context to move from incremental eco-design improvements to innovative eco-design. The eco-innovation approach developed during this period is based on eco-innovation existing approaches but has been completed with a prospection upstream phase and an action downstream phase to guarantee a continuity with our own project processes. A combination of tools linked to the environmental and innovation fields can today be used by our research teams to help

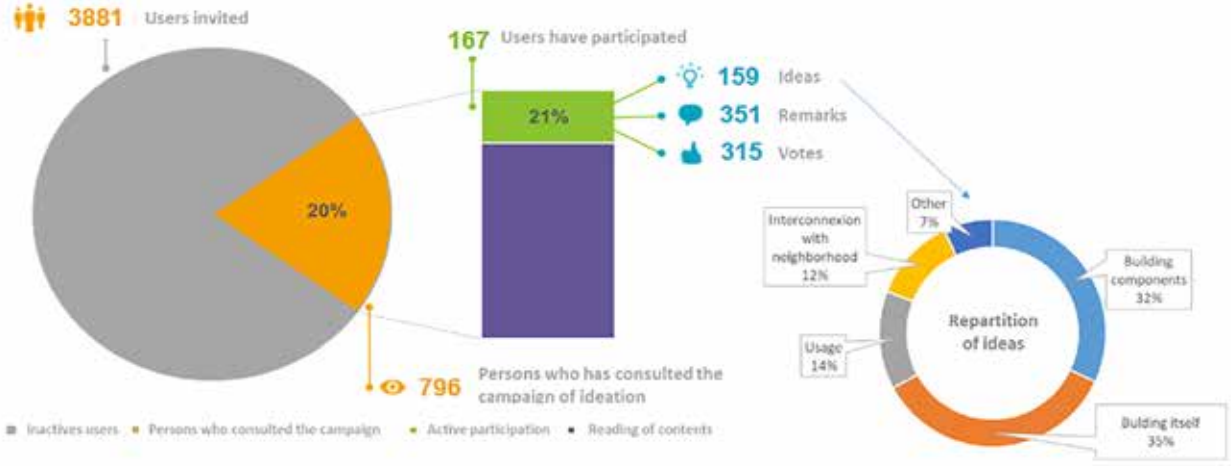

Fig. 8: Key data concerning the call for innovative ideas related to the building sector.

the emergence of new technological developments; outside existing trajectories. The testing of the methodology in three technological contexts helped its improvement and can be used today for any eco-innovation problem of our institute. In 2019, the use of the methodologies and the tools developed and tested within the Carnot project Eco-Innov'NTE, will be extended with the objective of implementing LCA and eco-innovation knowledge and expertise in all the R&D activities of the CEA-Liten. This will be done through the creation of a LCA and eco-design practitioner's internal network. With the training of environmental ambassadors in each department, the objective for future years is to improve the integration of environmental aspects in research activities and technological developments of our institute. For now, a training session has been organized and the LCA/Eco-innovation network is launched in June 2019. The main strategic orientations regarding eco-innovation activities for the CEA-Liten are in the process of definition in each department and include amongst other: circular economy activities, sustainable technological development regarding H_2 technologies or solar technologies (PV, thermal sensors...), and environmental database development for energy storage technologies. □

[1] 'ISO 14040: 2006 - Analyse du cycle de vie - Principes et cadre', AFNOR, X30-300.

[2] 'ISO 14044: 2006 - Analyse du cycle de vie - Exigences et lignes directrices', AFNOR, X30-304.

[3] European Commission and Joint Research Centre, ILCD handbook: general guide for life cycle assessment : detailed guidance. Luxembourg: Publications Office of the European Union, 2010.

[4] European Commission and Joint Research Centre,, ILCDHandbook: Recommendations for Life Cycle Impact Assessment in the European Context, Luxemburg: Publications Office of the European Union, 2011.

[5] S. Di Iorio et al, 'Protective coatings for SOFC SOEC interconnets: impact of fabrication technique on electrical conductivity' 13th European SOFC &SOE Forum, Lucerne, 2018

[6] T. Bauer, 'Concevoir un produit pour plusieurs vies : Propositions pour la conception et l'évaluation environnementale de solutions en cascade', PhD thesis, Université Grenoble Alpes, 2018.

[7] T. Bauer, G. Mandil, É. Naveaux, and P. Zwolinski, 'Lifespan Extension for Environmental Benefits: A new Concept of Products with Several Distinct Usage Phases', Procedia CIRP, vol. 47 (2016) 430–435.

[8] D. C. Pigosso, H. Rozenfeld and T. C. McAloone, "Ecodesign maturity model: amanagement framework to support ecodesign implementation intomanufacturing companies", J. Clean. Prod., vol. 59 (2013) 160-173

[9] H. Sharma, É. Monnier, G. Mandil, P. Zwolinski and S. Colasson, "Comparison of environmental assessment methodology in hybrid energy system simulation software", Procedia CIRP, vol. 80 (2019) 221–227.

[10] H. Teulon, "Le guide de l'éco-innovation: éco-concevoir pour gagner en compétitivité", Paris: Eyrolles, 2015.

[11] European Photovoltaic Industry Association. Market report 2011. ISO 14040. Environmental management – life cycle assessment – principles and framework; 2006.

[12] Fraunhofer Institute for Solar Energy, Photovoltaics Report, Fraunhofer ISE, Freiburg im Breisgau, 2015.

[13] N. Gazbour et al., "A path to reduce variability of the environmental footprint results of photovoltaic systems", J. Clean. Prod., vol. 197 (2018) 1607–1618.

[14] N. Gazbour, "Intégration systémique de l'éco-conception dès la phase de R&D des technologies photovoltaïques", PhD thesis, Université Grenoble Alpes, 2019.

[15] International Technology Roadmap for Photovoltaic (ITRPV), Seventh Edition, March 2016.

[16] http://criticalrawmaterials.org/european-commission-publishes-new-critical-raw-materials-list-27-crms-confirmed/

MATTER AND MATERIALS

TOWARDS FUTURE ADDITIVE MANUFACTURING METALLIC MATERIALS

RESEARCH TEAM (from left to right) Luc AIXALA, Gilles GAILLARD, Matthieu BUGEAU, Violaine SALVADOR, Céline RIBIÈRE, Marilyne ROUMANIE, Guilhem ROUX, Cécile FLASSAYER, Jean LEFORESTIER, Mathieu SOULIER, Michel PELLAT, Pascal FAUCHERAND, Richard LAUCOURNET, Julie MAISONNEUVE, Thierry BAFFIE, Pierre LASSÈGUE, Emmanuelle ROUVIÈRE, Claudia SALVAN, Mathieu OPPRECHT, Michaël BOUVIER, Florian PEYROUZET, Akash SONAWANE, Jean-Paul GARANDET

CONTACT emmanuelle.rouviere@cea.fr; jean-paul.garandet@cea.fr

1. Introduction to Metals Additive Manufacturing activity at CEA-LITEN

Additive manufacturing (AM) refers to a number of material fabrication technologies allowing to build parts layer by layer to Net Shape (or at least Near Net Shape) according to an a priori prescribed computer file. AM allows faster prototyping, weight reduction thanks to topological optimization, component customization, the production of complex shapes or the reduction of the number of assembly steps compared to traditional manufacturing processes. AM is in continuous industrial expansion, and it addresses virtually all types of markets, e.g. energy, aeronautics, oil and gas, medical and health care, luxury...

The LITEN developments in the field of AM are based on a widely recognized historical experience in powder metallurgy, that associates a scientific background in materials science (thermodynamics, chemistry and physico-chemistry, mechanics and thermo-mechanics) with a technical expertise in process engineering (powder functionalization, feedstock formulation, solidification and sintering, thermal processes and annealing), that covers both metallic and ceramic materials. Based on these historical characteristics, the AM developments in the LITEN Materials and Technologies department proceed mainly along two axes, one based on the implementation of a thin powder bed that is melted locally by means of a focused laser beam (Laser Powder Bed Fusion, L-PBF), the other relying on the selective curing of an organic-metallic feedstock (Vat Photopolymerization or Stereolithography, SLA).

The LITEN activities in the field of AM are mainly located within the 1400 m² POUDR'INNOV 2.0 platform, which includes a complete range of laboratory, semi-industrial and industrial equipment covering the entire component production process, from CAD design to parts characterization, and including a variety of equiments (formulation/mixing, debinding, sintering and post-treatments). The platform features six state of the art AM machines, namely L-PBF Prox200 (3D Systems), L-PBF FS271M (Prodways), L-PBF SLM125HL (SLM Solutions), L-PBF FormUp350 (AddUp), Vat Photopolymerization M120 (Prodways) and Vat Photopolymerization V6000 (Prodways).

The results presented here are restricted to the AM of metallic materials. We will first in section 2 briefly present the AM processes actually used on the POUDR'INNOV 2.0 platform and the associated materials. We will then proceed in section 3 to a few salient results on powder specification and functionalization input material preparation. We will then move in section 4 to a description of our research activities in the field of AM materials and processes, including a special focus on magnetic materials, a field of recognized LITEN expertise, where AM has the potential to be a game changer.

2. Focus on L-PBF and SLA processes

In L-PBF process (Fig. 1a), a metallic powder is first spread as a thin layer on platform thanks to a blade or a roller and then locally molten with a high power Yb fiber laser having a circa 1 µm wavelength. The duration of interaction with the material is very short (below 1 ms)

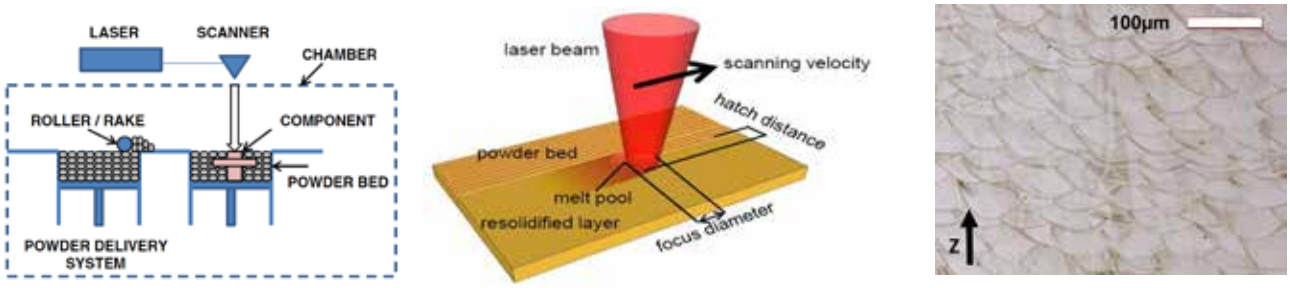

Fig. 1: a) Schematics of the L-PBF process [1]; **b)** Key parameters of L-PBF process [2]; **c)** Typical microstructure in as-built state along the building direction, after [3]

and the light intensity very high (often above 10^5 W/cm^2). The process is carried out under a protective gaseous flux to limit oxygen intake and remove fumes and fines particles. For each layer, the energy density transferred to the material is enough to melt it, but also to partially re-melt the underlying layer so that the layers are welded (Fig. 1c). Once the process is completed, the unused powder is removed and the part can be post-treated and detached from the platform. The main parameters of the process (Fig. 1b) are the laser power (generally in the 200-500 W range), the laser spot radius (30 to 100 µm), the laser scanning speed (500 to 1500 mm/s), the hatching distance between two adjacent scanning vectors (30 to 100 µm), the powder layer thickness (20 to 100 µm) and the scanning strategy. The used particle size distributions are in the 0-60 µm range. The productivity ranges from 1 cm^3/h to 150 cm^3/h. The surface roughness is around 20 µm and dimensional accuracy of parts ranges from 0.05 mm to 0.2 mm. In L-PBF field, we have up to now studied Iron-based alloys (stainless steels, low carbon steels), nickel-based alloys, aluminium alloys, copper alloys, metal matrix composites (hard metals), high entropy alloys and magnetics alloys (FeSi, FeCo, SmCo, NdFeB). The R&D topics address the compatibility of powders with the L-PBF process, determination of the process window, the effect of powder recycling on mechanical properties, the chemical functionalization of the powders surface (through wet or gas surface engineering, in order to increase their optical absorption at the laser wavelength) or the development of new alloys. M-SLA is a metal/polymer additive manufacturing technology, based on UV curable printing, completed by a thermal debinding and sintering cycle to produce dense metal parts (Fig. 2a). More specifically, the photoreactive composition is a blend of photoinitators (PI), oligomer and monomer acrylates filled with a high rate of metallic particles [4-5]. The prepared paste is spread into thin layers (25-100 µm) by a dual blade recoater (Fig. 2b) on a building platform. The UV light head projects a pattern of the layer slice of the part (Digital Light Processing technology: high spatial resolution (32 µm) - high dimensional tolerances (up to 1%)). An organic network ensures a mechanical strength of printed parts. The printed parts are removed from the platform and cleaned. The uncured paste can be re-used. Once the parts are manufactured by SLA, organic phase is burnt during the thermal debinding and the metallic parts are sintered.

In Vat Photopolymerization, we have undertaken process development for metallic alloys (titanium alloys, nickel alloys, iron alloy and copper) as well as ceramics (silicon carbide and zirconia); R&D topics address feedstock formulation, optical properties of powder-resin feedstocks, chemical and thermal debinding development and optimization to control organic contamination and density.

3. Powder issues

3.1. Powder specifications

One of pending issues in L-PBF metal additive manufacturing is the definition of powder specifications to ensure its compatibility with the AM process, in particular a high powder spreadability. To this end, a number of characterization techniques available on our POUDR'INNOV 2.0 platform (laser granulometry, morphogranulometry, He pycnometry, avalanche angle, apparent and tap density, optical reflectivity) have been implemented on a panel of available gas or water atomized 316L commercial powders [6]. Our objective is to set up a powder database in terms of morphology and particle size, flowability and apparent density. The database is used to feed a phenomenological predictive model that aims to adjust powder characteristics (particle size distribution, shape) to optimize the powder flow or apparent density. The aim of this work is to fine tune powder specifications to ensure powder suitability to processing while maintaining reasonable material costs and avoid too stringent powder specifications. This work will also bring valuable insights regarding the question of powder recyclability, which is presently an open question.

3.2. Low optical absorption of Cu- and Al-based powders

If laser/powder interaction generally exhibits good energy absorption, some metals are difficult to melt using L-PBF technology, due to an a priori too high

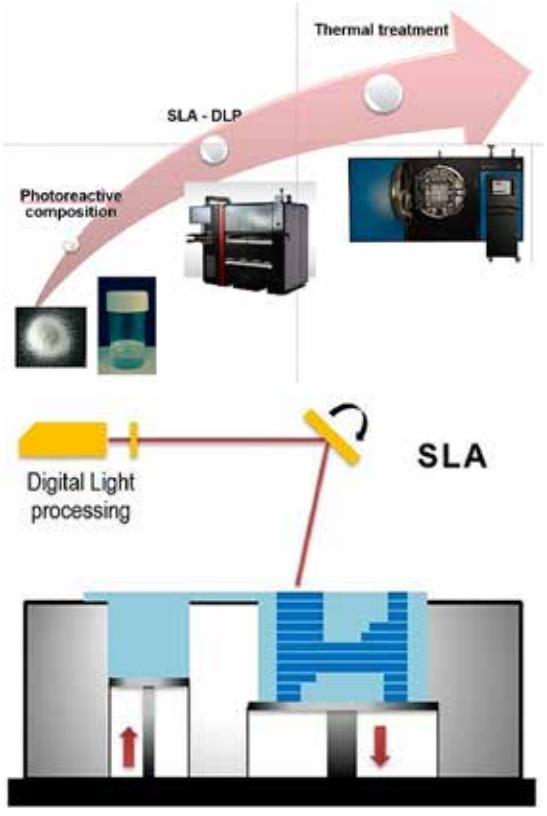

Fig. 2:
a) Metal Stereolithography: formulation, SLA technology, thermal treatment;
b) SLA process

reflectivity (Fig. 3). We have proposed a number of developments in order to address this problem.
In the case of Cu, a first approach is to add elements in small amounts such as chromium and zirconium. Part of these elements located on the surface of the particles allow reducing the optical reflectivity of roughly 3%. Another solution is to decrease the reflectivity of the powder by an absorptive coating. Optimal layer thickness is computed using numerical tools to achieve optical interference between laser wave and coated particles (Fig. 4). Another line of research is based on surface nanostructuration by means of electroless deposition [8] Coated powders manufactured present large reflectivity reduction (60% to 9% for Cu based powders) validating our patented approach [9] (Fig. 5).
Trying to extend this approach to more industrial processes, allowing high-rate uniform deposition on powders, fluidized-bed chemical vapour deposition (FB-CVD) is presently investigated.

3.3. Nanocomposite powders

The integration of a secondary nano-phase on standard micronic L-PBF powders phase can have several goals. In very small quantities, this can first of all allow to refine the grain structure of the material, and thus to increase its mechanical properties or to avoid hot cracking on materials sensitive to this mechanism, as is the case for some standard structural aluminium grades. In larger quantities, the second phase can make it possible to further increase the mechanical properties of the material by adding a second stable phase, able to block the dislocations during the plastic deformation of the material.
In the frame of the European HIPERCO project, the objective is to develop an industrial route to prepare a mix of aluminium/n-SiC nanocomposite powders compatible with the L-PBF process. Electrostatic bonding of silicon carbide nanoparticles at the surface of aluminium alloy particles ensures the stability of the powder mix (Fig. 6a). In addition, the mix process improve the flowability and apparent density of the nanocomposite powder through a reduction of hydrogen bonding between Al particles where surfaces become saturated by n-SiC. A similar approach was successfully implemented to graft ZrO_2 nanoparticles on top of Al-6061 powders [11]. These nanoparticles proved to be a key ingredient to the solidification process, with a significant grain size reduction and the promotion of an equiaxed structure (Fig. 6b and 6c).
The next step on this topic is to realise FA parts using these nanocomposite powders in order to quantify the improvement with respect to standard powders. Future work is also planned on nickel base alloys.

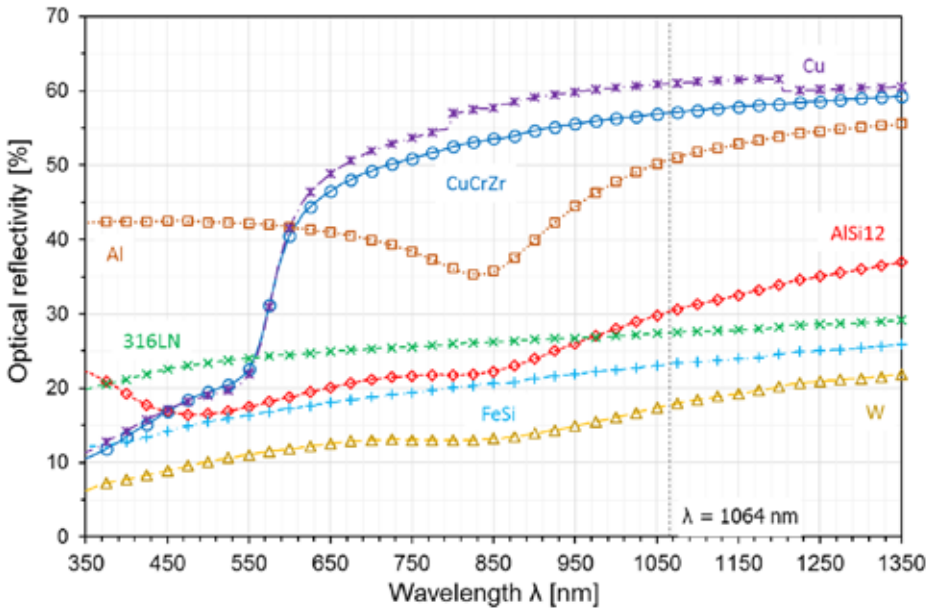

Fig. 3: Comparison of optical reflectivity curves versus wavelength for several L-PBF powders, after [7].

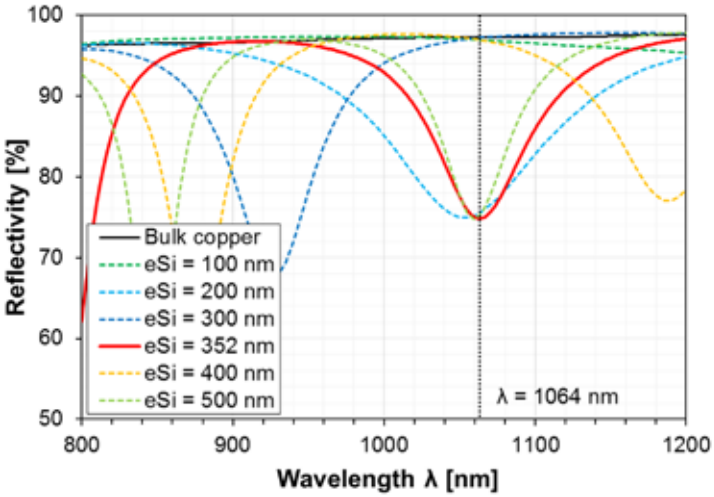

Fig. 4: Simulation of the silicon layer thickness influence on the reflectivity of bulk copper

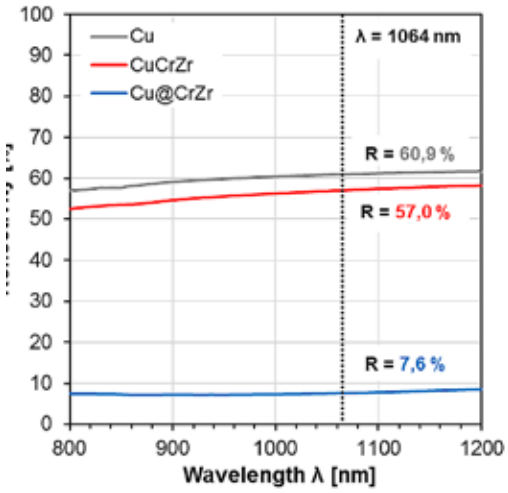

Fig. 5: Effect of layer coating on powder absorption, after [10].

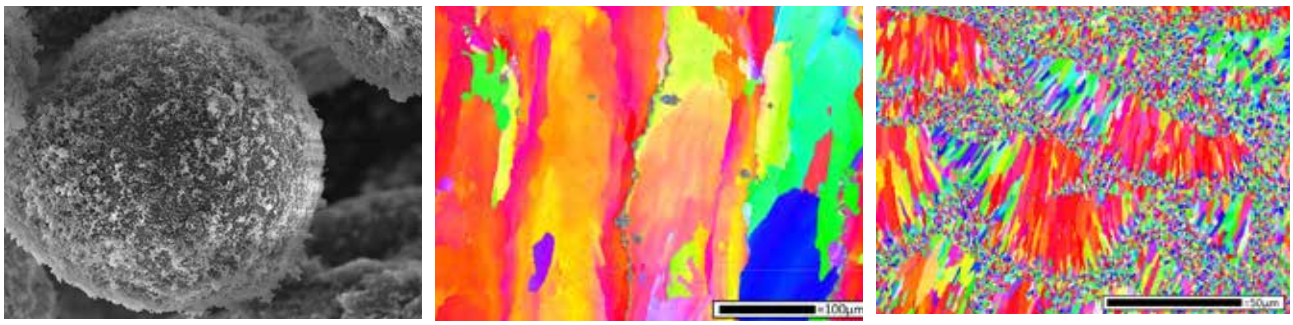

Fig. 6: a) Nanocomposite Al-SiC powders and EBSD solidification structures on Al-6061 alloy without b) and with c) ZrO_2 nanoparticles on the starting powders.

4. Materials and processes

4.1. Copper alloys

Apart from aforementioned reflectivity issue, the high thermal conductivity of copper alloys affects the solidification process in L-PBF (1064 nm). Varying laser power and speed through single tracks and walls building allowed to draw the process window of CuCrZr alloy (Fig. 7a) with a highest density of 8.84 g / cm^3 (i.e. 99.3 % in terms of relative density), obtained using a scanning speed of 160 mm/s, a laser power of 270 W and a hatch of 100 µm. Microstructure of cubes indicates columnar grains in the z direction (building direction), (Fig. 7b and 7c). The hardness after a heat treatment of L-PBF sample is 112 ± 4 HV1 in the z direction, comparable to the one of a wrought sample (116 ± 2 HV1).

4.2. Titanium alloys

Developments on titanium parts manufactured by stereolithography have shown that Metal Matrix Composites (MMC) could be synthesized by reaction between the metal and the carbonaceous residue from the binder thermal decomposition (Fig. 8a) [13-14]. The carbonaceous rate and therefore the TiC inclusions can be managed with the acrylate molecules (long or short molecular chain), the filler rate and the thermal conditions (Fig. 8b). Samples are cured with gamma-rays, debinded and sintered at 1250 °C under Ar. Mechanical properties like Vickers hardness could be increased according to the TiC inclusions (Table 1).

4.3. Magnetic materials

In the family of soft magnetic materials, Fe-Si alloys are widely used in rotating or static electrical machines. Their low cost associated with good magnetic properties (high permeability, low coercivity and high flux density) make them suitable candidates for the markets of non-integrated applications (e.g. industrial equipment). With L-PBF, it is expected to improve the performance of these machines especially through a new design of magnetic cores including (i) weight reduction through lattice structures while remaining robust to mechanical stresses, (ii) heat management of components (especially for permanent magnets), (iii) reduction of assemblies by reducing the number of elementary parts and (iv) fabrication of 3D magnetic structures in order to increase the torque.
Within the ADDIMO Carnot funded project, two compositions of soft magnetic

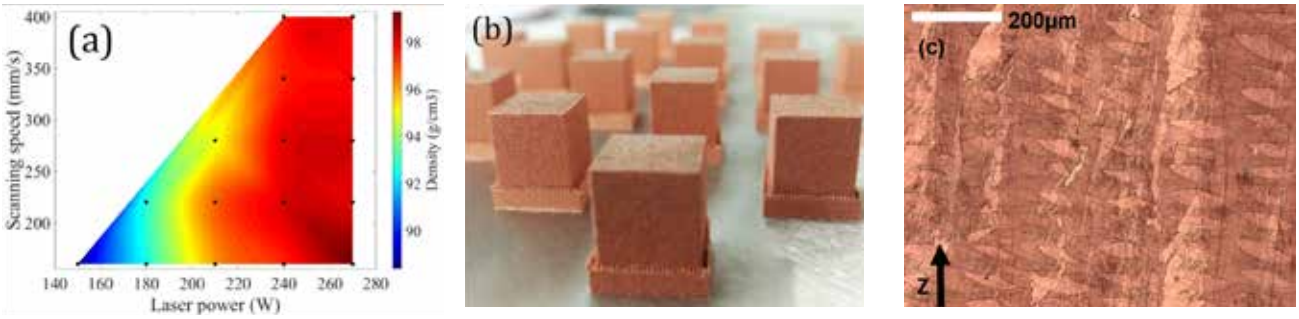

Fig. 7: a) Density map of CuCrZr L-PBF cubes constructed with a 100 µm hatch parameter ; **b)** Resulting cubes; **c)** Microstructure of as-built L-PBF CuCrZr sample after a chemical attack in the z direction. After [12].

Fe-Si alloys powders were successfully used to produce almost full-dense parts from an L-PBF process. An optimized annealing was performed on built parts to achieve the desired magnetic properties. Annealing conditions were correlated with microstructures and magnetic properties. The quasi-static magnetic properties obtained after annealing are comparable to those reported for commercially laminated Fe-Si alloys (cf. 3rd and 4th lines in Table of Fig. 9a). Finally, based on the results of simulations (electromagnetic, thermal and structural-mechanical), a first rotor concept for an electric machine, designed internally, was printed (Fig. 9b).

We are also active on the topic of the adaptation of rare earth (RE) permanent magnets to L-PBF processes. Indeed, the conventional powder metallurgy route does not allow shaping complex parts, due to the brittleness of these materials upon machining. Preliminary results have been obtained using a commercially available spherical isotropic and coercive powder synthesized by rapid solidification and gas atomization. The objective of the study was to define the process conditions allowing to obtain a high density, which is mandatory for high remanence magnets, while maintaining a fine grain microstructure. The influence of laser power, laser speed, hatching distance and strategy of the building has been investigated, and it has been shown that samples without visible cracks and with good magnetic properties can be obtained in a narrow window of L-PBF process parameters. Further work is planned on in-house manufactured powders to fine tune the material composition.

4.4. Protection of AM workers versus nanoparticles and fumes

To deal with HSE issues, we have developed an expertise on assessment of exposure to airborne particles throughout material life cycle [16]. These field campaigns in AM labs or companies consist in on-line measurements (number concentration, particle size distribution) and off-line analyses and characterization of samples (form, size, chemical composition). Based on measurement results (Fig. 10), environment, health, and safety recommendations are made to help industrial partners to limit occupational exposure by working on premise and equipment design, work organization, collective and personal protective equipment, waste management, worker training, etc.

5. General perspectives

Our ambition is to create an ecosystem of R&D and other services for additive manufacturing in conjunction with equipment manufacturers to facilitate the transfer of new technologies to industry such as with AddUp (JV Michelin_Fives) to accelerate the adoption of metal additive manufacturing by L-PBF and M-SLA across the energy industry. □

Fig. 8a: Titanium parts

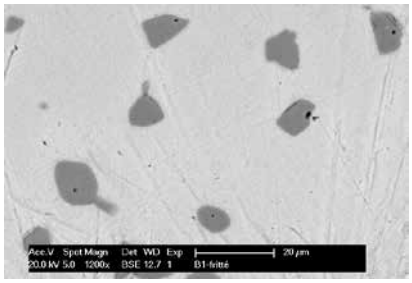

Fig. 8b: TiC inclusion in titanium matrix

Table 1: Mechanical properties (Vickers hardness) of in house Ti MMC and comparison to CHIP Ti reference.

Long chain resin formulation (C content 7.5 wt.%)	Short chain resin formulation (C content 1.8 wt.%)	Cold- and hot-isostatically pressed titanium
440 HV30 ± 12	289 HV20 ± 2	200 HV ± 10

	Main chemical elements	ρ (μΩ.cm)	Js (T)	Hc (A/m)		μ max	
				Annealing temp.		Annealing temp.	
				700 °C	1150 °C	700 °C	1150 °C
Fe-3Si	2.9 wt.% Si	47 ± 2	1.99	240	30	1060	15500
Fe-4Si	3.9 wt.% Si + 0.7 wt.% Cr	62 ± 2	1.90	167	15	1300	16600
Non grain oriented (NGO) Fe-3Si (*)	3 wt.% Si	47	1.8 – 1.9	11 – 60			
Grain oriented (GO) Fe-3Si (*)	3 wt.% Si	47	1.9 – 2.05	3.5 – 11			

Fig. 9: (a) Electrical and magnetic properties of Fe-Si alloys processed by L-PBF, after A. Krings, IEEE Trans. on Industrial Electronics, Vol 64, Issue 3 (2017) 2405-2414); **(b)** L-PBF as printed Fe-Si rotor parts, after [15]

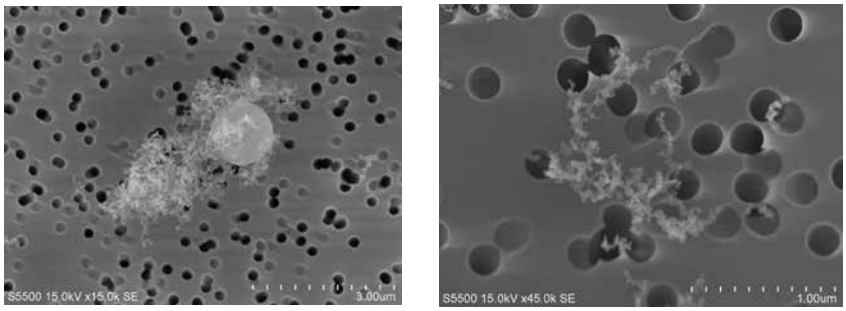

Fig. 10: SEM observations of samples collected during AM machines door's opening to recover AM parts after building ; two cases were observed: a) micronic and b) nanometric particles

[1] W. E. Frazier, Metal Additive Manufacturing: A Review, Journal of Materials Engineering and Performance, Vol. 23(6), (2014) 1917-1928.

[2] F. Doré, La métallurgie des poudres, "Les Rendez-vous de la Mécanique", October 13th 2016.

[3] T. Baffie et al., Physical, Metallurgical and Mechanical Characterization Of An Austenitic Stainless Steel Produced By Selective Laser Melting, in Proceedings of EuroPM2017 Conf., Ed. EPMA, Milan, Oct. 2017.

[4] M. Roumanie et al., Paste for use in a stereolithography method for the manufacture of titanium parts, Patent EP3473357, Oct. 2018.

[5] M. Roumanie, Paste for use in a stereolithography method for manufacturing a ceramic or metal part, Patent EP3473356, Oct. 2018.

[6] M. Soulier et al., Study of 316L Stainless Steel Powders Specifications on Parts Printed by Laser-Powered -Powder Bed Fusion (PBF), in Proceedings of EuroPM2018 Conf., Ed. EPMA, Bilbao, Oct. 2018.

[7] N. Tissot, "Amélioration du procédé LBM par nanostructuration de poudres d'aluminium", PhD Thesis, ENI St Etienne, 2019.

[8] N. Tissot et al., "Nanostructuration de la surface de poudres d'aluminium pour l'amélioration des procédés de fabrication additive par fusion laser", in Proceedings of the "Science et Technologie des Poudres" 2018 Conf., Compiègne, Juil. 2018.

[9] L. Aixala et al., Particle for manufacturing metal parts by 3d printing and method for manufacturing metal parts, Patent EP3409349, May 2018.

[10] P. Lassègue et al., Interest in the use of the fluidized-bed chemical vapour deposition process for additive manufacturing applications, Poster, EuroCVD 2019 conf., Luxembourg, June 2019.

[11] M. Opprecht, PhD thesis INP-Grenoble (in progress).

[12] C. Salvan, Microstructure and properties of Copper parts obtained by Laser Powder Bed Fusion (L-PBF) process of a CuCrZr powder, Talk, MATERIAUX 2018 conference, Strasbourg, Nov. 2018.

[13] M. Roumanie et al., Near Net Shape Parts Development By Additive Manufacturing Opportunities For Ceramics And Metals, in Proceedings of FIMPART 2017 Conf., Bordeaux, Juil. 2017.

[14] M. Roumanie et al., Manufacturing of metal parts by stereolithography, in Proceedings of EuroPM2017 Conf., Ed. EPMA, Milan, Oct. 2017.

[15] G. Gaillard et al., 3D Printing of a FeSi Soft Magnetic Alloy for Prototyping an Optimized Rotor for an Electric Machine, in Proceedings of EuroPM2018 Conf., Ed. EPMA, Bilbao, Oct. 2018.

[16] C. Philippot et al., Potential Workers Exposure Measurement in Metal Additive manufacturing and How to Manage It, in Proceedings of EuroPM2018 Conf., Ed. EPMA, Bilbao, Oct. 2018.

A STUDY OF ORGANIC SEMICONDUCTOR DOPING

P-doping of organic semi-conductor is a good way to increase printed device performances by improving material conductivity and polymer-metal contacts. This study investigates the mechanisms involved in intentional polymer doping. The characterization tools and methodology developed are then used to emphasize the impact of unintentional doping of organic semi-conductor with oxygen and its impact on organic photodetector physics.

With large area scalability, compatibility with flexible substrates, and low temperature processability, printed electronics offers an interesting alternative to conventional silicon-based electronics. To achieve better performances, hole and electron doping needs to be developed to improve the material conductivity as well as the polymer-metal electrode contact. Chemical intentional doping of organic semiconductors is used to increase the mobility and conductivity at low concentration due to trap filling. At higher concentration, doping helps enhancing charge injection through effective barrier lowering at the electrode/organic interfaces. However, the efficiency of molecular doping is limited and a deeper understanding of the charge transfer mechanism is necessary to push the boundaries of this new technology. In this work [1,2], we investigate the doping process at different regimes for PBDTTT-c p-doped with the complex Mo(tfd-$COCF_3$)$_3$. To carry out this study, complementary chemical and electrical characterization techniques are used. On the other hand, doping can be detrimental in printed devices. Although it is known that O_2 plasma treatment efficiently changes the surface tension of polymer layers, no study has been done on its impact on the device performances. Our study [3] highlights the p-doping character of oxygen and its impact when used to change the surface tension during organic photodiode fabrication process.

UV-visible spectroscopy and photoluminescence measurement suggest the creation of gap states with doping. In order to understand the origin of these gap states we carried out admittance spectroscopy at different temperatures. An energy level is extracted ca. 280 meV above the polymer HOMO for the pure polymer. For p-doped PBDTTT-c, the intensity of the peak associated with this energy level increases while a new peak is created suggesting the formation of a gap state ca. 450 meV above the polymer HOMO (Fig. 1). Thanks to the knowledge obtained on doping mechanism and characterization, the impact of unintentional doping with oxygen through oxygen plasma treatment on organic photodetectors performances was demonstrated. Electrical characterization shows the decrease of the External Quantum Efficiency (EQE) of the photodiode with a modification of its shape when an O_2 plasma treatment is used during the fabrication process (Fig. 2). Further analysis emphasizes an increase of the hole doping concentration and conductivity reminding the doping ability of oxygen. Admittance spectroscopy allows extracting a gap state due to the O_2 plasma treatment (Fig. 3). Finally, we were able to fit I(V) and EQE characteristics by simulating our device with and without acceptor traps using the activation energy measured by admittance spectroscopy, emphasizing the need to eliminate oxygen and find an alternative surface treatment to increase device performances and reliability. □

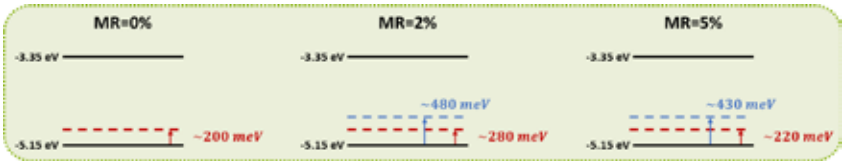

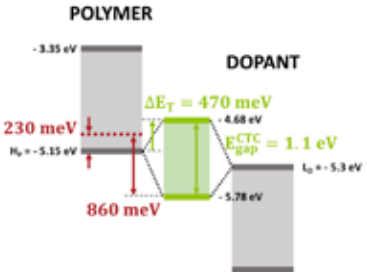

Fig. 1: Band diagrams showing (a) PBDTTT-c energy levels probed by admittance spectroscopy vs dopant concentration and (b) the hypothetical Charge Transfer Complex formed between the polymer HOMO and the dopant LUMO.

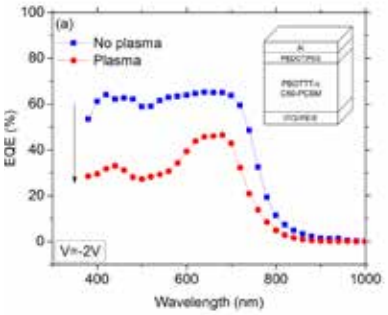

Fig. 2: EQE at -2 V with and without O_2 plasma treatment of the device (inset: OPD structure).

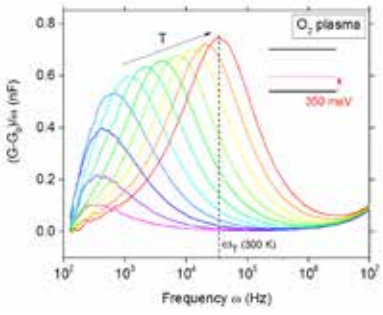

Fig. 3: Spectroscopic impedance as a function of temperature at 0 V for the device with O_2 plasma exposure.

[1] J. Euvrard et al., Organic Electronics, vol. 53, (2018) 135-140.
[2] J. Euvrard et al., Journal of Applied Physics, vol. 123, (2018) 225501.
[3] J. Euvrard et al., Organic Electronics, vol. 54, (2018) 64-71.

TEAM Julie EUVRARD, Amélie REVAUX
PARTNERS IEMN, Princeton University
CONTACT amelie.revaux@cea.fr

SEARCHING FOR NEW MATERIALS USING FIRST-PRINCIPLES CALCULATIONS AND MACHINE LEARNING

Many promising technologies, in particular in the field of energy, are hindered by the lack of performant materials. In the materials modeling group at CEA-LITEN, we develop techniques combining state of the art ab initio calculations with machine learning to look for new materials with relevant technological applications.

Ab initio calculations based on density functional theory have found numerous applications in materials science. However, due to computational costs, ab initio calculations have strong limitations when it comes to predicting properties of large systems, studying extended time scales or computing properties of materials at elevated temperatures. For example, calculating finite temperature phonon densities of states, or vacancy formation energy in solids require performing long molecular dynamics simulations in large supercells. Machine learning techniques offer a solution to this problem. Different machine learning approaches have been used in the attempt to overcome the limitations of density functional theory while keeping its accuracy for various applications. A most relevant one is that the system descriptors should be invariant with respect to rotations and translations of the system as a whole, and with respect to permutations in the ordering of the atom inputs (Fig.1) [1]. Another important feature is to be able to train the potential simultaneously with energies and forces, since both are obtained by density functional theory for the same effort. Recently, we have developed an approach using a deep neural network trained on ab initio data to build interatomic potentials that can be used for much larger systems or time scales while keeping density functional theory accuracy (Fig.2) [2].

We have prooftested our technique by calculating the vacancy formation free energy in aluminum as a function of temperature [2]. The accuracy and efficiency of the potential allowed us to obtain results which refine the state-of-the-art theoretical description of vacancy thermodynamics in metals. Namely, our results predict that the vacancy formation free energy as a function of temperature follows the Arrhenius law at low temperatures, in contrast with previous calculations, and that anharmonicity causes deviation from it only above 600 K. This study was for a monatomic system, but our neural network potential is also universal in terms of structure and chemical composition. Applications of this potential for more complex systems will be demonstrated in future works, notably in the field of materials for energy storage. □

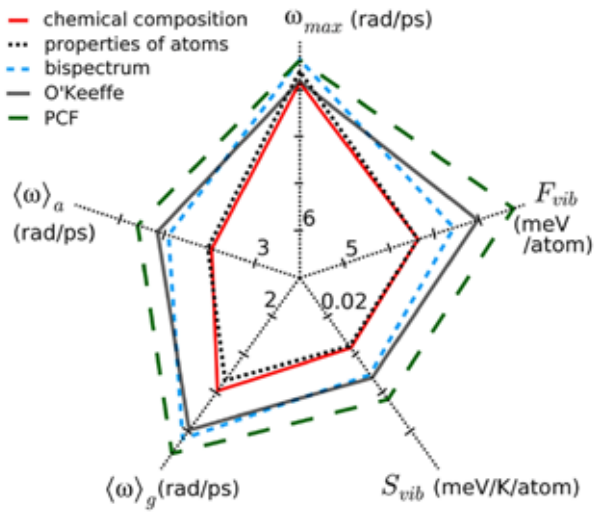

Fig. 1: Performance of different structural and chemical descriptors to predict the vibrational properties of solids.

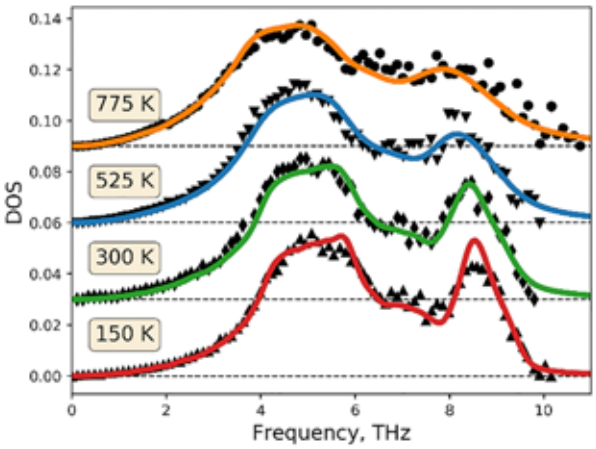

Fig. 2: Phonon density of states at finite temperature obtained from molecular dynamics simulations using an interatomic potential based on neural networks and trained with ab initio data.

[1] F. Legrain et al, Chemistry of Materials, vol. 29, (2017), 6220-6227.
[2] A. Bochkarev et al, Physical Review Materials under review (2019).

TEAM Natalio MINGO, Ambroise VAN ROEKEGHEM
PARTNERS GENCI-TGCC (Paris), APERAM
CONTACT natalio.mingo@cea.fr; ambroise.vanroekeghem@cea.fr.

HEAT ON DEMAND BY TRIGGERING NUCLEATION IN PHASE CHANGE MATERIALS

Thermal energy storage systems (TES) are used to partially solve the mismatch between energy needs and renewable energy availability. One type of storage materials used in TES are phase change materials (PCMs). Some of these PCMs have a metastable property (supercooling) whose use may constitute a breakthrough, as it would be possible to release the stored thermal energy on demand.

Phase change materials have a passive behavior as they melt above the liquidus temperature and solidify when the temperature drops below this point (short-term heat storage). Usually, the melting and the crystallization points are similar and the heat can be released only in a limited temperature range. However, for long-term heat storage application (heating up a device or seasonal thermal storage), the heat release needs to be triggered on a wide temperature range. PCMs that can be put in a supercooled state would be good candidates for this application. In that way, sodium acetate trihydrate has interesting properties: a melting point of 58 °C relevant for hot water production, good thermal storage properties together with a deep supercooling capacity. However, the uncontrolled activation of the crystallization is an important issue. Several techniques for triggering the nucleation are considered: seeding, electrical means, mechanical means, agitation.

We have reviewed [1] the different methods of triggering the nucleation on demand and identified the most favorable conditions and their limits. Most of the usual triggering techniques are intrusive and involve the contact with the PCM. We have developed a new experimental bench using ultrasounds in a non-intrusive way. Several characteristics were analyzed such as opacification related to the heat release duration (Fig. 1) [2] and nucleation probability for different ultrasound configurations (Fig. 2) [3]. The results show that nucleation can be triggered with a high probability (>90 %) with a few number of ultrasound periods (£ 3) for a 3.2 % duty cycle in a quartz container of 30 mL. The following steps of the analysis will focus on the analysis of the scaling and roughness effects and to the thermal aging of this salt hydrate. □

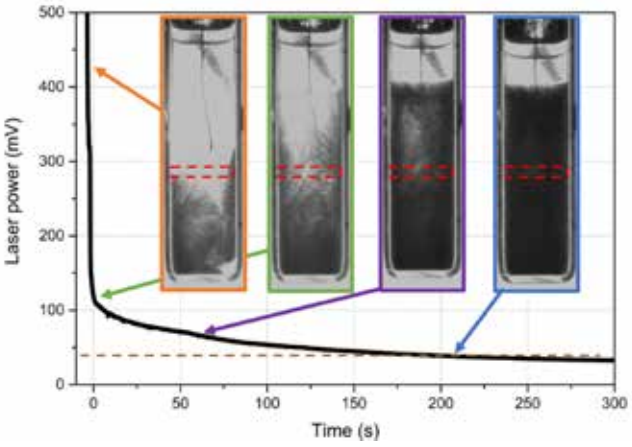

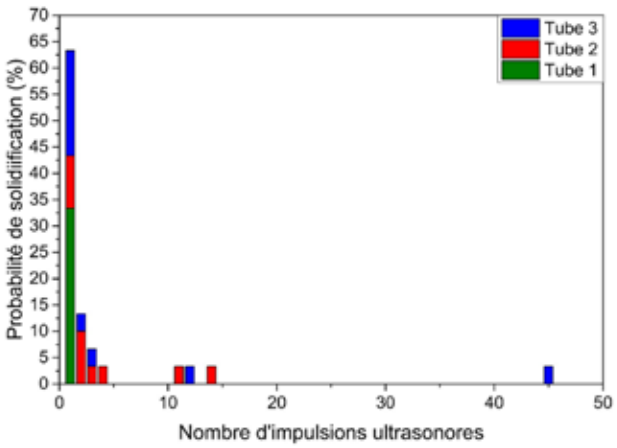

Fig. 1: Opacification under non-intrusive ultrasound triggering of PCM crystallization.

Fig. 2: PCM crystallization probability vs the number of ultrasound periods.

[1] N. Beaupere et al., Thermochimica Acta, vol. 670, (2018) 184-201.

[2] N. Beaupere et. al., 12th IIR Conf. on Phase-Change Materials and Slurries for Refrigeration and Air Conditioning (PCM 2018) Orford (Québec), paper number 0022.

[3] N. Beaupere et al., "Libération de la chaleur stockée dans un matériau à changement de phase surfondu, par cavitation ultrasonore", Congrès Français de Thermique, Nantes, 3-6 Juin 2019

TEAM Noé BEAUPERE, Nicolas DUNOYER, Ulrich SOUPREMANIEN

PARTNERS LGCgE (Lille)

CONTACT ulrich.soupremanien@cea.fr

STABILIZED COPPER NANOWIRE BASED TRANSPARENT ELECTRODES FOR THIN FILM HEATERS

Whereas the integration of silver nanowires as transparent electrode in devices has reached a fair level of maturity, the integration of copper nanowires still remains difficult, mainly due to their intrinsic instability in ambient conditions. Strategies of stabilization by organic and inorganic capping layers have been studied to elaborate stable transparent heaters.

Metallic nanowires are known to be very promising alternatives to non-flexible transparent conductive oxides [1-2]. The optoelectronic device market evolves toward flexible and stretchable products such as rollable displays or flexible solar cells. Metallic nanowires networks offer high level of flexibility while keeping excellent optoelectrical properties. Based on random percolative network, the conductivity is ensured by physical contact between metallic nanowires to form a continuous electrical pathway while transparency is ensured by the hole of the network that let the light to go through the sample. Made of one of the most conductive metals, copper nanowires [3] are intrinsically far less stable than silver based nanowires. In this work, the environmental ageing under different conditions (temperature, humidity, light) of copper nanowires was performed and their degradation in different conditions was monitored, in particular by electrical measurements, transmission electron microscopy, x-ray photoelectron spectrometry and Auger electron spectroscopy. In order to thwart the poor stability in ambient conditions, several routes were evaluated. Encapsulation by organic varnishes, laminated barrier films with optical clear adhesive and inorganic layers by spatial atomic layer deposition were assessed and compared for their potential interest for the fabrication of stable transparent film heaters.

The synthesis of copper nanowires through hydrothermal process led to the production of high aspect ratio Cu nanowires (100 nm in diameter and 33 µm in length). Highly conductive and transparent electrodes based on random networks of copper nanowires exhibiting 33 $\Omega.sq^{-1}$ at 88% of transparency were fabricated through a spray solution process. A fast degradation of the electrical properties was observed in ambient conditions, which is ascribed to the fast oxidation of copper demonstrated by different fine nano-characterization experiments. Appearance of a copper oxide shell around the copper core is presented in Figure 1 and detailed in the reference [3]. It points out the absolute need to stabilize the system by an efficient encapsulation layer to prevent oxidation and consequently failure of the electrical conductive network. Several organic or inorganic protecting coatings as polyurethane, polysiloxane, very thin alumina coating or barrier optically clear adhesives were compared. The best results were obtained thanks to the latter two materials as shown in time-dependent temperature curve and picture of Figure 1. Transparent film heaters made of copper nanowires protected by these materials were successfully produced. Very good performances were measured and the stability and cycling of the devices was greatly improved, with a lifetime exceeding 6 months. □

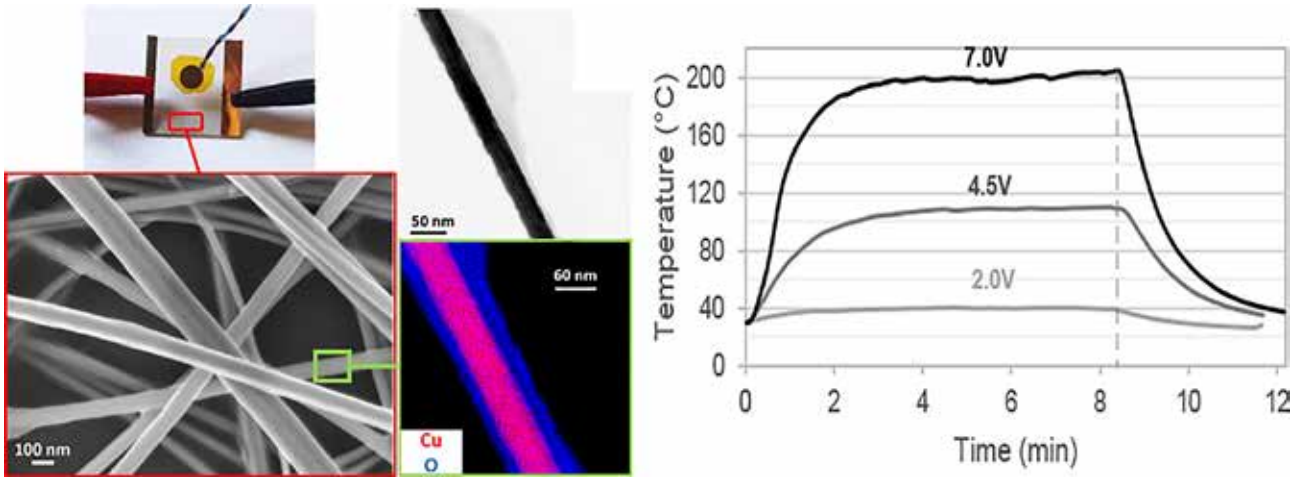

Fig. 1: Optical picture of transparent conductive electrode made up of copper nanowire network with SEM/XEDS magnification of the nanowire network and the oxidized surface of copper nanowire. Time-dependent temperature of transparent heater powered at low voltage (from left to right).

[1] D. Langley et al., Nanotechnology, vol. 24, (2013) 452001.
[2] T. Sannicolo et al., Small (2016) 6052–6075.
[3] C. Celle et al., Nanotechnology, vol. 29, (2018) 085701.

TEAM Antony CABOS, Caroline CELLE, Bruno LAGUITTON, Florence MASSE, Jean-Pierre SIMONATO, Maribel TOURON, Djadidi TOYBOU
PARTNERS LMGP (Grenoble)
CONTACT caroline.celle@cea.fr

PROTOTYPING AND TESTING EMBEDDED TRANSFORMER FOR 100 W - 1 MHZ GAN CONVERTER

High efficient and compact 1 MHz converters requires new magnetic cores for passive components. Soft ferrites, of formula $NiZnFe_2O_4$ with spinel structure, have low intrinsic iron losses at desired frequency (300 mW/cm³ at 1.5 MHz, 25 mT). Those materials have been embedded in a printed circuit board for building compact planar transformers.

The volume of passive components contributes to 40% of the whole volume of a converter. The size reduction of the transformers or inductances is possible thanks to the frequency increase. However, it implies a certain temperature rise of the magnetic core due to iron losses explained by microstructural changes in the material. Gaella Frajer's PhD [1], allowed us to understand those mechanisms generating magnetic losses in $NiZnFe_2O_4$ ferrite material and to optimize it. The establishment of a magnetic measurement tool in collaboration with G2ELab, and the choice of an optimal composition finally led to a material whose performances in terms of losses at 1 MHz, 25 mT are of the order of 350 mW/cm³ against 2200 mW/cm³ for commercial reference material. Based on this material characteristic, and with the help of application specifications coming from CEA-LETI, a prototype of transformer has been developed. The transformer has been characterized electrically to measure inductances at the primary and secondary, thermally to measure the surface heating of the PCB thanks to a set {thermal camera / thermocouple}, by tomography to visualize the presence or absence of cracks after heating of the component.

A transformer has been calculated to be able to transform 325 V into 20 V with targeted iron losses of 1 W. Powder injection molding was studied as well, to process the powder into a functional magnetic core and to take advantage of the possibility to access to complex details or cooling channels. The thermal exchanges of the transformer are optimized thanks to a planar design with a form factor of 25. A planar core, comprising commercial powder, was integrated into a 6 cm³ printed circuit and tested to validate the thermal management proposed above (Fig. 1). This consists of a stack of FR4 resin layers, copper tracks forming the windings of the transformer, and the processed magnetic core lying inside. The temperature measured at the surface is 140 °C at 60 W for this prototype. The tomography analysis showed that the core was not degraded (Fig. 2). A model has been developed to evaluate the thermal balance of the component and to calculate the temperature increase on its surface. This model is consistent with the experimental results. An estimation of the temperature increase at 60 W for a second prototype comprising an optimized material shows that the maximum temperature should not exceed 100 °C. This result brings the power density to about 6 W/cm² for this component that is beyond the state of the art (about 1 W/cm²). □

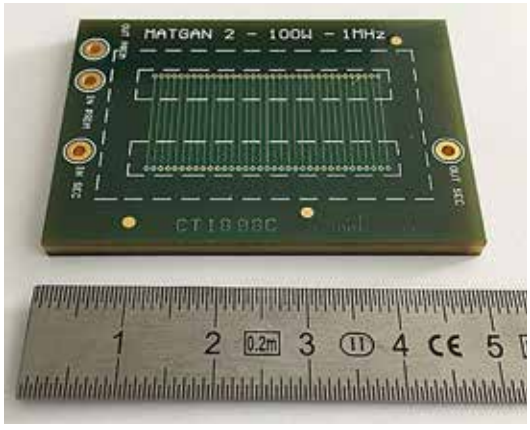

Fig. 1: Prototype of planar transformer integrated in the printed circuit board (50 x 35 x 3.2 mm³). The copper tracks constitute the primary and secondary windings.

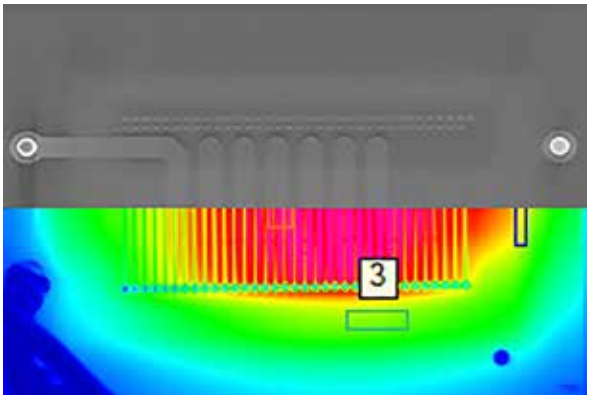

Fig. 2: Truncated tomographic image of secondary and primary revealing the configuration of the coil with respect to the thermal image of the printed circuit

[1] G. Frajer, PhD thesis, Univ. Grenoble Alpes (2018).

TEAM Marc BOHNKE, Céline DELAFOSSE, Gérard DELETTE, Pierre PERICHON, Cyril RADO.
PARTNERS CEA-LETI, G2ELab (Grenoble), CIRETEC
CONTACT marc.bohnke@cea.fr

SYNTHESIS OF HIGH PERFORMANCE SOFT MAGNETIC NiZnCu FERRITE FOR POWER ELECTRONICS COMPONENTS

GaN technology enables miniaturization of power converters but requires low core-loss components for operation at high frequency. Fine grained and multi-substituted (NiZnCu)(CoFe)2O4 ferrite material fulfil this requirement. The sol-gel technique based on the Pechini method is efficient to produce nanometric powder liable to be sintered with a limited grain growth.

High performance magnetic cores were obtained with the formulation $(Ni_{0.31}Zn_{0.49}Cu_{0.20})_{0.979}Co_{0.021}Fe_{1.9-d}O_4$ by the conventional ceramic process and constitute the reference samples [1]. The addition of copper is useful to perform the sintering at lower temperature and the low iron content promotes high resistivity. Ni/Zn ratio and cobalt content are fixed to minimize the magnetic core losses. A high densification rate (> 93% of the theoretical density) combined with a small grain size (< 1-2 µm) are key microstructural parameters for obtaining high performances. Besides the ceramic route, Pechini method has the advantage to produce nanometric powders for targeting further microstructure refinement after sintering. In this process, a gel is formed by evaporation of a solution containing precursors (nitrate metals) mixed firstly with citric acid and then with ethylene. The crystallization of the gel into the ferrite phase occurs during the calcination step, but the kinetics had to be clarified. The structural and magnetic properties were characterized and compared to the ones of the reference ferrite synthesized by classical solid-state reactions. Furthermore, we performed core loss measurements on toroidal samples up to 5 MHz in order to present a complete overview of this alternative synthesis method.

The optimal conditions for the chemical route are fulfilled with a molar ratio of metal cation to citric acid equal to 1:3 combined to a ratio of ethylene glycol to citric acid of 4:1. In-situ X-ray diffraction performed during the gel calcination revealed that the crystallization of the ferrite starts at 380 °C and that the reaction is complete at 550-570 °C. The size of the crystallites reaches then 15 nm. This characteristic allows the densification of the powder to begin around 500-600 °C during the sintering treatment, while a temperature of 800 °C is required for the conventional process. Eventually, the grain size is limited to 1.3 µm in the sample. The hysteresis loop measured at low frequency (Fig.1) on the reference sample is clearly broader compared to the Pechini method. The chemical route leads to a lower coercitvity and a higher induction improving the figure of merit of the soft magnetic material [2]. The Pechini method provides samples with low magnetic core-loss values for frequency values up to 5 MHz (Fig.2). The chemical route constitutes an alternative process that could be still optimized by further research activities involving low temperature sintering techniques. □

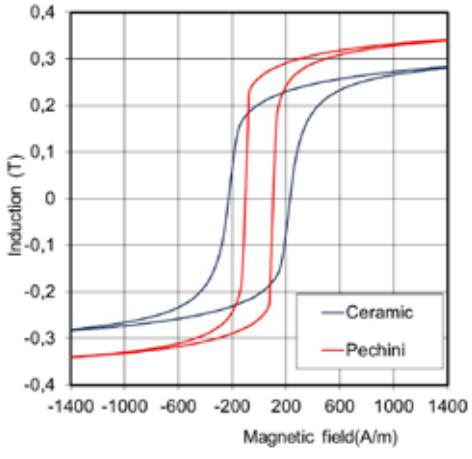

Fig. 1: Hysteresis loops of (NiZnCu) ferrite samples produced by the conventional ceramic process and by the Pechini method. Chemical route provides better properties revealed by a narrower hysteresis loop

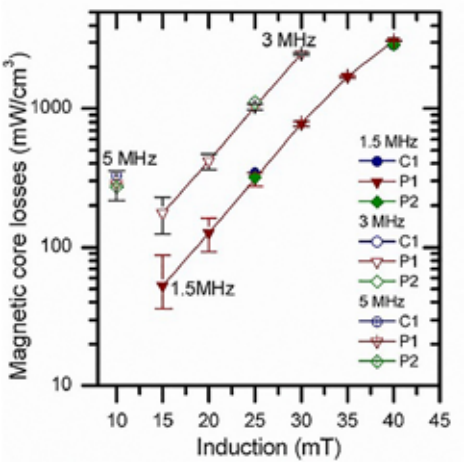

Fig. 2: Magnetic core loss measured on (NiZnCu) ferrite samples produced by the conventional ceramic process (C1) and by the Pechini method (P1, P2).

[1] G. Frajer, PhD thesis, Univ. Grenoble Alpes (2018).
[2] G. Frajer et al., AIP Avdances, vol. 8, (2018) 047801.

TEAM Gérard DELETTE, Gaëlla FRAJER
PARTNERS NEEL Institute, G2Elab (Grenoble)
CONTACT gerard.delette@cea.fr

PRINTED NEAR FIELD COMMUNICATION TAG FOR COLD CHAIN BREAK MONITORING

The domain of connected objects is growing up. Indeed, objects of everyday life are provided with a capacity for data communication. In this field, we develop and test Near Field Communication (NFC) printed tag with embedded temperature sensors [1]. The goal is to demonstrate the potential of screen printing processes in the field of smart food packaging.

We uses large surface printing technologies for the development of NFC tag (13.56 MHz) on paper substrate. It is of great interest to print the antenna, an environmental sensor (here a temperature sensor) and conductive tracks in the same process sequence. The reduction in the number of steps required to produce a tag will thus have a significant impact on the manufacturing cost. To do this, we carried out a demonstrator by screen printing process on Arjowiggins' Powercoat™ paper substrate (Fig. 1). Pick and place of a commercial chip and laser ablation were performed in order to include the component into the substrate and minimize the thickness of the system. We used a carbon-based ink to produce a thermistor connected to the output of the analogue-digital converter of the chip [2]. An estimation of the tag temperature can be made after conversion of the resistance variations recorded by the chip. In this field, a direct temperature-reading interface was developed. The validation was carried out through the comparison of a reference temperature recorded by a thermocouple regarding the temperature recorded by the external printed sensor during a cold chain break simulation (Fig. 2a).

We first measured the resonant frequency and bandwidth of the screen-printed antenna using a spectrum analyser. Q-factor, which characterizes how the LC resonator circuit is tuned with the antenna coil, is about 8.3. It is based on the ratio of the resonant frequency and its 3 dB bandwidth. Using the tag in a cold chain break simulation, we also demonstrated a temperature measurement with a ±1 °C accuracy regarding the reference temperature recorded by a thermocouple (Fig. 2b). This accuracy was established for slow temporal variations of the temperature between 20 °C and 55 °C. When a quick temperature variation occurs, the low thermal diffusivity of the paper induced a time lag between the reference and the measured temperatures. Further experiments performed at lower temperatures showed the same result. Due to the difference in thermal conductivity and diffusivity of the tag itself and the material that served as a reference (a metallic thermocouple), one can conclude that the reference temperature is non-representative of a real cold chain break. Thus, the proposed solution seems to be realistic to monitor products temperature during storage. It has the advantage of being fully integrated into the food package with a minimum additional cost. Following this work, we are involved in the development of multi-sensors smart tags in the INNPAPER H2020 European Project. □

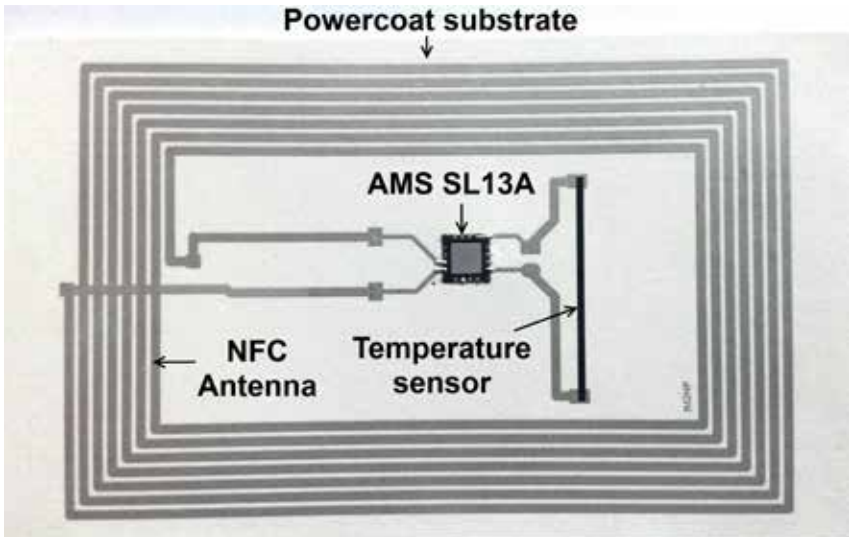

Fig. 1: Printed NFC Tag on PowercoatÔ substrate using AMS SL13A silicon chip.

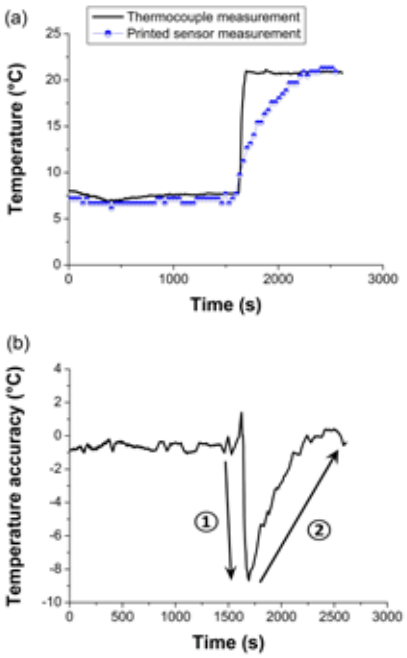

Fig. 2: (a) Monitoring of a cold chain break using the NFC printed tag – (b) Temperature measurement accuracy of the printed sensor regarding the reference temperature recorded by the thermocouple.

[1] A. Pereira et al., Flex. Print. Electron., vol. 3, (2018) 014003.
[2] A. Aliane et al., Microelectonics Journal, vol. 45, (2014) 1621-1626.

TEAM Romain COPPARD, Olivier HAON, Alexandre PEREIRA, Julien ROUTIN, Laurent TOURNON
PARTNERS IM2NP, ARJOWIGGINS CREATIVE paper
CONTACT alexandre.pereira@cea.fr

RENEWABLE ENERGY

EXTENDED PAPER

HIGHLIGHTS

HETEROJUNCTION TECHNOLOGY OF SILICON PV CELLS: FROM MATERIAL TO MODULES

RESEARCH TEAM (from left to right) Olivier BONINO, Renaud VARACHE, Fabien OZANNE, Frederic FASOLA, Joel KINFACK LEOGA, Jordi VEIRMAN, Julie STENDERA, Johann JOURDAN, Van Son NGUYEN, Mathieu TOMASSINI, Ravi VASUDEVAN, Charles ROUX, Wilfried FAVRE, Valentin GIGLIA, Julien HOTEL, Daniel SAPORI, Romain DELCROIX, Martin VANDENBOSSCHE, Julien SUDRE

CONTACT pierre-jean.ribeyron@cea.fr

1. Introduction

The photovoltaic industry is looking for ever higher performances in order to reduce the cost of modules expressed in €/Wp. Indeed, the photovoltaic module plays a key role in the cost of electricity of a photovoltaic plant and the continuous power increase at reduced cost is a strong trend. Thus, this race for increased performance exists both at the R&D and industrial levels, and there are global gains of around 0.2 to 0.5% per year in the crystalline silicon sector. Also, in order to respond to this strong trend, CEA-LITEN has been committed for more than ten years in the development of a new photovoltaic cell technology called silicon heterojunction (SHJ). Indeed, we have selected this technology as a major axis for R&D development because it meets most of the criteria for the emergence of an alternative to the current standard. It has many advantages over competing technologies:

- Record efficiency and module power (internal roadmap towards 25% efficiency, which is the practical limit of silicon);
- A potentially competitive production cost compared to the standard;
- A compatibility with bi-facial architectures close to 100% and a low temperature coefficient, guaranteeing a higher productivity (up to 20% more over certain periods of the year);
- Proven reliability compared to standards: an absence of degradation phenomena such as PID, LID and LETID[1] which reduces the risk of initial degradation in PV power plants.

Since the beginning, the developments focused on increasing cell efficiency to prove the potential of this technology. Later, the main objective was to demonstrate the industrial feasibility and competitiveness with the implementation of the hetero-junction pilot line whose core equipment is able to process up to 2400 wafer/h with yields higher than 23% on average since 2016. In addition, the CEA-LITEN has a roadmap to approach the maximum efficiency of 25% in the coming years. Moreover it is looking to the next generation of cells to exceed this efficiency thanks to the contribution of a semiconductor material complementary to silicon in terms of gap, perovskite being the most interesting candidate, allowing to increase the overall conversion efficiency of the cell beyond 30% in tandem mode. In parallel with these cell-centered developments, it is essential to address the upstream parts of the value chain, such as ingot and silicon wafers, because the heterojunction cell requires the use of n-type silicon combined with excellent characteristics in terms of charge carrier lifetime. In addition, it is also necessary to pursue the developments up to the module because the heterojunction cell requires an original interconnection process, and must be specifically encapsulated within the module to ensure reliability equivalent to or better than mainstream technology (Fig. 1).

Fig. 1: Development of hetero-junction technology across the entire value chain at CEA-LITEN

1/ PID: Potential Induced Degradation; LID: Light Induced Degradation; LETID: Light and Elevated temperature Induced Degradation.

2. Importance of silicon material on high-performance cell technologies

2.1 Czochralski growth and related challenges

The manufacturing process for high-efficiency cells (in particular heterojunction technology) use monocrystalline silicon wafers from Czochralski (Cz) growth technology. In recent years, considerable efforts have been made by ingot and wafer manufacturers to improve the volume quality of the material. The main known sources of defects in Cz ingots that can affect the quality of the material are intrinsic defects (vacancies, interstitials) and defects related to dopants (B, P), metallic impurities (Cu, Fe,...), and oxygen. We focused mainly on reducing the amount of oxygen. The challenges consist in reducing or neutralizing the defects caused by oxygen since the crystallization stage. The oxygen source is the quartz crucible in which the silicon charge is melted. Reducing the amount of oxygen incorporated in the ingot (and therefore the associated defects) requires a detailed understanding of the mechanisms of oxygen diffusion in the silicon melt, the transport within the melt during the process, and the evaporation of oxygen at the free surface. To this end, a complete numerical model of a Cz furnace (Fig. 2) capable of taking into account all these physical phenomena is being developed at CEA-LITEN. The model aims to evaluate the impact of growth parameters, of changes in the furnace thermal configurations (optimized gas evacuation, hot zone geometry, crucible position, cooling jacket...), and of technological developments (Cz, RCz, CCz)[2] on the quantity of oxygen incorporated along the ingot height and width. As part of E. Letty's thesis work [T1], this tool enabled to evaluate the thermal story of the ingot during the drawing process by defining the residence times of the different regions of the ingot in the temperature ranges where oxygen-related defects appear and develop (Fig. 4). An original method has also been proposed to validate the ingot thermal cooling model by comparing experimentally and numerically determined thermal donor (TD) concentrations [1,2].

Fig. 2: Cz furnace model developed under ANSYS Fluent. Thermal modelling of ingot and convection in the Si melt

3. Oxygen, thermal donors and dopants

Not all silicon substrates, although metallic in appearance and shape, are equal in terms of cell yield. Indeed, a silicon wafer cannot be considered as a black box because each wafer, even from the same ingot, does not have the same properties or the same thermal story as its neighbor. But what defines a substrate compatible with a silicon heterojunction cell? Of course, the answer is intimately linked to the point of view. For a buyer, for example, a good substrate is a low-cost substrate that can be delivered quickly and in quantity. For a high power module integrator, a good substrate will have a square shape to maximize the spatial filling of the cells in the photovoltaic panel. Let us now focus on the intrinsic quality of the n-type silicon material itself, which governs the conversion efficiency of the device. What is expected from a substrate is that the photo-generated carriers by the photovoltaic effect can accumulate in significant concentration, before reaching the front and rear surfaces of the cell, in order to increase the voltage and current respectively at the terminals of the photovoltaic device. As shown in Figure 4, the prerequisites for optimally fulfilling the two functions mentioned above are to have (1) a long lifetime (LT) of photo-generated carriers - i.e. a long duration between photo-generation and recombination loss on a defect -, associated with (2) a rather low substrate resistivity (typically 1 Ω.cm).

2/ RCz: Recharged Czochralski ; CCz: Continuous Czochralski

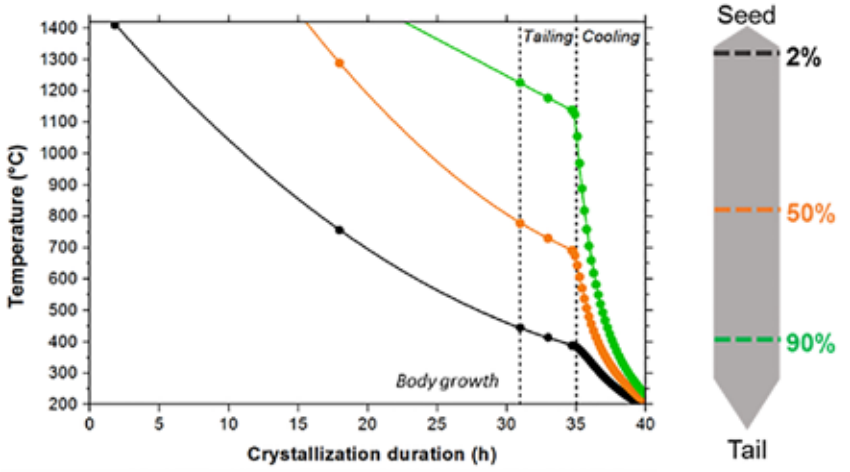

Fig. 3: Example of thermal stories obtained by simulation for different solidified fractions (2, 50 and 90 %). The different stages of the drawing are indicated: growth of the body, the final tip, and cooling of the ingot.

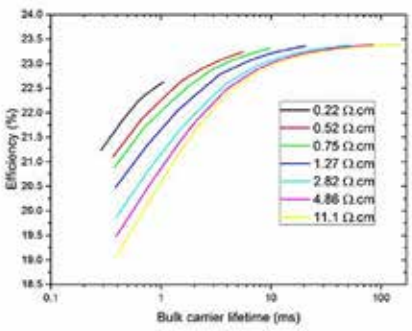

Fig. 4: Prediction of the variation of the conversion efficiency as a function of the volume lifetime for several substrate resistivity values [P1].

While resistivity can be adjusted relatively easily when pulling the ingot, LT is a more complex parameter to control and improve. Indeed, many defects may scatter the silicon lattice, such as impurities introduced during the pulling or manufacturing of the cell (O, Fe, Cu…), or crystalline defects (dislocations). While some defects are harmless to LT (e. g. O in the interstitial position), others are on the contrary virulent and their presence should therefore be limited such as thermal donors (TDs). We have focused intense research efforts both on understanding the effects of TDs on the properties of substrates/cells and on evaluating options for their measurement/removal.

In the literature, it is commonly accepted that DTs are aggregates of oxygen atoms that are formed during ingot cooling/cell process in the 350-600 °C range and whose formation kinetics are very strongly dependent on the oxygen content of the material. We began their study in 2008, through the PhD research work of J. Veirman [T2], in partnership with the INL and co-financed by the CEA and ADEME. This work has led to the development of a patented technique for quick, easy and reliable measurement of oxygen and DT contents on as-cut substrates [3]. This technique was then industrialized with the partner AET Technologies, which marketed the equipment called OxyMap®. The technique has been the subject of about fifteen scientific communications [4], and is regularly used in CEA projects/publications (with academics such as the Norwegian university NMBU [5] or industrial partners such as the equipment manufacturer Semilab [6] or the substrate manufacturer Norsun [7]).

In parallel with the industrial transfer to AET Technologies, we specified the recombination properties of the DTs. The cross section and the position of the energy levels introduced in the band gap were determined. Also the maximum allowable content, beyond which DT affects the conversion efficiency, has been specified. Since this defect may be present in concentrations significantly over this threshold value, it has become imperative to develop techniques to quantify them on substrates at the beginning of a cell manufacturing line. In this context, three patents have been filed, which make it possible to detect and quantify the presence of DT in as-cut substrates based on photoluminescence measurements [8-10].

It is important to note here that the prerequisites mentioned above do not necessarily concern the substrates as received from the supplier, but they should be met when the cell is under outdoor operation. This let us carry out a specific research effort in order to study/strengthen the stability of the substrate properties under illumination. Such work was initiated through E. Letty's thesis [T1], in collaboration with INL and funded by INES2 program[3]. A major result of this study was the demonstration of an LT reduction under illumination in n-type substrates from different sources [11]. This result was particularly striking in that until then, only boron-doped p-type substrates seemed to be affected by such instabilities. Although the mechanism(s) behind this discovery remain to be determined, this work has made it possible to support the involvement of DTs in the observed degradation, possibly in interaction with silicon self-interstitials [12].

Since DTs are harmful to the carriers lifetime and its stability under illumination, we have also patented techniques to limit/suppress their influence [13] or, on the contrary, to take advantage of them when present at concentrations below the threshold value of 5 10^{14} cm^{-3} [14-15], for example to produce an ingot of constant longitudinal resistivity.

3. Challenges of conversion efficiency improvement in heterojunction cell technology

The breakthrough of heterojunction technology in the PV market is conditioned by its ability to provide conversion efficiencies that cannot be achieved by other technologies, and by stable and robust production (equipment, processes). The processes implemented at the various technological steps have improved dramatically in recent years (preparation of textured and ultra-clean surfaces, deposition of amorphous silicon layer, etc.). To continue to increase yields, it is now essential to focus on persistent defects largely related to the production equipment (defect, plate edges) while pursuing intensive research on improving the materials used, particularly for transparent conductive oxides.

3.1. Defectivity

As it enters its mass production phase, the hetero-junction cell must see its production rate increase, typically beyond 3000 cells per hour and per production line. This implies having silicon wafer transport systems with increasingly high throughputs. By increasing the transport speed of the wafers, they are subject to damage due to contact with the transport elements (trays, belts, vacuum grippers, centering devices, etc.). All these degradations, commonly referred to as defects, are revealed by a spatially resolved photoluminescence (PL) measurement. On a PL map such as Figure 5, the dark areas show areas where the surface passivation is degraded, resulting in a locally lower efficiency of the device.

As part of a post-doctoral fellowship in 2013 and an internship in 2018, we have implemented an image processing method and an appropriate software to analyze these PL images and link defect metrics to cell performance [17]. From Figure 6, it is evident that the level of defect, quantified as the average of local defects over the total cell surface, is directly related to the fill factor FF. In the example given here, the average conversion efficiency of the 10 best cells is 0.6 % higher than the efficiency of the ten most defective cells (+2 % on the FF). Extrapolation to a near-zero level of defect makes it possible to quantify a potential yield gain at around +1 % absolute (provided, of course, that no other factor limits the cell's performance).

The means implemented to limit the defects include process optimization (surface preparation in particular), design and fine adjustment of automation (transport speed, coordination, etc.) as well as environmental control in terms of particles. In parallel, we recently initiated a research work in collaboration with the Lyon Institute of Nanotechnologies on understanding the inhomogeneity influence on hetero-junction cells via 2D simulations and a comparison with typical experimental cases.

3.2. Wafer edges impact

With the increase in silicon wafer sizes (125x125 mm, then 156x156 mm, still increasing), the edges-to-surface ratio is increasingly favorable to the area where the structural properties can be macroscopically considered as uniform (layer thickness, crystal orientation, etc). At the same time, the performances improvement of the devices makes them increasingly sensitive to inhomogeneity. At the wafer edges, several phenomena occur:

- Emergence of texturing singularities: the change of crystalline plane at the level of the chamfers (pseudo-square wafers) disturb texturing and new ridges appear,

3/ INES2 program grant n°ANR-10-ITE-0003

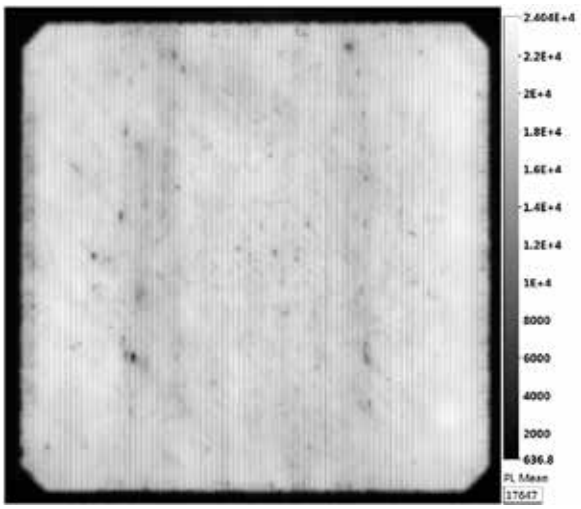

Fig. 5: Typical photoluminescence image on a completed cell.

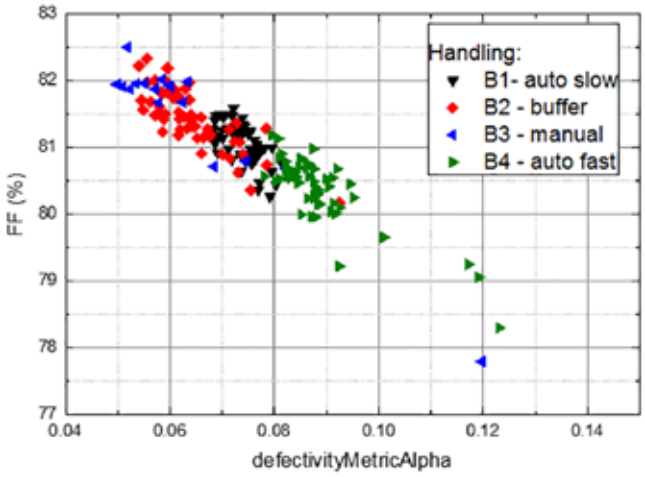

Fig. 6: Conversion efficiency as a function of the overall defect metric on the cell, for different production modes.

which are areas not very favorable to an optimal passivation.

- Degraded passivation: the wafer edges are areas where the deposition of amorphous silicon layers is potentially of lower quality than on the light-receiving surfaces. Photo-generated charges near the edges therefore have an increased probability of rapidly recombining because one more surface is accessible to them, including one potentially of lower quality. This passivation drop at the edge of the wafer is illustrated in Figure 7.
- Transparent conductive oxide (TCO) deposition not extended up to the edge of the wafer to avoid any short circuit ("shunt" of the p/n junction) between the front and rear face of the cell: this absence of TCO alters the optical properties at the edge (no anti-reflective effect) as well as the collection of charges.

A device for detecting carriers' recombination at the wafer edges using photoluminescence has been developed (patent pending) based on a non-zero signal outside the wafer, to keep sufficient resolution at the cell edges. A more elaborate version is under construction and will allow to study finely the losses due to the degraded passivation on the edges of the wafers. Once correctly characterized, the wafer edges can be treated specifically at the as-cut wafer level (chamfers on the edges) or at the process level (specific chemical preparation, dedicated passivation...).

3.3. Transparent conductive oxydes (TCO)

TCO plays a key role in the hetero-junction structure: photo-generated carriers must pass through the TCOs since the amorphous silicon layers are too thin and not enough-conductive for lateral transport. The TCO currently mainly used is indium-tin oxide (ITO) deposited by sputtering (PVD - Physical Vapor Deposition). At present, this deposition technique considerably restricts the field of potentially usable materials and results in passivation degradation due to the ion and electron bombardment during deposition [18].

Other deposition methods address these two drawbacks, including RPD (Remote Plasma Deposition). We are actively working on these new techniques and materials in collaboration with other institutes, with the aim of integrating better optical and electrical quality materials into the devices, as well as reducing damage to the passivation layers. Thus, within the framework of the European AMPERE project, we have integrated indium-tungsten oxides (IWO) into cells at our pilot line. The first results are promising in the sense that IWO gives more favorable optoelectronic properties than ITO for heterojunction cells.

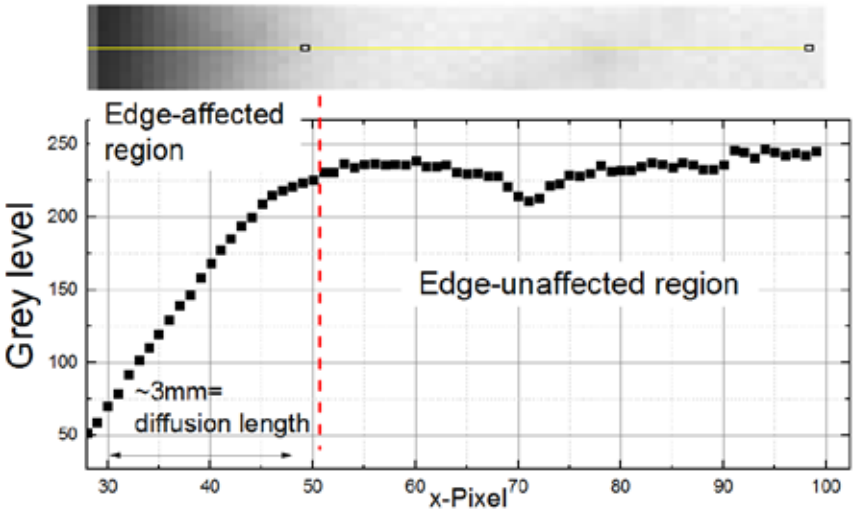

Fig. 7: PL signal profile at the edge of the wafer: the signal drops to the edge of the cell, a sign of loss of passivation.



3.4. Champion industrial solar cells

In parallel, champion industrial phototovoltaic cells were processed, incorporating all the scientific advances presented above. Record yields were thus obtained on industrial-sized cells (Fig. 8). These results place CEA-Liten among the world leaders in this technology.

4. Module integration and its specific constraints

The manufacture of modules based on heterojunction cells requires adaptations of the processes used for homojunction cells. The two main differences are due to:

- The serial connection of several cells or interconnection (usually 12 cells are connected in series) by a low temperature process,
- The use of encapsulation materials allowing better reliability and durability.

4.1. The different interconnection modes and their respective challenges

New processes, different from conventional welding, must be used to connect heterojunction cell because of their sensitivity to high temperature processes (>200°C), and the limited adhesion with the copper ribbon if un-sintered low temperature silver paste are used for metallization. Therefore, we are studying different approaches:

- SmartWire Connection Technology (SWCT), developed by the equipment manufacturer Meyer Burger (MB), which uses wires glued on a transparent polymer to facilitate their placement on the cells. The electrical contact between the wire and the metallization finger is made during the lamination step at a temperature of 150-160 °C.
- The use of conductive adhesives (ECA) to interconnect ribbons and cells. These conductive adhesives can be applied to the cells by different processes, such as screen printing or dispensing.

These low temperatures (<180°C) processes limits residual thermomechanical stress and increases reliability in thermal cycling. Another advantage of these two processes is that they do not require the use of ribbons or wires containing lead (eco-toxic) or indium (rare). We have performed repeated thermal cycling tests [P2]. One of the objectives is to reduce the amount of glue applied in order to gain competitiveness while maintaining reliability.

Using these two approaches, we made different high-power modules, including a record 412W module. -Equivalent results were obtained in bus interconnection with a 72-cells module with a power greater than 420W (BiFi10 measurements - IEC60904). Finally, a half-cell module was made thanks to the new Meyer Burger equipment. Conventional soldering also remains a possible way for heterojunction provided that specific screen printing pastes are used, specific metallization is carried out and/or ribbons are used with low melting temperature alloys but cost effectiveness is not yet achieved.

5. Encapsulation and reliability

The encapsulation of the module must make it possible to protect the previously assembled cell skeleton from the external environment (humidity, UV, rain/hail...), while guaranteeing the adhesion of the sandwich of the various elements composing the module. A qualification and evaluation process for the different materials (encapsulants, backsheet, foil, ECA) has been set up to meet the challenge of module reliability. It is based on various material studies (by DSC, DMA, spectro-photometry) as well as tests in mini-modules or real modules. The aim of this method is to develop and innovate in the choice of the materials in order to meet the constraints of performance, reliability and competitiveness. It allow to design specific modules adapted to more demanding environments, such as the Atacama Desert in Chile (UV, fouling, high thermal constraints). We have obtained reliability results at twice the standard of heterojunction modules, via tests of thermal cycling (CT), wet heat (DH), freezing humidity (HF) or ultraviolet (UV).

These studies made it possible to obtain internal certification for modules of 60 cells by identifying a reference encapsulant, which effectively protects hetero-junction cells from moisture (DH test - loss <2% after 3 times the standard). They also allow us to support our industrial partners for their certification.

6. Conclusion

We have reviewed the scientific developments implemented at CEA-Liten to increase the performance of heterojunction cells among the highest level in the world. We demonstrate that the development of this technology not only requires continuous R&D efforts in the field of cells but also requires specific development along the entire value chain, from material to module. This expertise also allows us to look to the future with a clear vision of the steps needed to continue to improve performance, while ensuring that performance can be maintained at the module level. Indeed, reliability remains an essential step in the maturation of a new technology, particularly for photovoltaics. □

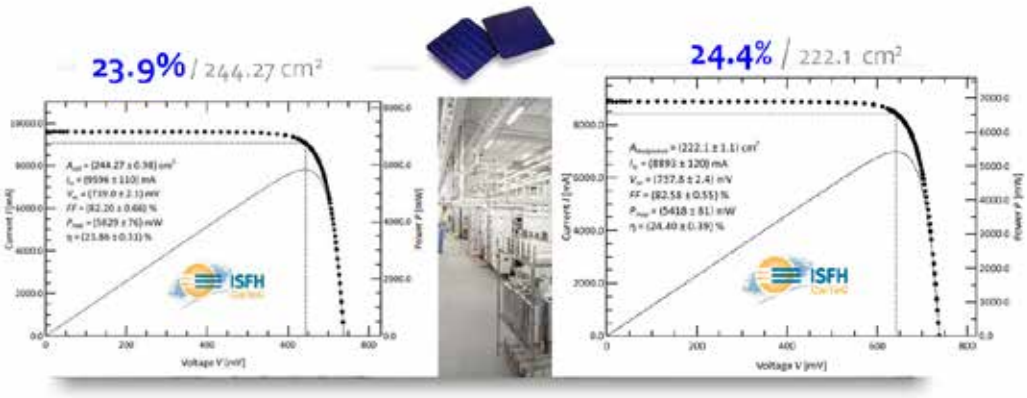

Fig. 8: Certified record cell yields reaching 23.9% and 24.4% conversion efficiency respectively.

Publications / Patents

[1] J. Veirman et al., "Novel way to assess the validity of Czochralski growth simulations", submitted to Phys. Status Solidi A (2019).

[2] M. Albaric et al., "Combined experimental and numerical investigation of Cz growth conditions on thermal donors generation", oral communication, EU PVSEC, (2019).

[3] J. Veirman, S. Dubois and N. Enjalbert, "Procédé de cartographie de la concentration en oxygène", Patent application: FR1003510, 2010.

[4] see J. Veirman et al., "Oxygen-defect characterization for improving R&D relevance and Cz-Si solar cell efficiency", 23 Photovoltaics Int., (2016) 33 and included references.

[5] T. Mehl et al., "Oxygen-related defects in n-type Czochralski silicon wafers studied by hyperspectral photoluminescence imaging", Energy Procedia, vol. 124 (2017) 107–112.

[6] F. Korsos et al., "Efficiency limiting crystal defects in monocrystalline silicon and their characterization in production", Solar Energy Materials and Solar Cells, vol. 186 (2018) 217–226.

[7] M. Tomassini et al., "Recombination activity associated with thermal donor generation in monocrystalline silicon and effect on the conversion efficiency of heterojunction solar cells", J. of Appl. Phys., vol. 119 (2016) 084508.

[8] E. Letty, W. Favre, J. Veirman, T. Mehl, E. Olsen, I. Burud and L. Kvalbein, "Method for determining the thermal donor concentration of a semiconductor sample", Patent application: EP18306196.9, 2018

[9] E. Letty, J. Veirman and W. Favre, "Procédé de tri de plaquettes en silicium en fonction de la variation du dopage net", Patent application: FR1658365, 2016

[10] E. Letty et al., "Bulk defect formation under light soaking in seed-end n-type Czochralski silicon wafers – Effect on silicon heterojunction solar cells", Solar Energy Materials & Solar Cells, vol. 166 (2017) 147–156.

[11] W. Favre et al., "On the nature and recombination properties of the defect responsible for the carrier-induced lifetime degradation in uncompensated n-type Cz silicon", MRS, Boston (2018), oral presentation.

[12] S. Dubois, B. Martel, J. Veirman, A. Danel and J.-P. Garandet, "Procédé de fabrication d'un lingot de silicium monocristallin de type n à concentration en donneurs thermiques à base d'oxygène contrôlée", Patent application: FR1460855, 2014

[13] J. Veirman, M. Tomassini, S. Dubois, J. Stadler and M. Albaric, "Procédé pour ajuster la résistivité d'un lingot semi-conducteur lors de sa fabrication", Patent application: FR1562311, 2015

[14] J. Veirman, J. Stadler and M. Albaric, "Procédé de fabrication d'un lingot en matériau semi-conducteur enrichi en oxygène et four de cristallisation", Patent application:FR1562313, 2015

[15] J. Veirman, S. Dubois and N. Enjalbert, "Procédé de formation d'un lingot en silicium de résistivité uniforme", Patent application: FR1202826, 2012.

[16] O. Nos et al., "Quality control method based on photoluminescence imaging for the performance prediction of c-Si/a-Si:H heterojunction solar cells in industrial production lines", Sol. Energy Mater. Sol. Cells, vol. 144 (2016) 210–220.

[17] W. Favre et al., "Influence of the transparent conductive oxide layer deposition step on electrical properties of silicon heterojunction solar cells", Appl. Phys. Lett., vol. 102 (2013) 181118.

Thesis defended

[T1] E. Letty, "Identification and neutralization of lifetime-limiting defects in Czochralski silicon for high efficiency photovoltaic applications", PhD thesis, Grenoble, 2017.

[T2] J. Veirmann, "Effects of doping compensation on the electrical properties of silicon and on the photovoltaic performance of solar silicon cells purified by metallurgical means", PhD thesis, Grenoble, 2011.

Projects

[P1] CHIC project, bilateral partnership CEA-Meyer Burger).

[P2] GOPV project, H2020



INFLUENCE OF CRYSTALLOGRAPHIC DEFECTS ON OXYGEN-RELATED THERMAL DONORS FORMATION KINETICS

Thermal donors are oxygen-related defects that can affect the bulk quality of silicon wafers. They form less effectively in multicrystalline than in Czochralski monocrystalline silicon. Carbon and extended crystallographic defects are candidates that can account for this feature. Using a carbon-lean Czochralski-grown multicrystalline ingot, we demonstrate that thermal donors formation kinetics are not affected by crystallographic defects.

The thermal donors (TD) formation kinetics at 450 °C in standard Czochralski-grown monocrystalline silicon (Cz-Si) can be well described from the interstitial oxygen content ([Oi]) with linear semi empirical models [2]. Although TD have been mostly investigated in Cz-Si, a few studies also report on their observation in multicrystalline silicon (mc-Si) obtained from directional solidification (DS) processes. Nevertheless their formation usually proceeds markedly slower than predicted in Cz-Si counterparts with the same [Oi]. This is evidence that other factors, not relevant in Cz-Si, inhibit the formation of TD in such materials. In this respect, substitutional carbon (Cs) in high concentrations ([Cs] > 10^{17} at.cm^{-3}) is known to hinder TD formation presumably owing to Cs-Oi interactions. On the other hand, high dislocation densities (typically 10^3 to almost 10^7 cm^{-2}) and/or grains boundaries in mc-Si could potentially interact with individual Oi chains and thus modify the TD formation. Discriminating the effect of extended defects from that of Cs is tricky, as they are simultaneously present in large amounts in mc-Si. To circumvent this constraint, the formation of TD has been investigated in a Cs-lean Czochralski-grown ingot that featured a multicrystalline fraction, following an instability during growth.

For this study we used a 90 kg (100)-oriented 9" Cz-Si ingot grown at CEA-INES. After 315 mm of pulling, a growth instability occurred and resulted in the crystal being increasingly multicrystalline therefrom. A sample was taken in the fully multicrystalline region with [Cs]=1.3×10^{16} at. cm^{-3} (< 10^{17} at.cm^{-3} threshold) as measured by FTIR. The [TD] evolution was monitored using 4-points probe resistivity measurement performed after successive 450 °C annealing steps. A comparable distribution is obtained with the expected [TD] evolutions computed using the Cz-Si Wijaranakula's semi-empirical model (Fig. 1). An Electron BackScatter Diffraction (EBSD) analysis was used to reveal the grain orientations in the multicrystalline area of the sample. It showed the presence of significantly disoriented grains. Additionally Wright solution was used to reveal surface-intersecting dislocations (Fig. 2). The presence of twin boundaries, the large number of orientation present suggest the presence of a wide variety of grain boundary configuration with similar properties in terms of crystal defects to DS material. Our findings revealed that extended defects in standard multicrystalline silicon wafers are unlikely to affect thermal donor formation. Additional investigations on point defects such as carbon could explain the donor generation slowdown observed in these materials. □

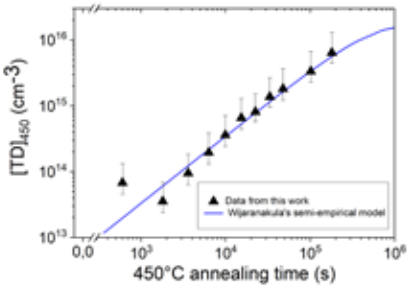

Fig. 1: Experimental and calculated evolution of the thermal donors concentration for multicrystalline sample.

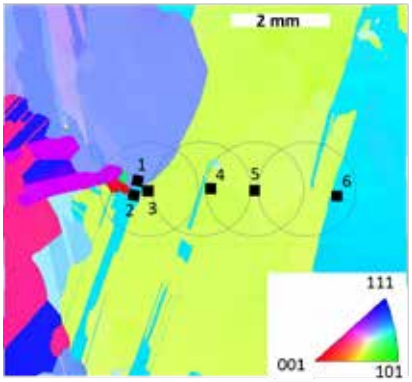

Fig. 2: a) EBSD image showing the different grain orientation in the area of interest. The positions of the 4 probes of the resistivity setup used to study the thermal donor formation kinetics are located within the depicted circles. The black squares represent the areas where dislocations counting was performed.

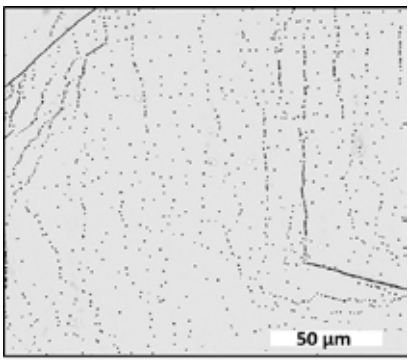

Fig. 2: b) Example of dislocations revealed with Wright solution.

[1] R. Bounab *et al.*, J. of Crystal Growth, vol. 510, (2019) 23-27.
[2] M. Tomassini *et al.*, J. Appl. Phys., vol. 119, (2016) 084508.

TEAM Mickael ALBARIC, Remzi BOUNAB, Jordi VEIRMAN
CONTACT mickael.albaric@cea.fr

EARLY INDUSTRY-COMPATIBLE CHARACTERIZATION OF DEFECTS IN MONOCRYSTALLINE SILICON FOR SOLAR CELLS

We investigated the suitability of innovative industry-compatible characterization techniques developed by CEA and by our long-term partner Semilab to detect already at the wafer/brick level, the early stage of defect formation, which subsequently become harmful during cell processing. We demonstrate that the investigated characterization techniques allow for a relevant selection of the silicon material.

The first step was to source a full ingot that is comparable to nowadays industrial crystals. For this purpose, we pulled a 8" diameter 1 m long crystal, and then subsequently chopped it up into bricks and wafers, following a comparable scheme to what is custom in industry. The capacity to crystallize internally this ingot allowed for the exact knowledge of all wafer positions in the parent ingot, which is in practice not possible in commercial ingots. Subsequently, the ingot was thoroughly characterized at the brick/wafer level using different characterization techniques, such as PhotoConductance Decay techniques (PCD) or Light Scattering Tomography (LST) (Semilab), as well as OxyMap [1]. High temperature n-PERT (Passivated Emitter Rear Totally diffused) solar cells were in parallel fabricated and characterized on the CEA research cell-manufacturing platform. The analysis of the results was carried out collectively with Semilab. This study has benefited from the internal expertise on the material/cell interplay developed for both homojunction and heterojunction silicon cell technologies.

The results evidenced that the LST technique is capable of detecting the presence of the main harmful defects for the solar cell efficiency in very early phase of the cell processing. Significant defect density (Bulk Micro Defects - BMD) was detected in test samples from the part of the ingot that later led to degraded cell efficiency. Despite the increase of BMD size/harmfulness in the course of the solar cell manufacturing, the defect quantities already detected in the as-grown material provide a clear evaluation of the monocrystalline silicon material. Our findings also revealed a very good correlation between the solar cell efficiency and the OxyMap outputs, that is to say the wafer oxygen content, as well as the Thermal History Index, which is a metric to quantify the cool-down speed of the ingot after crystallization (Fig. 1). OxyMap measurements being conducted on as-cut wafers or even on bricks, we demonstrated its potential to be very helpful in the early detection of any silicon material bound to result into poor efficiency cells [2]. □

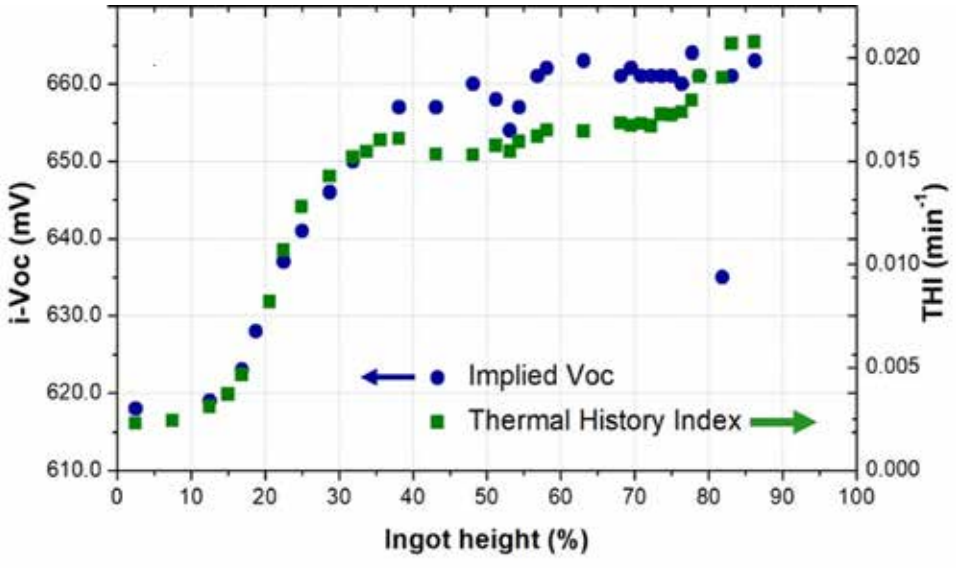

Fig. 1: Remarkable correlation between OxyMap output (THI) obtained on as-cut wafer, and characterization at the cell precursor level (implied open-circuit voltage Voc), demonstrating the possibility of an early prediction of the material quality for solar cells.

[1] Veirman et al., Photovolt. Int., vol. 33, (2016).
[2] F. Korsós et al., Sol. En. Mat. and Sol. Cells, vol. 186 (2018) 217-226.

TEAM Mickael ALBARIC, Karim DERBOUZ, Sebastien DUBOIS, Jordi VEIRMAN
PARTNERS SEMILAB, AET Solar Tech
CONTACT jordi.veirman@cea.fr

POLYCRYSTALLINE SILICON ON OXIDE PASSIVATED CONTACTS FOR HIGH EFFICIENCY SOLAR CELLS

Passivating the contacts of silicon solar cells with a poly-crystalline silicon (poly-silicon) layer on top of a thin silicon oxide is currently sparking interest for reducing carrier recombination at the metal/substrate interface. Blister-free boron-doped poly-silicon on oxide contacts were successfully fabricated, featuring high conductivity and surface passivation properties.

Passivated contacts made of poly-silicon layers deposited on thin silicon oxide films offer an interesting approach to decrease the carrier recombination at the metal/substrate interface and therefore to increase the photovoltaic conversion efficiency. Poly-silicon layers can be obtained by Plasma Enhanced Chemical Vapour Deposition (PECVD) of hydrogenated amorphous silicon layers (a-Si:H) followed by annealing steps. However, this approach can induce blistering of the layer due to its high hydrogen (H) content. This blistering causes a severe degradation of the passivated contact properties. To solve this issue we focused on the optimization of the a-Si:H deposition temperature and gas ratio. Then, the conductivity and the surface passivation level were improved by adapting the annealing temperature. Eventually, a post-process hydrogenation step based on the deposition of hydrogen-rich silicon nitride layers was conducted to cure dangling bonds at the interface and further improve the surface passivation.

By increasing the a-Si:H deposition temperature (from 220 °C to 300°C) and the H_2/SiH_4 gas flow ratio (from 25 to 65), the H content in the film was reduced. This enabled to obtain blister-free poly-silicon (Fig.1) on oxide structures [1]. By decreasing the density of blisters, both the poly-silicon conductivity and the surface passivation level were increased. Furthermore, this reduction of blisters improved the stability of the electric properties of the structure. The subsequent optimization of the temperature of the post-deposition annealing step allowed to find a good trade-off between the field effect passivation developed by the highly doped poly-silicon layer (rather enhanced by high temperature) and the preservation of the oxide quality (high temperature can alter the oxide integrity, particularly via the formation of pinholes). The passivation level was further improved by adding the post-process hydrogenation step [2]. A mean open-circuit voltage potential (i-Voc) of 714 mV was obtained (Fig.2) with chemically polished large area wafers (156x156 mm^2). Recently the whole process was applied on higher quality wafers leading to a maximum i-Voc of 734 mV, performance among the best values obtained so far with such structures. Thus, the structure is ready for future integrations in high efficiency solar cells. □

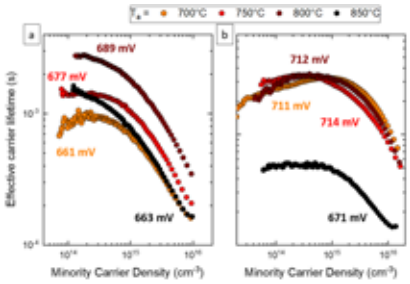

Fig. 2: Effective carrier lifetime versus the minority carrier density measured after the post-deposition annealing step, conducted at various temperatures (T_a) right after annealing (a) and after the hydrogenation treatment (b). The corresponding i-V_{oc} values are presented.

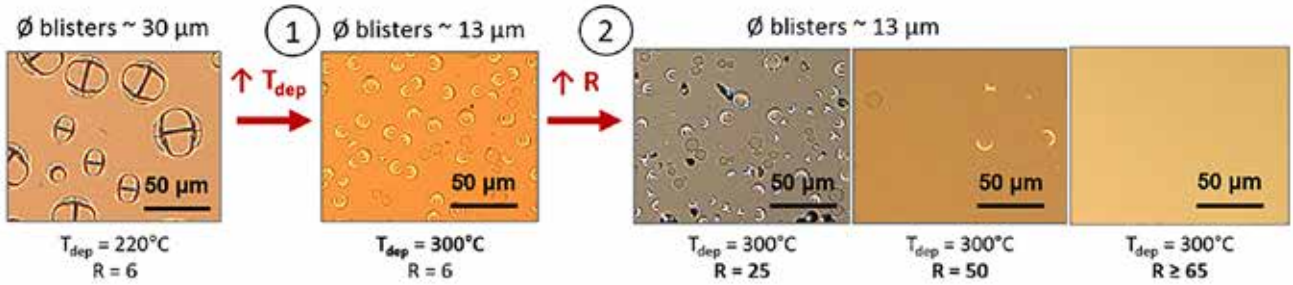

Fig. 1: Optical microscope images (×20) of poly-silicon (B-doped) layers after annealing at 700 °C. The deposition conditions were optimized to reduce the blistering: 1/ Increase of the deposition temperature T_{dep}, 2/ Increase of the gas flow ratio R=H_2/SiH_4.

[1] A. Morisset et al., AIP Conference Proceedings, vol. 1999, (2018) 040017.
[2] A. Morisset et al., Physica Status Solidi A, vol. 216, (2019) 1800603.

TEAM Raphaël CABAL, Sébastien DUBOIS, Bernadette GRANGE, Audrey MORISSET
PARTNERS IPVF, GeePs (Gif sur Yvette)
CONTACT sebastien.dubois@cea.fr

HIGH EFFICIENCY OF PEROVSKITE PHOTOVOLTAIC DEVICES TOWARDS TANDEM ARCHITECTURES

In the context of photovoltaic technologies, the question of cost remains central. The current strategy to stay competitive is to increase the efficiency of the cells. To this end, we work to combine silicon heterojunction cells (SHJ) and perovskite (PK) ones to obtain tandem device with the target of highly efficient conversion up to 30 %.

Perovskite Solar Cells (Fig. 1) have recently emerged as one of today's most promising upcoming photovoltaic technology. Yet, a number of challenges are still to be met to ensure a bright industrial future for tandem architecture. Significantly improving device active area while maintaining similar initial power conversion efficiency and over time is probably one the most important. The main focus of this work is to provide new industrialisable processing routes towards the elaboration of highly efficient large area PK device. In parallel the relevance of this work mainly lies in the selection of the best materials and architectures that led to the highest stability under temperature and illumination for large area device.

The developments performed at lab-scale combining spin coating process and laser structuration allowed us to obtain PK modules on 50x50 mm² substrates with efficiencies up to 17 % (Fig. 2) with little loss in comparison to performance obtained on mm² cells (best performance reached 18 %). This result is actually among the best international records for this device area. In parallel, industrial coating process is developed in replacement of the spin coating one in order to be able to transfer the technology on larger area at industrial scale. Slot-die coating combined to nitrogen gas quenching was selected and validated, as a first step on small area device, with photovoltaic efficiency >16 % [1]. Homogeneity of the thickness has to be further controlled to elaborate device up to 150x150 mm². Moreover, first stability results were also obtained under continuous illumination (AM1.5G, 1000 W/m²) with limited losses (<10 %) after 1200 hours. These results were obtained by optimizing interfacial layers in combination with the tuning of the chemical composition of the perovskite active layer. The perspective is now the integration of this perovskite junction onto a heterojunction silicon cell in order to develop new generation of silicon-based tandem PV cells with increased efficiencies. □

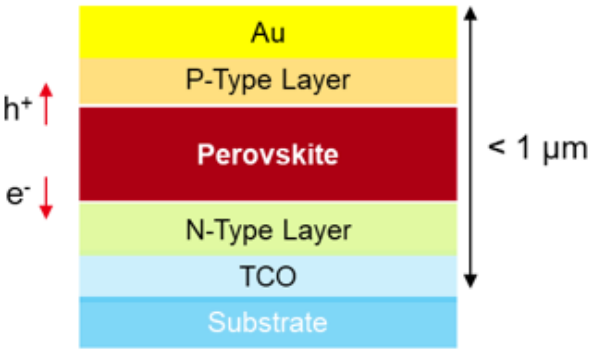

Fig. 1: Typical architecture of Perovskite photovoltaic cell

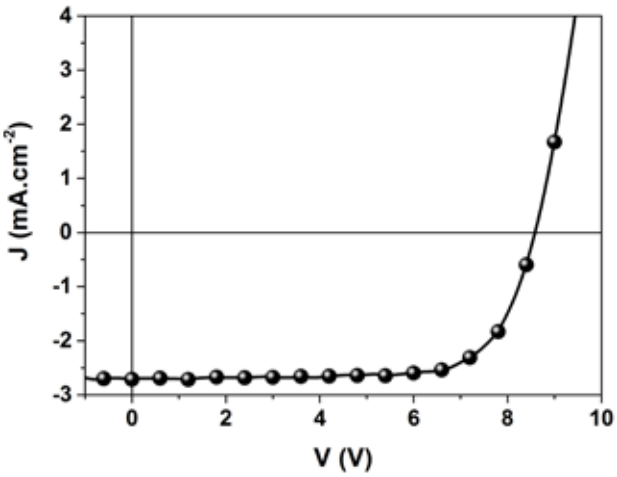

Fig. 2: J-V curve of best Perovskite module

[1] M. Fievez et al., to be published 2019.

TEAM Florence ARDIACA, Solenn BERSON, Stéphane CROS, Mathilde FIEVEZ, Matthieu MANCEAU, Carine ROUX
PARTNERS NTU Singapour
CONTACT matthieu.manceau@cea.fr; solenn.berson@cea.fr

THE MICRO-SCALING OF CONCENTRATOR PHOTOVOLTAIC MODULES IMPROVES THE EFFICIENCY

The actual trend of Concentrator PhotoVoltaic (CPV) development is going into micro-scaled CPV modules to optimize the balance between cost and efficiency. Based on a complete analysis of the Cell-To-Module (CTM) loss chain in micro-CPV, this work proves that the micro scaling of CPV modules improves their efficiency.

Photovoltaic cells have seen an important increase in efficiency (> 38.8 %) with the emergence of III-V multi-junction solar cells (MJSC). Since solar cell efficiency increases logarithmically with the light intensity, the CPV technology is based on focusing light onto a receiver composed of the MJSC, eventually covered by a secondary optic with a heat sink on the backside of the module. The module efficiency is up to 46 %. The Cell-to-Module ratio, which is the fraction of the module efficiency with respect to the cell efficiency at the concentration, is in within the range 65 % to 75 % for the commercial CPV modules. Today, the current trend in CPV technology is to create compact modules with simplified manufacturing processes. This trend inspired by micro and nanotechnology integration implies a decrease in focal length and cell size to conserve a high concentration ratio. Consequently, it reduces material consumption, and, by reducing area of light collection per solar cell, heat spreader becomes no longer necessary. Therefore, miniaturisation of CPV modules is interesting both economically and technically. The aim of this study is the impact evaluation, in addition, the impact of the miniaturisation on the CTM ratio of the micro-CPV modules.

First, we reviewed the state of the art of micro-CPV systems. Based on concentrating optics principles, micro-CPV optical designs are not compliant with a standard configuration. Concentrating optics can be reflective, refractive or both. Moreover, the short focal length implies thinner modules and the chassis can integrate sun-tracking mechanisms interesting for BIPV applications. Figure 1 presents the module efficiencies of the main micro-CPV modules as a function of their concentration and their CTMs ratio. Concentration ratio varies from 150X to 1111X, and the module efficiency from 29.7 % to 36.5 %. Our best micro-X module has an efficiency of 33.4 % at AM1.5D at 25 °C for a geometrical concentration of 1000X [1]. The list of main loss sources (reflection, absorption, scattering, current mismatch, light no-uniformity, mechanical assembly, misalignment) in the CTM ratio are quantified (Fig. 2) [2]. Other losses, like dispersion, tunnel junction current limit and electrical interconnection losses are negligible. The CTM ratio of the micro-CPV modules ranges from 71.4 % to 86.7 %. For the first time in the CPV reported results, a quantified loss chain diagram is compiled which enhances that micro-CPV systems are economically and technically better and more efficient than classical CPV. □

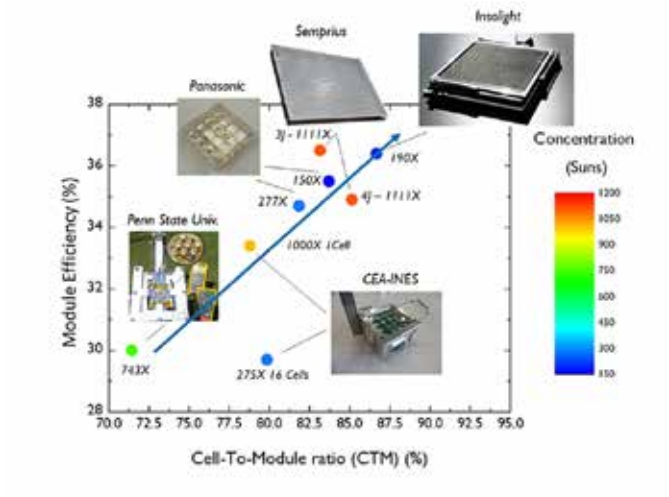

Fig. 1: CPV micro-module efficiency as a function of Cell-To-Module ratio and concentration ratio for a sample of micro-concentrators representative of the state-of-the-art.

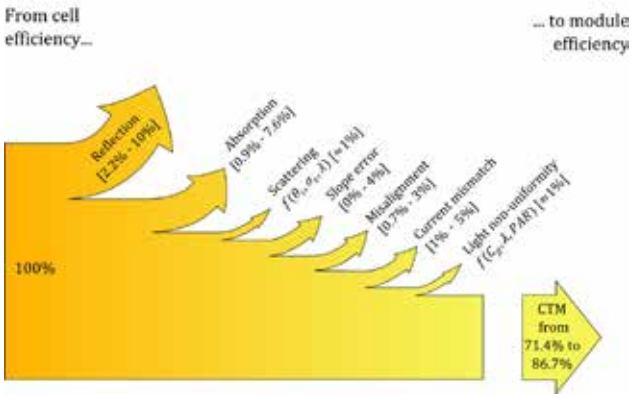

Fig. 2: State-of-the-art micro-concentrator Cell-to-Module loss chain. The minimum and maximum values of loss are given in percentage of cell efficiency.

[1] A. Ritou et al, AIP Conf. Proc., vol. 1881, (2017) 030007.
[2] A. Ritou et al, Solar Energy, Vol. 173, (2018) 789-803.

TEAM Arnaud RITOU, Olivier RACCURT, Philippe VOARINO
CONTACT philippe.voarino@cea.fr

ENCAPSULATION RESILIENT FLEXIBLE ORGANIC PHOTOVOLTAIC DEVICES

Encapsulation is a crucial step to obtain reliable organic photovoltaic devices (OPVs). For flexible OPVs, the mechanical stress induced by roll-to-roll encapsulation may lead to device efficiency loss due to solar cell internal failure. Therefore it appears necessary to find a solution to make them resilient against encapsulation. We have demonstrated that a relatively simple peeling technique allows understanding the role of the interfaces inside a multilayered OPV device supported by a flexible substrate.

The approach developed here consists in quantifying the peeling strength for each interface inside the encapsulated solar cell. The mechanical resilience of OPV devices was evaluated with 180° peel tests (also known as T-peel tests). Encapsulation foils were used as mechanical arms during the device peeling test, as presented on Fig. 1. The peeling strengths between each layer were measured using a series of partial devices. This provided a quantitative analysis of the mechanical strength or quality of each interface. Complementary characterization techniques such as IR spectrometry, EDX-SEM and photoluminescence were performed on the peeled samples to identify the fracture location within the initial stack. Thus we were able to study the effect of the treatment of some specific interfaces.

In accordance with literature, two weak interfaces of the encapsulated solar cells were identified: namely the AL (Active Layer)/PEDOT:PSS and ZnO/TCO interfaces. We applied a UV-ozone surface treatment to the ZnO n-layer, which led to a tremendous improvement of adhesion with the TCO electrode: from less than 0.1 N/cm up to 6 N/cm (Fig. 2). After encapsulation, such treated devices show a significantly higher efficiency than untreated ones with an increase of 33% in the PV performances. The surface treatment altogether modifies the ZnO surface chemistry, allowing a stronger adhesion and a better charge transfer within the solar cell, as denoted by a lower series resistance (13 W.cm² against 23 W.cm²). Such an approach could be broadened to improve all interfaces within OPVs, perovskites, and other optoelectronic devices, which could be subject to the same kind of stress during processing, encapsulation and use. Such mechanical characterizations could also be coupled to device imaging to spatially localize defects within the layers. □

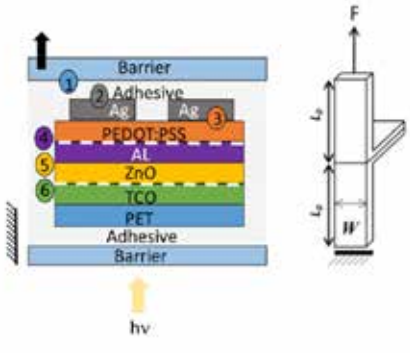

Fig. 1: Architecture of the encapsulated solar cell studied with the interfaces characterized by the peeling test at 180° as described by the attached scheme.

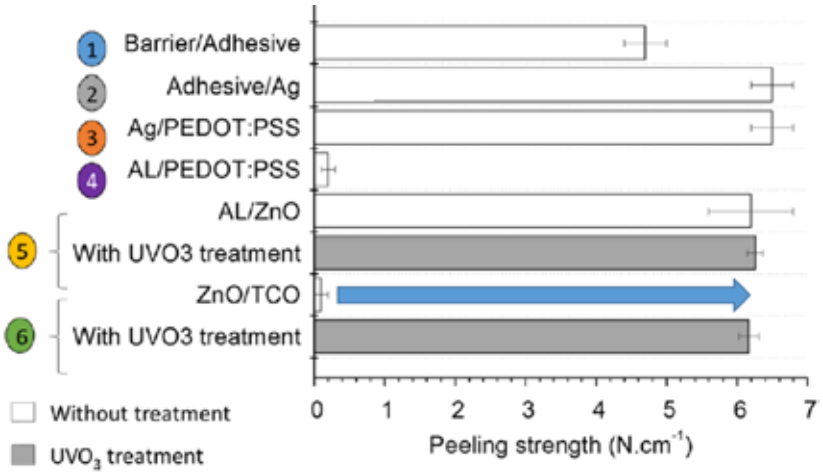

Fig. 2: Peeling strengths determined for a bare and a treated device.

[1] S. Juillard et al., ACS Appl. Mater. Interfaces, vol. 10, (2018) 29805–29813.

TEAM Solenn BERSON, Sacha JUILLARD, Muriel MATHERON
PARTNERS LEPMI (Bourget-du-Lac)
CONTACT muriel.matheron@cea.fr

DURABILITY AND LIFETIME PREDICTION OF MATERIALS FOR SOLAR TECHNOLOGIES

Over the past 30 years, the development of solar technologies has accelerated in order to meet the challenge of renewable and low-carbon energy production. However, the materials used must have a service life of more than 20 years to be profitable. We present here a methodology to determine the lifetime of these materials.

Global warming and climate changes are probably the major challenge for humanity today, which implies the reduction of the anthropogenic CO_2 emissions into the atmosphere. In the context of increasing energy demand, renewable energies with a low carbon footprint have then to be developed, and among them, solar energy constitute a viable option. However, their deployment depends on the cost of the produce energy, which is directly linked to the lifetime of materials and components. To make a plant profitable, the service life aims to reach about 20 to 30 years. The energy production of solar plants, either photovoltaic or concentrating solar power (PV or CSP) plants, is also impacted by the solar radiation available on site. There is a paradox because locations on Earth with the better levels of this resource have high aggressive environment as well, with a lot of stress factors such as temperature, humidity, UV, etc., which can shorten the plants lifetime. When a new solar technology is developed such as PV panel or solar mirrors for CSP plants, it is necessary to evaluate its lifetime faster than waiting for many years that the material undergo degradation on site.

Accelerated test, by increasing the level of stress or the cycles number in laboratory, were used to test materials.
The stress factors of interest depend on the location considered for power plant installation. The objective of such tests is to determine either a degradation law or an acceleration factor of the test compared to the site of interest, which can be defined by the ratio of the time to failure on site to the time to observe the same degradation on the accelerate test. As the time to failure on site is equal to the lifetime and so is obviously unknown, a relationship is needed to link a quantification of the stress level to time. A review of accelerating ageing test modelling was used to identify the law associate to stress factor [1]. The durability of solar mirrors was studied at different level of temperature, humidity and light irradiance to accelerate the degradation. By measuring the degradation kinetic as function of stress level, we determine the model parameters (Fig. 1). With the knowledge of the climatic condition of site, we calculate the acceleration factors for each type of mirrors (Fig. 2) related to the site of solar plant to determine lifetime [2]. □

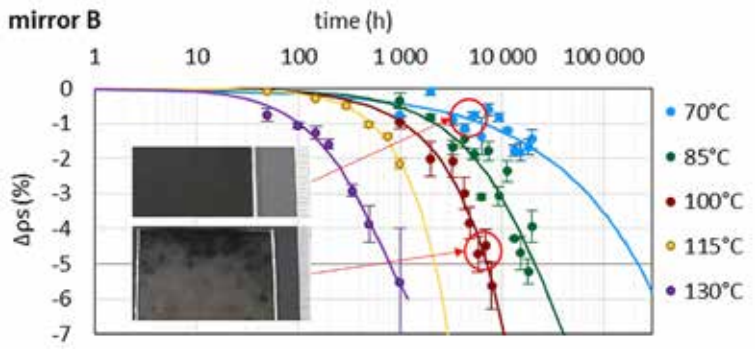

Fig. 1: Specular reflectance loss of mirror B during temperature aging tests with the picture of two mirrors (after 8000 h at 70 °C and 7900 h at 100 °C).

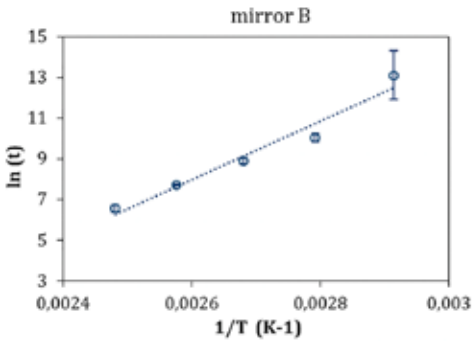

Fig. 2: Graphical representation based on Arrhenius law to determine the apparent activation energy for mirror B.

[1] C. Avenel et al., Solar Energy Materials and solar Cells, vol. 186, (2018) 29-41.
[2] C. Avenel et al., npj Materials Degradation, vol. 3 (2019) Article number: 27.

TEAM Coralie AVENEL, Angela DISDIER, Olivier RACCURT
PARTNERS Univ. Clermont Auvergne - ICCF
CONTACT olivier.raccurt@cea.fr

ENERGY STORAGE AND CONVERSION

STEAM AND CARBON DIOXIDE CO-ELECTROLYSIS AT HIGH TEMPERATURE

RESEARCH TEAM Jérôme AICART, Lucile BERNADET, Jérôme LAURENCIN, Federico MONACO, Marie PETITJEAN Magali REYTIER, Guilhem ROUX, Pauline THIBAUDEAU

CONTACT Jerome.laurencin@cea.fr; marie.petitjean@cea.fr

1. Introduction

The climate change, the rarefaction of fossil fuels in conjunction with the growing worldwide demand for energy have drastically increased the need of clean and sustainable energy sources. Due to the intermittency of renewable technologies such as solar panels or wind turbines, new solutions for energy storage are required to match the fluctuations between the demand and the production. In this frame, the high temperature co-electrolysis of steam and carbon dioxide in Solid Oxide Electrolysis Cells (co-SOECs) appears as a promising way to convert electricity into chemical energy [1,2].[1,2] The produced syngas, which is composed of hydrogen and carbon monoxide, can be further transformed by Fischer-Tropsch or other catalytic processes into gaseous or liquid hydrocarbons (methane, methanol, dimethyl ether, etc.) [3-5].[3,4,5] The final synthetic fuels can be easily stored or even injected in the existing natural gas grid. This 'power-to-gas/liquid' route based on the high temperature co-electrolysis was identified as one of the most efficient solutions to produce synthetic hydrocarbon fuels [6].[6] Indeed, compared to low temperature technologies, SOECs presents the ability to reduce simultaneously H_2O and CO_2 in the same device by using non-noble metal catalysts. Besides, from a thermodynamic point of view, the electricity demand to split the H_2O and CO_2 molecules decreases with increasing the temperature [7].[7] In particular, the electricity requirements can be significantly reduced if the water vaporization is achieved using waste heat from other industrial or downstream catalytic processes [1,2]. Moreover, an operation of the co-electrolyser under high pressure offers several advantages. Indeed, the conventional catalytic processes (such as the Fischer-Tropsch reactor) require high operating pressures between 5 and 100 bar (depending on the catalyst, the temperature and the produced hydrocarbon) [10].[8] Furthermore, the synthetic fuels are usually stored and transported under pressure. Finally, an integrated system operating under pressure could be energetically favored since the compression of liquid water is less energetic than the compression of steam [11,12].[9,10] Nevertheless, only few studies have been dedicated to estimate the real influence of pressure on the cell response.

In this frame, we have developed an approach coupling experiments and modelling to investigate the behavior of a conventional cell operated under pressurized co-electrolysis conditions. Thanks to a specific experimental set-up [3], polarization curves and gas composition at the cell outlet have been

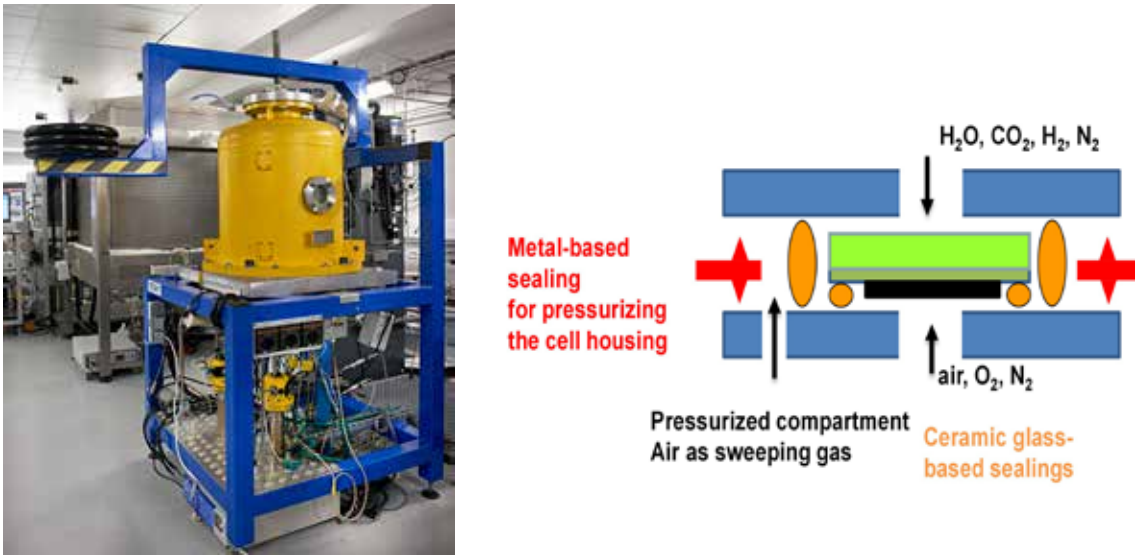

Fig. 1: (a) Photography of the test rig and **(b)** scheme of the cell housing for pressurized tests.

1/ S.D. Ebbesen et al., J. of Electrochem. Soc., vol. 159 (8), (2012) F482-F489.
2/ Y. Wang et al., Fuel Process. Tech., vol. 161, (2017) 248-258.
3/ W.L. Becker et al., Energy, vol. 47, (2012) 99-115.
4/ J. Hartvigsen et al., ECS Transactions, vol. 12 (1), (2008) 625-637.
5/ T. Ogawa et al., J. Nat. Gas Chem., vol. 12, (2003) 219–227.
6/ C. Graves et al., Renew. and Sustain. Energy Rev., vol. 15, (2011) 1–23.
7/ S.D. Ebbesen et al., Chem. Rev., vol. 114, (2014) 10697–10734.
8/ M. Röper, In: "Catalysis in C1 Chemistry", Ed. by W. Keim, D. Reidel Publishing Compagny, 1983, pp. 41-88.
9/ E. Giglio et al., J. Energy Storage, vol. 1, (2015) 22–37.
10/ J.B. Hansen et al., ECS Transactions, vol. 35 (1), (2011) 2941-2948.

measured up to 10 bar in co-electrolysis mode. The experimental data have been used to validate a kinetic model that includes both H_2O and CO_2 electrochemical reductions. Kinetic expressions for the reverse water gas shift reaction and reactions of CH_4 formation have also been taken into account. Once the model was validated under pressure, simulations have been carried out in order to study the operating mechanisms of pressurized high-temperature co-electrolysis. A special attention has been paid to investigate the close interaction between the electrochemistry and the chemical reactions and the amount of produced CH_4 has been simulated according to operating conditions.

2. Experimental studies for Co-SOEC

2.1. Test rig for pressurized operation

For single cell testing under pressurized conditions, an original test rig has been developed at CEA-Liten to perform electrochemical tests in SOEC and co-SOEC modes (Fig. 1) [3,4]. A "counter-pressure" chamber is added to withstand the pressure differential between the furnace (at atmospheric pressure) and the standard cell housing (at high pressure). A metallic gasket, which is electrically insulated, is used at the periphery of this chamber to handle the pressure differential between the cell and the furnace. Two other internal ceramic glass seals ensure the gas tightness between the anodic and cathodic compartments and between the cathodic compartment and the "counter-pressure" chamber. Thanks to this specific design, the ceramic glass seals do not undergo any significant pressure difference inside the cell housing (Fig. 1b). The effective gas tightness is realized by gravity load applied on the top of the housing through a rod crossing the furnace insulation (Fig. 1a). This applied clamping force was required to compress the metallic seal but also to optimize the contact resistances between the grids and the electrodes. Besides, in order to control the load on the electrodes, the dimensions of the housing is precisely adjusted by taking into account the deformation of the compressive metallic gasket. The pressure control is managed by section variations on the downstream flow, before water condensation, i.e. by closing more or less specific valves. Furthermore, a fine pressure regulation control has been developed to ensure limited pressure differentials between the O_2 and H_2 compartments and between the cell and the counter-pressure chamber as low as 30 mbar. Thanks to this specific design, the cell housing remains gas tight even at high pressure and the pressurized exhaust gases can be collected at the test rig outlet, released

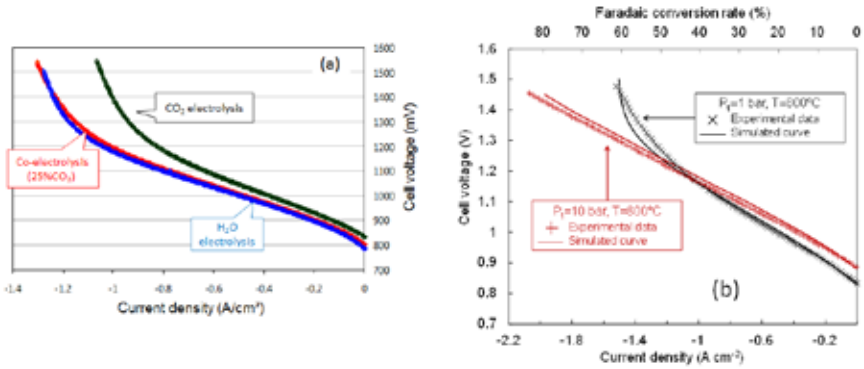

Fig. 2: (a) Effect of CO_2 on cell performances at a total pressure of P_t=1 bar, at 800 °C, with a faradaic conversion rate of 64 % at -1 A/cm² and **(b)** experimental and simulated polarization curves at P_t=1 bar and 10 bar, T=800 °C and for an inlet gas composition of $H_2O/H_2/CO_2$=58.5/6.5/35 vol.% [5].

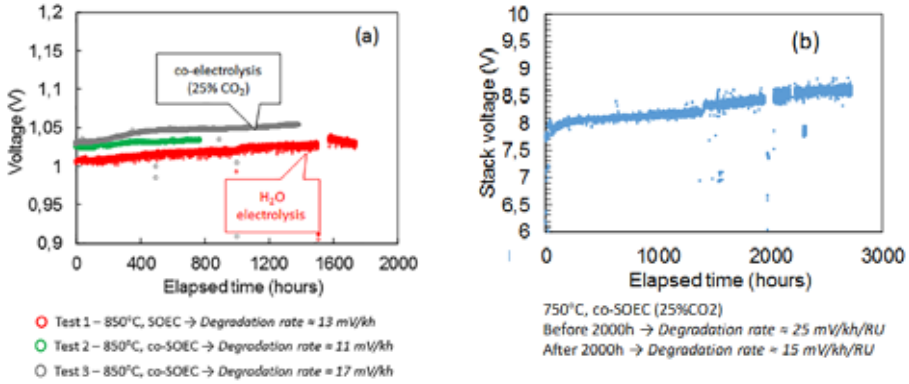

Fig. 3: Endurance curves of SoA button cells carried out at 850 °C and 750 °C in SOEC and co-SOEC modes. Tests 2 and 3: **(a)** Reproducibility of the durability test in co-SOEC mode, at -0.75 A/cm² and faradaic conversion rate =48 %, with 65 vol.% H_2O+25 % CO_2+10 % H_2 at the inlet, Test 1 in pure SOEC mode, at -0.75 A/cm² and SC=48 %, with 90 vol.% H_2O+10 vol.% H_2 and **(b)** Endurance curve of a commercial 6-cells stack at 750 °C in co-SOEC mode, with 65 vol.% H_2O+25 % CO_2+10 % H_2 at the inlet, at -0.85 A/cm² and faradaic conversion rate =54 %.

to atmospheric pressure and then analysed (water is condensed and weighted while dried gases are analysed by micro chromatography).

2.2. Impact of CO_2 and pressure on performances

The cell performances decrease when going from SOE to co-SOE gas mixtures containing more and more CO_2 as shown in Fig. 2a at atmospheric pressure, mainly due to the increase of gas transport and conversion contributions. Under pressurized conditions (Fig. 2b), it has been shown that, in co-SOEC mode at low current density (or low voltages), the OCV increase is predominant and better performances are measured at atmospheric pressure [5]. On the other hand, at high current density, the hydrogen or syngas production is improved under pressure, especially at the thermoneutral voltage 1.3 V and at high steam conversion rate. Indeed, the decrease of concentration overpotentials at high pressure for this type of cell allows reducing the electricity demand for the syngas production (cf. section 3.2).

2.3. Impact of CO_2 on durability

To check the reproducibility of the durability experiments, two long-term tests (800 h and 1400 h) have been performed in co-SOEC at 850 °C, with 65% H_2O+25% CO_2+10% H_2 at the inlet, and a faradaic conversion rate equal to 48% at -0.75 A/cm². In parallel, a test in pure SOEC mode at the same current density and conversion rate, with 90% H_2O+10% H_2 at the inlet, has been carried out to compare the two operating modes. The endurance curves are reported in Figure 3a. In co-electrolysis mode supplied with 25% of CO_2, the voltage degradation rate was between 11 and 17 mV/kh at 850°C as shown in Figure 3a. In pure electrolysis mode, the degradation rate was 13 mV/kh at 850 °C. In other words, the presence of 25% of CO_2 in these testing conditions does not influence significantly the degradation as confirmed by the test performed at the stack level reported in Figure 3b.

3. Understanding of the co-SOEC operating mechanisms by modeling

3.1. Model description and experimental validation

Brief model description - The underlying mechanisms of co-electrolysis, which are not precisely understood, still need to be unravelled. For this purpose, an in-house modelling framework, which has been initially developed at CEA-LITEN for Solid Oxide Fuel Cells (SOFC) and High Temperature Steam Electrolysis (HTSE), has been extended to take into account the CO_2 electro-reduction. A special effort has been paid to include in the model the impact of the elevated operating pressures [5,6]. The multi-scale numerical tool combines two micro-scale models for both electrodes [7,8] with a macroscopic cell approach. At the macroscopic scale, a two dimensional cell description has been adopted which is extensively detailed in references [5,6,9]. The macro-model enables to take into account the radial co-flow configuration of the test bench (cf. section 2.1) and allows determining the distribution of local parameters along the cell radius (such as the gas concentration, the current density, the ohmic losses or the electrode overpotentials). Nevertheless, at this macroscopic scale, the thin electrode active layers, in which the reactions take place, are reduced to the interface with the electrolyte. Therefore, to adapt this model to co-electrolysis, each elementary surface has been divided in two distinct zones, and , dedicated to the H_20 and CO_2 electro-reduction:

$$idS=i_{H_2O}dS_{H_2O}+i_{CO_2}dS_{CO_2} \qquad (1)$$

where is the local cell current density while and are the current densities related to the steam and carbon dioxide electrolyses, respectively. The repartition between the two active surface areas is defined through a parameter expressed as the relative fraction of steam and carbon dioxide content along the cathode/electrolyte interface [10,11]. In co-electrolysis operation, it has been widely

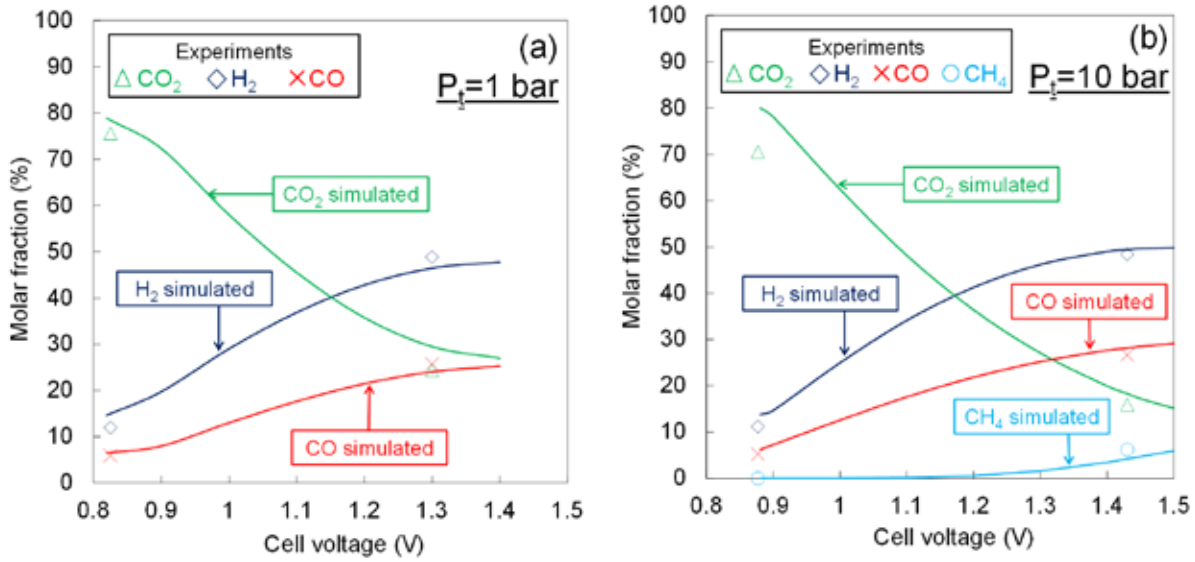

Fig. 4: Simulated and measured dried gas outlet composition plotted as a function of the cell polarization at 800 °C, (a) 1 bar and (b) 10 bar (and for an inlet gas composition of $H_2O/H_2/CO_2$=58.5/6.5/35 vol.%) [5].

demonstrated that the Reverse Water Gas Shift (RWGS) reaction takes place in the classical Ni-YSZ cathode and participate to the global process even under atmospheric condition. At higher operating pressure, it was suspected that the Reverse Steam Reforming (RSR) and the Reverse Dry Reforming (RDR) reactions could be also activated resulting in a methane production at the cathode side. To take into account these possibilities, the RSR and RDR reactions have been introduced in the model in addition to the RWGS [5].

$CO_2+H_2 \leftrightarrow CO+H_2O$ (RWGS) (2a)
$CO+3H_2 \leftrightarrow CH_4+H_2O$ (RSR) (2b)
$2CO+2H_2 \leftrightarrow CH_4+CO_2$ (RDR) (2c)

For this chemical reactions, the kinetic rate expressions are dependent on the total pressure trough the activities of the reactants and products. The pressure also plays a role on the Open Circuit Voltage (OCV) thanks to the Nernst equation while the impact of pressure on the electrode exchange current densities has been neglected in the model. Finally, a special attention has been paid to include in the description the effects of pressure on the diffusive and convective mass transfer through the porous electrodes [5].
Elements of validation - A set of simulations have been carried out in the same conditions than the experiments. Without any specific fitting, it was found that the model is able to accurately simulate the polarization curves for co-electrolysis (Fig. 2b). To go further in the validation, the syngas compositions analyzed at the cell outlet has also been compared to the computations. As shown in Figure 4, the simulations and the experimental data are fully consistent whatever the cell voltage. The evolution with the pressure of both the cell polarization curves (Fig. 2b) and the gas composition (Fig. 4) are also well captured by the simulations. Based on these statements, the model was considered validated and used for the studies.

3.2. Impact of CO_2 and pressure on the cell operating mechanisms

Performances under pressure and role of the gas diffusional process - The operation under pressure yields to shift the cell limiting current density toward higher conversion rates. This evolution results in higher performances at 10 bar than at the atmospheric pressure as soon as the cell voltage exceeds »1.2 V (Fig. 2b). As shown in Figure 2b, this phenomenon is well reproduced by the simulations. To analyze this behavior, a sensitivity analysis has been performed by changing the model input parameters. This numerical analysis has revealed that the quasi disappearance of the cell limiting current density is explained by an improvement of the multi-component gas diffusion under pressurized co-electrolysis while the convective flow remains negligible [5].
Formation of methane in the electrode - It can be noticed in Figure 4 that the methane formation is activated at 10 bar for a cell voltage exceeding a threshold of ~1.2 V. In other words, the formation of CH_4 by the RSR and RDR is only activated at high pressure and cell voltage. To understand this observation, the distribution of methane within the electrode has been computed with the model. It has been found that its concentration increases along the cell radius and is higher at the electrolyte interface. This result points out that the production of CH_4 is favored in a volume located at the cell outlet and close to the electrolyte interface (where the concentration of H_2 and CO are the highest and the H_2O and CO_2 concentrations are the lowest). This statement means that the two reactions of methanation (2b) and (2c) need the accumulation of their reactants and the depletion of their products to be activated under pressure. A close interaction was thus highlighted between the electrochemical and chemical reactions for the internal production of CH_4 within the cermet [5].
Role of the electrochemical reactions - Except for the methane only produced by chemical routes, it is important to understand the precise role of the electrochemical and chemical reactions on the production/consumption of each gas

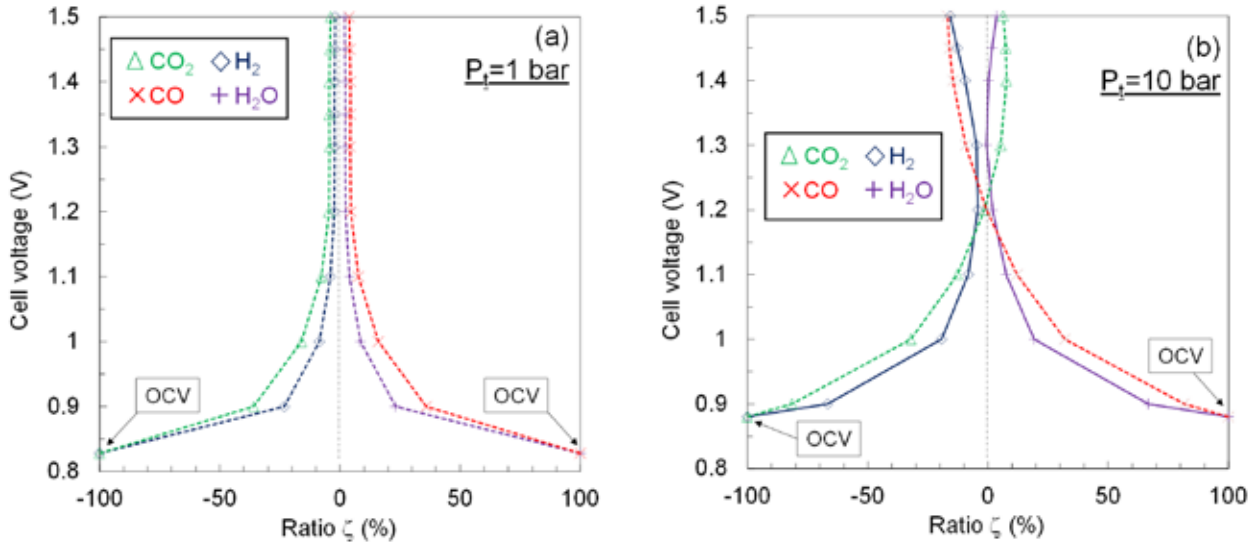

Fig. 5: Relative contribution of the chemical reaction in the global process to produce or consume each gas specie at 800 °C, (a) 1 bar and (b) 10 bar (for an inlet gas composition of $H_2O/H_2/CO_2$=58.5/6.5/35 vol.%) [5].

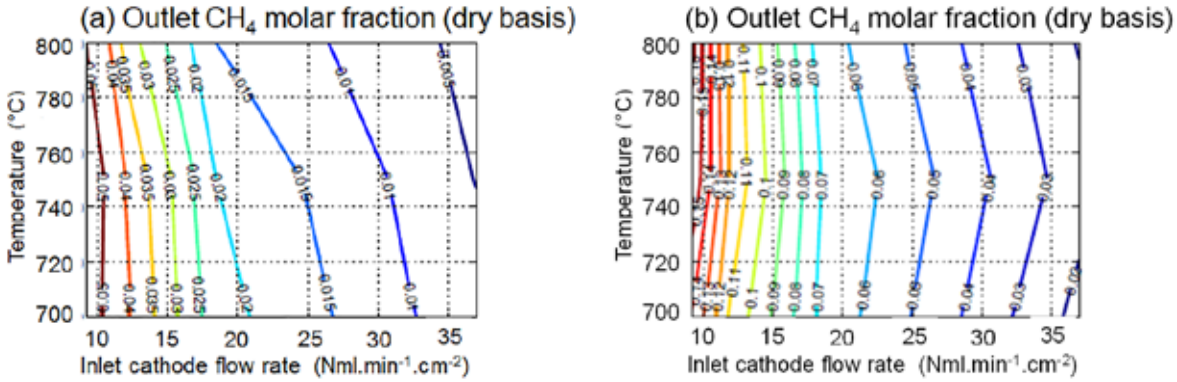

Fig. 6: Molar fraction of CH_4 after steam condensation are plotted as a function of temperature and inlet cathode flow rate at (a) 10 bar and (b) 30 bar (at 1.3 V and for an inlet gas composition of $H_2O/H_2/CO_2$=58.5/6.5/35 vol.%). The molar fractions are given after steam condensation [5].

specie. For this purpose, a parameter z_j has been defined as the ratio between the quantity of each gas compound *j* produced (or consumed) by the chemical reactions and the net quantity resulting from both the chemical and electrochemical reactions. When z_j® ±1, the specie is thus only produced (or consumed) by the chemical means. The ratio is plotted in Figure 5 for all the species at 1 bar (Fig. 5a) and 10 bar (Fig. 5b). All the ratios decrease continuously with increasing the current density. They fall to very low levels at intermediate cell voltages meaning that the steam and the carbon dioxide electrolysis are also the major route to produce H_2 and CO under pressurized co-electrolysis current.

3.3. Operating maps of pressurized Co-SOEC

The previous studies have unraveled the entwined mechanisms for the pressurized co-electrolysis. Once the processes understood, the model can be used to compute the operating maps with the objective to identify the main operating parameters controlling the cell performances, the temperature gradients, and the gas outlet composition [15]. Such approach has allowed demonstrating the technological relevance of co-electrolysis by defining the best strategy of operation for the system. As an illustration, a set of simulations have been carried out in order to investigate the possibility to promote the *in-situ* production of CH_4 in the co-electrolyser. The cartographies of CH_4 molar fraction are plotted in Fig. 6 as a function of the temperature and inlet flow rates. It is shown that formation of CH_4 in the co-electrolyser remains limited even at 700 °C and 30 bar.

4. Conclusion and perspectives

Experiments have been performed in atmospheric and pressurized co-electrolysis mode with a state-of-the-art SOC. It has been shown that the cell performances are improved under pressure at 1.3 V. The gas analyses have revealed that the methane formation is only activated under polarization and pressure. These results have been used to validate a physical-based model for pressurized co-electrolysis. This model is now able to predict accurately the polarization curves, the syngas compositions at the cell outlet as well as to analyze the specific underlying operating mechanisms for pressurized co-electrolysis. For instance, operating maps have been computed at 10 bar and 30 bar from 700 °C to 800 °C. These simulations have shown that formation of CH_4 in the co-electrolyser remains limited at 700 °C and 30 bar for a SOC fed with 25% of CO_2. In terms of durability, long-term experiments have revealed that the degradation rates in co-SOEC mode fed with 25% of CO_2 are in the same range than those obtained in SOEC mode. The next steps will be to investigate the links between the performances, the SOC materials and their degradations upon various operating conditions thanks to the coupled approach between electrochemical tests, physico-chemical post-test characterizations and multi-scale modeling. □

Publications / Patents

[1] J. Laurencin and J. Mougin, In: "Hydrogen Production by Electrolysis", Ed. By A. Godula-Jopek, Wiley, 2015, pp.197-208.

[2] M. Reytier et al., "Stack performances in high temperature steam electrolysis and co-electrolysis", Int. J. Hydrogen Energy, vol. 40, (2015) 11370-11377.

[3] M. Planque, M. Reytier, and G. Roux, Patent application: FR1462699, 18 Dec. 2014.

[4] M. Reytier, M. Planque, and G. Roux, Patent application: FR1659876, 12 Oct. 2016.

[5] L. Bernadet et al., "Effects of Pressure on High Temperature Steam and Carbon Dioxide Co-electrolysis", Electrochimica Acta, vol. 253, (2017) 114-127.

[6] L. Bernadet et al., "Influence of pressure on solid oxide electrolysis cells investigated by experimental and modeling approach", Int. J. of Hydrogen Energy, vol. 40, (2015) 12918-12928.

[7] E. Lay-Grindler et al., "Micro modelling of solid oxide electrolysis cell: From performance to durability", Int. J. of Hydrogen Energy, vol. 38, (2013) 6917-6929.

[8] J. Laurencin et al., "Reactive Mechanisms of LSCF Single-Phase and LSCF-CGO Composite Electrodes Operated in Anodic and Cathodic Polarisations", Electrochimica Acta, vol. 174, (2015) 1299-1316.

[9] J. Laurencin et al., "Modelling of solid oxide steam electrolyser: Impact of the operating conditions on hydrogen production", J. of Power Sources, vol. 196, (2011) 2080–2093.

[10] J. Aicart et al., "Experimental Validation of Two-Dimensional H_2O and CO_2 Co-Electrolysis Modeling", Fuel Cells, vol. 14, (2014) 430-447.

[11] J. Aicart et al., "Accurate predictions of H_2O and CO_2 co-electrolysis outlet compositions in operation", Int. J. of Hydrogen Energy, vol. 40, (2015) 3134-3148.

Thesis defended

[T1] J. Aicart, "Modélisation et validation de la co-électrolyse de la vapeur d'eau et du dioxide de carbone à haute température", PhD Thesis, University of Grenoble, France, 2014.

[T2] L. Bernadet, "Étude de l'effet de la pression sur l'électrolyse de l'H_2O et la co-électrolyse de H_2O et CO_2 à haute pression", PhD Thesis, University of Bordeaux, France, 2016.

Projects

[P1] DEMETER: Démonstration de la faisabilité technique et économique d'une boucle de stockage/déstockage d'électricité renouvelable sur méthane de synthèse au moyen d'un électrolyseur à haute température réversible, ANR-SEED 2011.

[P2] CHOCHCO: CHaîne Optimisée flexible de Co-électrolyse et d'Hydrogénation de CO en méthane de synthèse, ANR-SEED 2013.

[P3] MINERVE, KIC InnoEnergy, grant agreement n° 76_2012_IP35_MINERVE.

[P4] SOPHIA: Solar integrated pressurized high temperature electrolysis, FCH-JU-2013-1, grant agreement n° 621173.

[P5] ECo: Efficient Co-Electrolyser for Efficient Renewable Energy Storage, H2020-JTI-FCH-2015-1), grant agreement n° 699892.

[P6] CatVIC: Catalytic Valorization of Industrial Carbon, ANR-BMBF, 2019

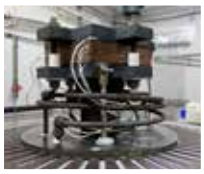

OPTIMISED STACK FOR REVERSIBLE ELECTROLYSER/FUEL CELL OPERATION (rSOC)

Solid Oxide Cell (SOC) technology is able to operate in both electrolysis (SOEC) and fuel cell mode (SOFC). Thus, the SOC systems allow to store excess electricity by producing hydrogen through electrolysis, or to produce electricity (and heat) through fuel cell mode from hydrogen or any other fuel locally available when energy needs exceed local production. CEA-Liten works on the optimization of its SOEC stack for the SOFC mode.

We have developed a stack, made of 25 cells of 100 cm² active area, able to be highly efficient in SOEC mode, reaching high current densities and high fuel utilisations [1-2]. Even if intrinsically able to operate in SOFC mode, it was needed to modify and optimise it in order to perform well in this mode. Indeed, the fuel cell mode requires a higher air flow rate as compared to the electrolysis mode. This is because, first, the air flow provides the oxidizing species needed for the electrochemical reaction and, secondly, an excess air flow rate allows to evacuate at least partly the heat generated. Starting from the reference 25-cells stack, we improved the fluidic distribution to the cells on the air side to cope with high flow rates as those needed for SOFC operation. Most of the work has been carried out to decrease the pressure drop on air side. In addition, works have been undertaken to improve the sealing mechanical resistance to internal pressure, to extend stack robustness and to increase the gas flow rate. Those improvements required some re-design phase and the manufacturing of the modified components. Then they were first validated at the scale of a Single Repeat Unit (SRU) before integration into a full scale stack.

Figure 1 shows the pressure drop reduction as a function of the inlet air flow rate before and after stack modification experimentally demonstrated at the SRU level at 800 °C. The pressure drop was reduced by a factor higher than 2 by comparison of SRU scale data. A gas path modification was then applied to 25-cells stacks [3]. The pressure drop on the 25-cells stacks is significantly decreased as compared to the value recorded at SRU level before modification even if a bit higher than for the modified SRU. We have verified that the electrochemical performance through i-V curves (Fig. 2) was not significantly affected by this modification. The modification of the sealing solution design was validated in terms of tolerance to several levels of internal pressures. No leak was observed after six hours at 800 °C with a pressure of 460 mbar on air side while at similar level of temperature, the previous sealing design failed after one hour at a pressure of 380 mbar. Those results validate the stack design modification for reversible operation (rSOC). It will be generalised, and deployed for in field test in the frame of the European REFLEX project (H2020 FCH-JU, grant agreement No 779577). □

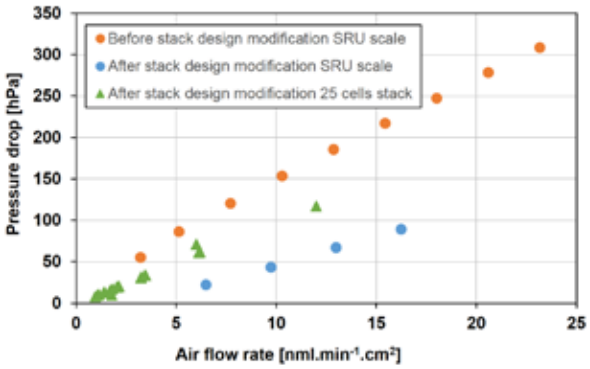

Fig. 1: Pressure drop evolution at 800 °C as a function of the inlet air flow rate before and after design modification as measured at SRU level; and after design modification at 25-cells stack level.

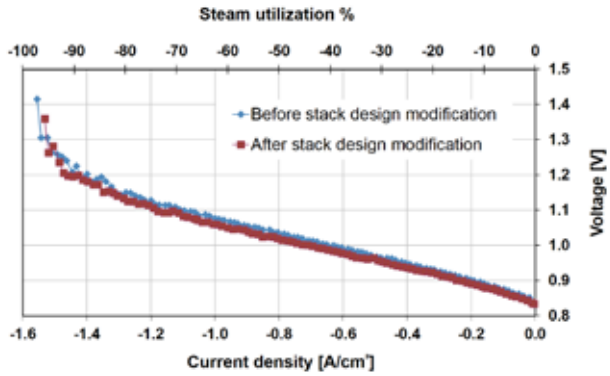

Fig. 2: I-V curves in SOEC mode at 800 °C with 90:10 ratio of H_2O:H_2 on fuel side (12 Nml min^{-1} cm^{-2}) and air on oxygen side, recorded at SRU level before and after design modification.

[1] J. Mougin et al., ECS Transactions, vol. 78, (2017) 3065-3075.
[2] M. Reytier et al., Int. Journal Hydrogen Energy, vol. 40/35 (2015) 11370-11377.
[3] A. Ploner et al., ECS Transactions, vol. 91, (2019) 2517-2526.

TEAM Géraud CUBIZOLLES, Stéphane DI IORIO, Pierre HANOUX, Thibault MONNET, Julie MOUGIN, Bruno ORESIC, Philippe SZYNAL
PARTNERS SYLFEN, H2020 REFLEX project partners
CONTACT julie.mougin@cea.fr

UNDERSTANDING INTIMATE OPERATION OF PEMFC BY COUPLED ADVANCED NEUTRONS AND X-RAY CHARACTERIZATION

Coupling advanced characterization tools with pseudo-3D two-phase flow models allows giving unique insight in the correlation between water distribution, performance and degradation of Proton Exchange Membrane Fuel cells. This is a prerequisite for the large-scale commercialization of this very promising carbon-free alternative energy conversion system for transportation and stationary applications.

Proton Exchange Membrane Fuel cells (PEMFC), as a highly efficient energy conversion technology, and hydrogen, as a clean energy carrier, have a great potential to reduce both carbon dioxide emissions and dependence on mainly imported hydrocarbons. However, in view of extending their use to a broad range of customers and to compete with existing technologies, progress has still to be done on current PEMFC stack technologies in terms of cost, performance and lifespan. Nevertheless, degradation mechanisms are not clearly understood because of their coupling, and also due to the complex composition and intricate nanostructure of the PEMFC components. We have been developing in parallel, for more than a decade, both original and unique multiscale modeling and characterization tools in order to understand the correlation between the heterogeneous water distribution and PEMFC operation and degradation mechanisms. This is particularly important to improve its performance reliability. Complementary imaging and scattering techniques based on Neutron and X-Ray probes available at large scale research facilities are used to study operando the water distribution and the microstructure of the components. Recently, a novel pseudo-3D two-phase flow model has been developed to quantify and predict the distribution in water content in real stack design.

We provide unique insights into structural aging of the proton conducting polymer electrolyte membrane in dependence of the local hydration and helps to identify the relevant scale for physical degradation [1]. In addition, by comparing neutron imaging and small angle scattering (SANS), we emphasize how large the in-plane and through-plane gradients in relative humidity are at the sub-mm and mm scales, within each cell and that two-phase flows with evaporation/condensation probably govern the water distribution in an operating PEMFC (Fig. 1) [2]. Neutron imaging results on a small power fuel cell stack made with industrial large surface bipolar plates, allow validating a recently developed multi-physic pseudo-3D model including two-phase flow aspects (Fig. 2) [3]. Once validated, this model is used to quantify the heterogeneities in the water content in the different components of the heart of the PEMFC, and also decipher the relative weights of the driving forces leading to liquid water formation in the whole cell of an operating stack, which is not directly accessible by the experiment. We aim at improving the models as well as both spatial and time resolutions of the experimental methods to be able to compare in a near future the measured and simulated water content profiles within the electrodes and their evolution upon aging. □

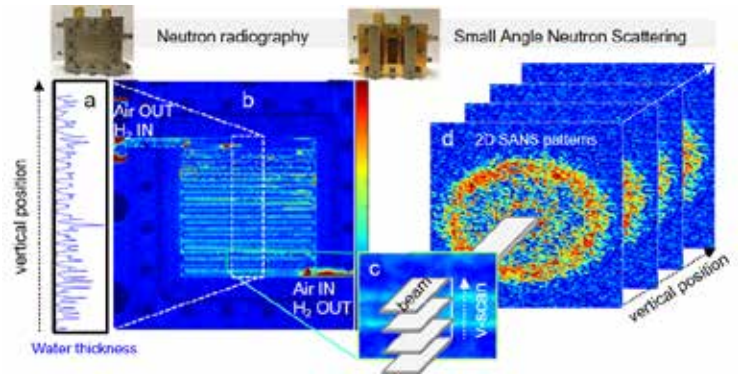

Fig. 1: Combination of neutron radiography and Small Angle Neutron experiments

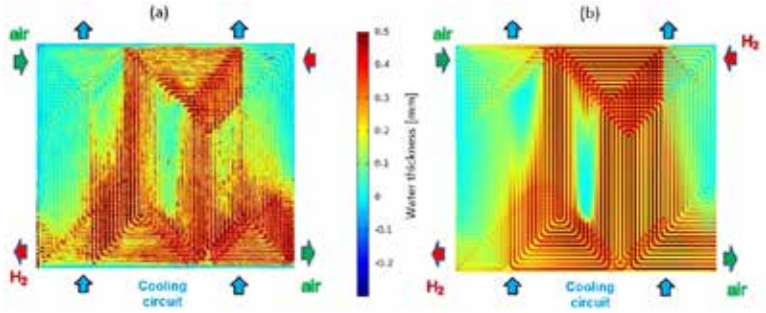

Fig. 2: (a) measured and **(b)** simulated total water thickness for 5 cells stack.

[1] N. Martinez et al., ACS Appl. Energy Mater., vol. 2, (2019) 3071–3080.
[2] N. Martinez et al., ACS Appl. Energy Mater., under review.
[3] E. Tardy et al., International Journal of Heat and Mass Transfer, under review.

TEAM Marion CHANDESRIS, François COURTOIS, Sylvie ESCRIBANO, Gérard GEBEL, Jongmin LEE, Sandrine LYONNARD, Nicolas MARTINEZ, Jean-Sébastien MICHA, Fabrice MICOUD, Arnaud MORIN, Jean-Philippe POIROT, Sébastien ROSINI, Erwan TARDY.
PARTNERS Laue Langevin Institute, Néel Institute, French CRG beamline D2AM @ ESRF, LEPMI (Grenoble)
CONTACT arnaud.morin@cea.fr

TOWARDS THE PRINTING OF PEMFC FUEL CELLS

The fuel cells are electrochemical converters alloying the production of electricity from hydrogen. Numerous manufacturers, mainly dealing with mobility, are interested in such energy sources. Classically, the Original Equipment Manufacturers (OEM) developed stamped metallic bipolar plates designs leading to power densities up to 3 kW/L and thicknesses of the cell of about one millimetre. The use of printing processes for the fluidic circuit manufacturing should permit to go one-stage further allowing power densities as high as 6 kW/L associated with few hundreds of microns of thickness reduction. The whole lot being produced at decreasing costs.

After identification of the most pertinent material and processes, the developments were oriented on the realisation of an active area of 100 cm^2. Parallel ribs, presenting a width of 400 µm and a height of about 150 µm were screen-printed at a step equal to 800 µm (Fig.1). The substrate consists in a 50 µm thick gold-coated metal foil. New fluidic circuits integrating homogenisation zones were specified and the designs were validated thanks to fluidic and thermal simulations. The printed fluidic circuits were assembled to realise a single cell. The insertion of a homemade micro-structured gasket generated the tightness. The measured pressure losses confirmed the calculated values and a working test was run. Figure 2 presents the polarisation curve of a cell integrating printed components. The electric power is lower than those from standard reference cells but some improvements have been pointed out. This first result validates the potential of these new printed components.

The development of innovating technologies to realize the PEMFC components by printing led to a first patent actually extended worldwide [1]. The development of the intellectual property still goes on. New designs are specified to reach higher power densities, notably through the reduction of the gasket surface. Technical-economic studies point out important decreases of the cost of fabrication generated by the use of these new techniques. Current studies are interested in the development of « roll to roll » processes. □

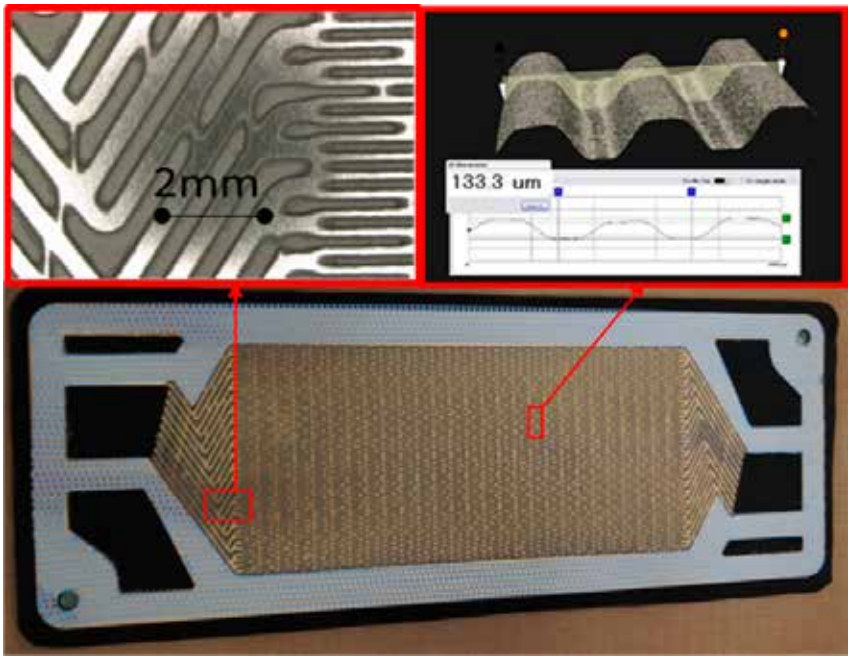

Fig. 1: observation and metrology of a printed cooling circuit.

[1] J. Salomon, B. Amestoy, J.-F. Blachot and D. Tremblay, Patent application E.N. 1871024, 12 September 2018

TEAM Jérémie SALOMON, Benjamin AMESTOY, Jean-François BLACHOT, Denis TREMBLAY
CONTACT jean-francois.blachot@cea.fr

BIOMASS BASED CARBON MATERIALS FOR NA-ION BATTERIE ELECTRODES

This work targets to identify the relationship between the physico-chemical properties of the biomass precursors and the electrochemical properties of the final hard carbons to be used as negative electrodes in Na-ion batteries. The aim is to give an added value to biomasses and agricultural wastes that are not currently being developed and use them as low-cost precursors for the production of hard carbon.

Several studies have explored the production of hard carbon from different types of biomass, mainly lignocellulosic biomass, such as forest residues and agricultural wastes. However, given the vast diversity of these types of biomass, it is crucial to quantify the impact of their physico-chemical properties on the structure and final composition of the hard carbon produced, and thus, identify the characteristics that induce the best electrochemical performance. Nowadays, the understanding of the properties of hard carbon from biomass is not the subject of systematic studies. To accomplish the objective we chosed four biomasses taking into account our previous study [1]: the pine as a coniferous wood, the beechwood as a deciduous wood, the miscanthus as an herbaceous crop and the wheat straw as a cereal agricultural waste (Fig.1). First, the precursors underwent a thermal treatment until 450 °C under an inert atmosphere, followed by a second thermal treatment under inert atmosphere up to three different temperatures: 1000 °C, 1200 °C and 1400 °C. The obtained hard carbons were characterized by several techniques such as CHNS, EDX-SEM, XRD, SAXS, and Raman spectroscopy. The electrochemical performances were measured by assembling half-cells of hard carbon electrodes against metal sodium as counter and the reference electrode. The half-cells were cycled in a galvanostatic test.

The hard carbons derived from woody biomasses (pine and beechwood) have a constant morphology along with the different thermal treatment. Figure 2 presents a particle of pine hard carbon obtained at 1400 °C. These hard carbons also have the characteristic XRD pattern of hard carbon, which also evidences that no mineral matter is present at 1400 °C. By the other hand, micanthus and wheat straw hard carbons have a changing morphology, with heterogeneous microstructures evidenced by the XRD patterns, in which important mineral phases are present even at 1400 °C and correspond to SiC compounds, given the important quantity of Si present in the precursors as SiO2. The electrochemical performances are presented in Figure 3. The commercial hard carbon exhibits less irreversibility than the biomasses derived hard carbons; however, its reversible capacity is less important. The hard carbons derived from woody biomasses present better electrochemical performance than the miscanthus and wheat straw hard carbons. The inorganic content of the raw biomass seems to have a significant impact on the performances. The content of cellulose, hemicellulose and lignin might also have an impact in the final microstructure and performance of the hard carbon. This work continues toward the constitution of a database of 25 biomasses to perform a statistical analysis and correlate the physico-chemical properties of the precursors with the final hard carbon performances. □

Fig. 1: Reference biomasses for this study.

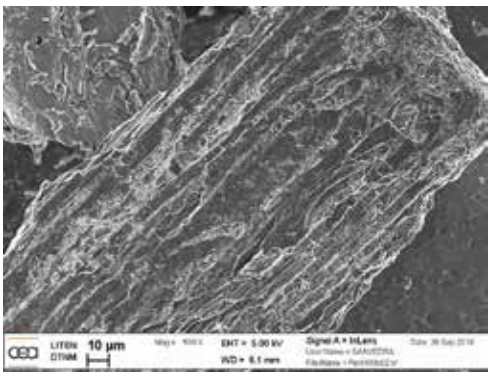

Fig. 2: SEM image for Pine hard carbon obtained at 1400 °C.

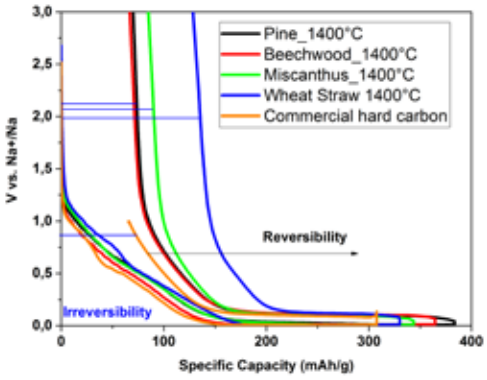

Fig. 3: First charge-discharge cycle for hard carbons obtained at 1400 °C.

[1] C. del M. Saavedra Rios et al., Biomass Bioenergy, vol. 117, (2018) 32-37.

TEAM Capucine DUPONT, Carolina SAAVEDRA, Loïc SIMONIN
PARTNERS Delft Institute for Water Education (IHE)
CONTACT loic.simonin@cea.fr

LITHIUM LAYERED OXIDE NANOPARTICLES TO ENHANCE THE BATTERIE PERFORMANCES

Cathode material nanoparticles can offer new perspectives for improving electrochemical performances. However, no robust and scalable synthesis procedure of such materials exists and there is a dearth of literature discussing the implementation of such materials in relevant cathode electrodes. We obtained first promising results on this thematic in 2018 in the frame of H2020 BASMATI project (grant agreement N° 646159).

We developed a tuned scalable co-precipitation synthesis, using processes with well-known industrially scaled analogs, to produce submicronic and isolated NMC particles ($LiNi_{1/3}Mn_{1/3}Co_{1/3}O_2$) [1]. The idea is to increase the electroactive specific surface area by limiting the number of grain boundaries. It is expected that the lithium diffusion will be improved and the electrochemical behavior enhanced at high C-rate. To produce NMC submicronic particles, synthesis conditions were adapted to favor rapid nucleation with little observed agglomeration. The resulting particle morphology is different of the large and spherical aggregates obtained by the classical synthesis process. Then, an environmentally-friendly water-based formulation was developed to implement the material and to produce highly loaded electrodes. The main technical challenge is related to the high sensitivity of Li-containing materials towards water which leads to strongly alkaline slurries. The pH of the slurry has to be adjusted and controlled during the electrode manufacturing process to avoid aluminum current collector corrosion upon coating for instance. At the end, high loaded water-based cathode with submicronic NMC are successfully produced and are assembled in a commercially relevant pouch cell configuration for electrochemical testing.

Our new synthesis process leads to monodispersed flake-shaped particles below 200 nm and a thickness of 80 nm (SEM picture in Fig. 1a). X-ray powder diffraction analysis indicates the material crystallizes without any crystalline impurity phase detected (Fig. 1c) and HR-STEM imaging confirms the well-ordered layered structure (Fig. 1d). In terms of electrochemistry, submicronic $LiNi_{1/3}Mn_{1/3}Co_{1/3}O_2$ particles performed better than classic dense micron-sized aggregates in half coin at all tested C-rates. It is clear that the non-agglomerated state of particles improves the rate of lithiation/delithiation in the material. Then, the C-rate behavior of our environmentally-friendly water-based formulation is compared to the classic organic-based formulation and similar results were obtained (Fig. 2c.). To complete the investigation, a high loaded submicronic $LiNi_{1/3}Mn_{1/3}Co_{1/3}O_2$ electrode (18.8 mg.cm-²) formulated in aqueous media has been assessed in a Li-ion system in a pouch-cell. A total capacity of 29 mAh was measured at a discharge rate C/20 and the capacity at 1C is 87 % of the initial capacity, which is quite an interesting result for this loading. The pouch cell shows very stable capacity at 1C, after 500 cycles, it retains more than 90 % of its initial capacity [2]. □

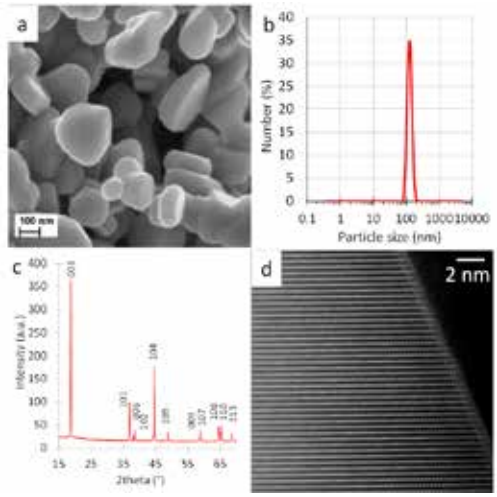

Fig. 1: Submicronic $LiNi_{1/3}Mn_{1/3}Co_{1/3}O_2$ physicochemical characterizations: (a) SEM image, (b) PSD analysis, (c) XRD pattern (d) HR-STEM imaging.

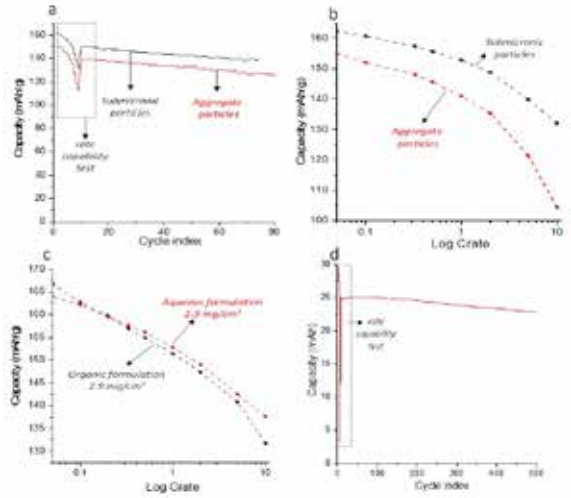

Fig. 2: Submicronic and dense particles aggregates performances: (a) cycle life and (b) C-rate capability, (c) comparison of the aqueous and organic formulations, (d) cycle life in pouch cell configuration.

[1] D. Peralta et al., patent application FR1750435, January 2017.

[2] D. Peralta et al., J. Power Sources 352 (2017) 194-207.

TEAM Benjamin AMESTOY, Didier BLOCH, Adrien BOULINEAU, Carole BOURBON, Jean-François COLIN, Frédéric FABRE, Elise GUTEL, Sébastien PATOUX, David PERALTA, Jérémie SALOMON

CONTACT david.peralta@cea.fr

FAST-CHARGING OF LITHIUM-IRON-PHOSPHATE BATTERIES

This work targets to identify the relationship between the physico-chemical properties of the biomass precursors and the electrochemical properties of the final hard carbons to be used as negative electrodes in Na-ion batteries. The aim is to give an added value to biomasses and agricultural wastes that are not currently being developed and use them as low-cost precursors for the production of hard carbon.

In the context of electrical vehicles (EV) applications, fast-charging methods are applied in order to minimize the battery charging time. We have evaluated an original fast charge with ohmic drop compensation (ODC) method comparatively to a standard charge protocol. A post-mortem study allowed to understand the degradation phenomena that lead to the decrease of the life time of the ODC charged cells. This analysis provided useful information to improve the ODC fast charge parameters.

Fast charge can accelerate the battery ageing and increase the cell temperature. In the present study, we contributed to evaluating an original fast charge with ohmic drop compensation (ODC) method proposed by M. H. Noh et al., *J. Energy Storage, vol. 8 (2016) 160–167*. Two charging methods were compared: (i) the reference charging method at 1 C-rate with an upper-bound voltage limit of 3.65 V; (ii) the ODC fast charging method at 6 C-rate until an upper-bound voltage limit defined by where is the compensation rate and the internal battery resistance. Two compensation rates of 57% (low level) or 93% (high level) were considered. During fast charge with ODC, the cells are degraded by cycling due to both the high temperature increase and the high cell voltage reached at the end of the constant-current stage (Fig. 1). Indeed X-ray tomography and post mortem analysis revealed a jelly-roll deformation and delamination of the graphite electrode leading to the loss of active materials [1]. The graphite electrode as well as of the components of the liquid electrolyte are degraded leading to a rapid loss of the lithium inventory. Post-mortem SEM observations (Fig. 2) show a mossy deposition of lithium for the high level ODC method at 6 C-rate.

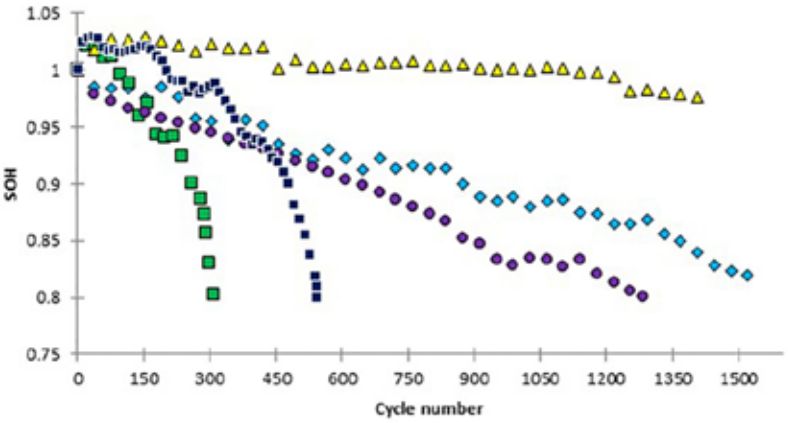

Fig. 1: Evolution of the battery's SOH
■ High level ODC method at 6 C-rate
◆ Low level ODC method at 6 C-rate
■ High level ODC method at 6 C-rate with air force convection
● Reference method inside 45 °C enclosure (50)
△ And reference method at ambient temperature, after M. H. Noh et al., *J. Energy Storage, vol. 8 (2016) 160–167*

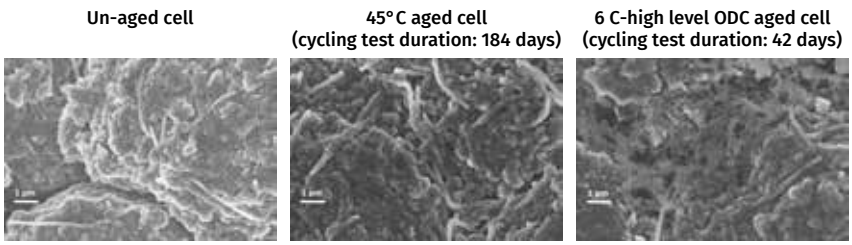

Fig. 2: SEM images of the un-aged, the 45°C aged and the 6 C-high level ODC aged negative electrodes.

[1] X. Fleury et al., J. of Energy Storage, vol. 16 (2018) 21–36.

TEAM Xavier FLEURY, Sylvie GENIES
PARTNERS LEPMI (Grenoble)
CONTACT sylvie.genies@cea.fr

The development of fast charging method for lithium ion batteries remains a key point of their deployment. Even if the high level ODC method induces a very fast battery ageing, the low level has extended the cell service life up to 1500 cycles and still shortened the overall charging time to less than 30 minutes for a full charge. Moreover, optimization of the compensation rate will allow to mitigate the ageing effect due to overcharge impact. Among many other fast charging protocols that could be implemented onto electric vehicles, the ODC fast charging method may be an alternative one to be used occasionally. Moreover, this work has demonstrated the interest of coupling electrochemical test and post-mortem study for a better understanding of the origin of performance degradations. □

DATABASES FOR SHARING AND COMPARING ENERGY STORAGE TECHNICAL DATA AND PHOTOVOLTAIC MATERIALS/PROCESSES

We have developed, at first internally, databases to capitalize the knowledge of the various laboratories involved in energy storage technologies and photovoltaic materials and processes technologies. Their design enable precise comparison between objects of similar or different technologies. They now comprise hundreds of records for battery cells, fuel cell stacks and photovoltaic materials.

The ESTOR database for energy storage systems includes both generic data (such as energy or mass) and specific data for a given type of object (such as detailed performance in various operating conditions). The photovoltaic database includes many technical data (optical, mechanical, electrical...) of materials used in the fabrication of a photovoltaic module: cells, encapsulant, frontsheet, backsheet, junction boxes...It aggregates in a consistent structure nominal data from manufacturer datasheets with test results from CEA laboratories. The type of data and tests included ranges from performances to safety, ageing, or fine characterization of dismantled components. Therefore, it helps improve the choice of the best technological solution to meet the specifications of a given application, dealing with trade-offs between energy, power, operating conditions, reliability, lifetime mass, cost, efficiency...It is implemented using the Granta MI software, which allows to finely tune access control in order to manage data confidentiality. It provides a simple web interface, and a Python interface which paves the way to its use by simulation software and for data mining.

Today, more than 500 battery cell records and more than 100 fuel cell stack records are populated, together with several other technologies as shown in Figure 1. It is also possible to perform automatic extraction of data and to derive meaningful visualizations as shown in Figure 2. The first applications for direct use by simulation software are emerging, together with automatic data checking and completion. However, to fully encompass the goal of ESTOR, a lot of additional work is necessary by adding:

- New types of storage: thermal storage, larger systems rather than components, SOFC/SOEC, ...
- New type of data: environmental impact, economic cost,...

In the frame of the H2020 project TEESMAT, ESTOR database structure will be extended to centralize the results of advanced characterizations on battery components and materials from 20+ partners, even after the project end, giving a much finer insight in the specificities of each kind of chemistry. Locally at CEA-LITEN, the same structure improvement will be used to automatically populate data from the raw results of our test benches in electrochemical and safety tests. The ambition is to avoid any further data loss or inconsistency, and increase the fluidity of exchanges between projects and laboratories. □

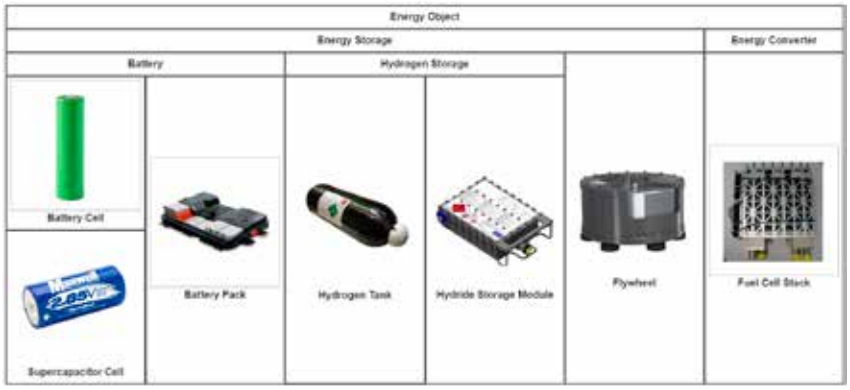

Fig. 1: Taxonomy of the objects described in ESTOR database. Reading from top to bottom gets from the most generic to the most specific data.

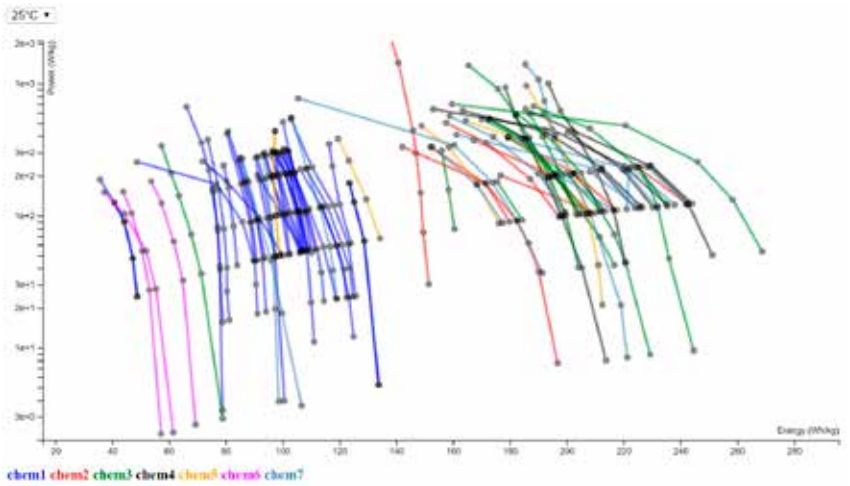

Fig. 2: Anonymised Ragone plot (Power vs Energy) of various battery cells: one line is a cell, one point is a test at a given current, one color is a chemistry.

[1] F. Perdu et al., in 2018 IEEE Intern. Energy Conference (ENERGYCON 2018), (2018) 483-488.

TEAM Boris BERSENEFF, Lise DANIEL, Cyrille DESMOULINS, Sébastien FIETTE, Yannick FOURNERON, Julien GAUME, Grégory LARGILLER, Gilles LAVIALLE, Loïc LONARDONI, Elise MONNIER, Lionel de PAOLI, Fabien PERDU, Eric PINTON, Sébastien ROSINI, Romain TESSARD
CONTACT fabien.perdu@cea.fr

ENERGY EFFICIENCY

INNOVATIVE SOLUTIONS FOR DISTRICT HEATING AND THERMAL STORAGE

1. Introduction

District Heating (DH) systems should continue to grow rapidly in France in the next years. This prospect lies on i) the statement that space heating and domestic hot water preparation remain significant contributors to national greenhouse gas emissi[1]ons[2], ii) on the natural ability of these systems to integrate intermittent, renewable and/or waste sources[3], iii) and finally on their central role in the development of smart energy systems, i.e. a system taking advantage of positive synergies between energy carriers[4].

In this context, our R&D team works both in the technological and algorithmic domains to optimize existing systems and prepare future ones. More specifically, we firstly work on new production systems and the integration of solar thermal energy into DH networks. Second, we develop technological components like heat storage solutions and bi-directional sub-stations. Finally, linked to the "digitalization" trend observed for thermal networks and consumers, we develop operational optimization decision support algorithm and tools.

2. Demonstrating a multi-carrier energy system

Hybrid Energy Networks (HEN), coupling gas, heat and electricity have the potential of addressing various types of energy needs in a more efficient and sustainable way, by leveraging the synergies between energy carriers. In particular, a HEN uses the most efficient storage technologies depending on the needs, and helps integrating a higher share of intermittent energy resources. However, such networks feature a higher complexity and require advanced control strategies to manage the energy generation, storage and consumption. In the European Project PENTAGON [P1], some of these key issues are addressed. A multi-carrier flexibility platform is developed, to manage the optimal operation of a HEN (Fig.1). The service based IoT (Internet of Things) platform is validated on specific scenarios, numerically by simulations, and experimentally on the micro district heating network facility of CEA. Key Performance Indicators are calculated for each scenario, eg. the storage flexibility or the share of renewable energy.

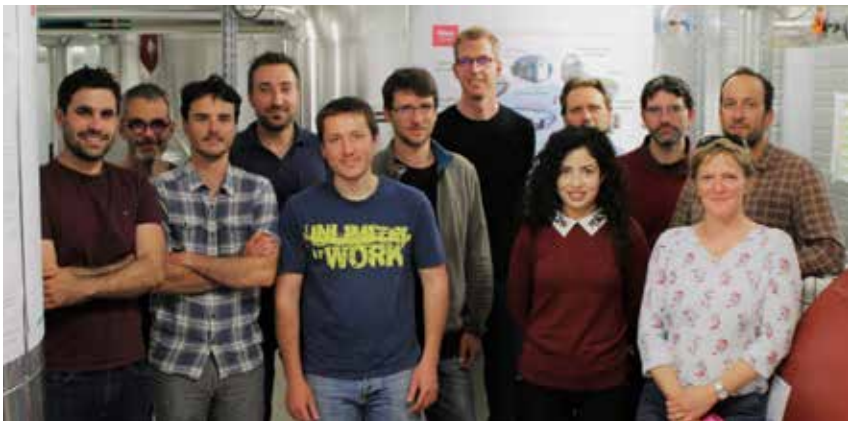

DISTRICT-HEATING RESEARCH TEAM (from left to right) N. Lamaison, J.-F. Robin, A. Aurousseau, C. Paulus, R. Joubert, F. Lefrançois, R. Bavière, N. Aoun, M. Vallée, F. Bruyat, D. Bourdon, M. Descamps

HEAT-STORAGE RESEARCH TEAM (from left to right) G. Matringe, R. Couturier, B. Lagorsse, S. Vésin, F. Bentivoglio, O. Soriano

CONTACT roland. baviere@cea.fr

3. Integrating thermal solar energy on heating grids

In the field of solar DH we focus on the development of specific solar thermal collectors, system integration, control, detection and faults diagnosis, as well as the monitoring of demonstrators. We have contributed to the development of two new large solar collector technologies being respectively based on vacuum tubes and on flat plate technology associated to a multiport extrusion absorber. This work led to significant progress in internal hydraulic distribution thereby limiting the occurrence of partial stagnation. These collectors were

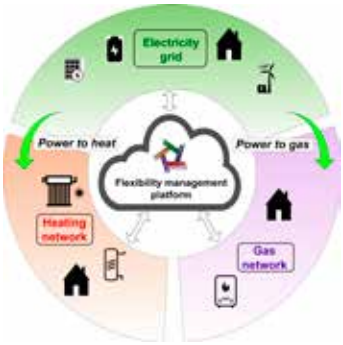

Fig. 1: Management of a Hybrid Energy Network using a flexibility platform (EU Project PENTAGON – [P1])

1/ *"Contenus CO_2 des réseaux de chaleur et de froid"*, Cerema, 2017
2/ "Scénario négatWatt 2011-2050: Hypothèses et Méthodes", Rapport technique négaWatt, mai 2014
3/ H. Lund et al., "4th Generation District Heating (4GDH)", Energy, vol. 68, (2014) 1–11.
4/ H. Lund et al., "Smart energy and smart energy systems", Energy, vol 137, (2017) 556-565.

then deployed on two demonstrators located in the French cities of Juvignac and Balma [1].
The PhD work of Gaelle Faure [T1] focused on faults detection and automated diagnosis of large-scale solar thermal installations with the target of helping to maintain nominal performances over their entire operating life. In this context, physical modeling in normal and degraded operation was realized and validated from experimental measurements (Fig. 2). The influence of various faults has been determined at the system scale [2], and automated fault detection methodologies have been developed [3].

4. Design and assessment of a bi-directional DH substation

A potential solution to increase the share of renewables in DH networks is to feed-in surplus solar heat produced by distributed consumers, in a similar manner as for photovoltaic solar panels and power grids. In the frame of the European Project THERMOSS [P2], an innovative substation (SST) allowing the bidirectional transfer of the heat, i.e. from the DHN to the consumer and vice-versa, has been specified and modeled. A prototype for a multi-family building is currently being assembled into the micro DHN facility of CEA-LITEN at INES.
The objective of the thermo-hydraulic modeling, based on the in-house Modelica[5] *DistrictHeating* library [4] was to find the most promising architecture and control strategy. Figure 3 presents simulated results of the bidirectional SST. Generally, the SST consumption is superposed with the building consumption. However, during periods of irradiation part of the solar heat is self-consumed, reducing the SST consumption. In periods of excess production, the heat is fed into the network, significantly increasing the share of useful solar heat.

5. Phase change materials for heat storage

A key hardware component for a smart DH is Heat Storage (HS). HS provides the following virtues: peak shaving, easing the integration of intermittent renewable and recovery energies like solar thermal and waste heat, increase the flexibility of sector coupling concepts (e.g. combined heat and power production plant, large scale heat-pump …) and improve the efficiency of generators sensitive to variable heat loads (e.g. biomass boiler). Decentralized HSs can also virtually strengthen a DH network by temporarily contributing to the satisfaction of heat demand despite limited network distribution capacity.
Besides our work on sensible HS (e.g. fluid stratification, energy management, multi-temperature level injection …), we focus on improving storage density using Phase Change Material (PCM). This paves the way to HS reaching 100 kW.h/m^3 while the traditional thermocline solution peaks at 30 kW.h/m^3. Researches carried out in our laboratory address on the one hand the PCM itself, on the other a concept of a shell and tube storage (Fig. 4) with particular attention payed on heat transfer behavior. At the end of 2018, we started-up a first demonstrator of a PCM HS in the Flaubert eco-district, in cooperation with the Grenoble DH operating company [P3]. The demonstrator uses a fatty alcohol as PCM and reaches 70 kW.h/m^3 (Fig. 5).
Our next step will be the integration of higher performance PCM such as sugar alcohols to reach densities above 100 kW.h/m^3. This requires the development of an additional crystallization promoter system. Two promising prototypes using an innovative bubbling technique have already been developed [T2].

6. The micro district-heating network facility

As part of an effort to assess the operation and management of DH networks, we have deployed a small scale DH network, located at INES premises. This experimental facility is representative of typical heating and cooling networks, in terms of assets and usage (Fig. 6).
In terms of technologies for heat generation, the district heating network is equipped with solar thermal panels, a gas boiler and a heat pump which produces heat and cold simultaneously. The heat is distributed to buildings using the

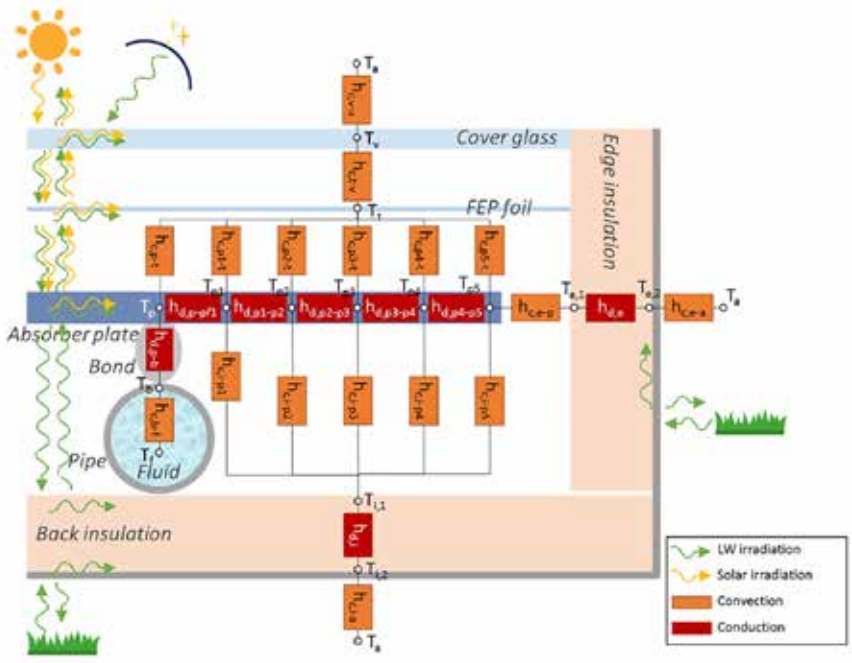

Fig. 2: Schematic representation of the model formulated to represent a solar collector in normal and degraded operation [T1].

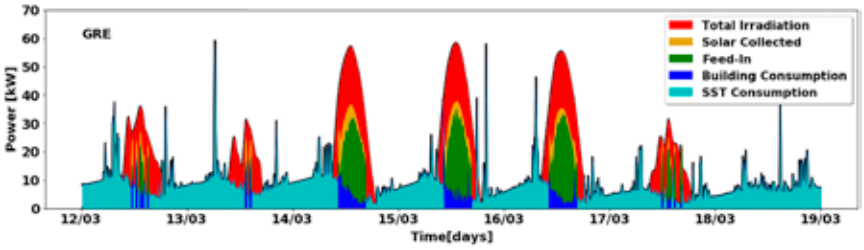

Fig. 3: Simulated weekly operation of the bidirectional substation, from [5] and [6].

5/ Modelica Association, *"Modelica- A unified Object-Oriented Language for Systems Modeling – Language Specification, Version 3.3 Revision 1"*, July 2014.

hot network. A thermocline water tank is used for storing the excess heat thereby allowing to shift heat loads. The facility is fully monitored and the experimental data can be used for the validation of numerical models which are developed in an in-house Modelica library called *DistrictHeating* [4].

7. Optimal temperature control of large scale district heating systems

Optimal temperature control of large scale DH systems is a domain in which our team has been recognized in the last 5 years. This success is rooted in the strong collaboration with the DH operator in Grenoble, which ranks second in energy in France and is amongst the large-scale DH networks in Europe. In such networks, distribution of heat to the final consumer can last several hours, so that temperature control is essential in order to minimize losses as well as to leverage the so called "network storage effect".
While leveraging this effect has long been a challenge, our team developed a model and software for providing DH operators with optimal temperature and differential pressure trajectories, optimizing costs while taking into account system constraints. This solution is based on fast and accurate simulation of the DH system as well as on the use of model predictive control (MPC). This solution was developed in several phases: first, the PhD work of Loic Giraud [T3] provided a demonstration at the scale of a small district. Second, this algorithm has been generalized and scaled to the city level, taking into account a more complex and meshed network structure as well as multiple heat injection points [7]. Third, the models and algorithms have been integrated into a package software, called PEGASE, allowing operational use [8]. This work has received a prize at the DHC student award in 2016 [9]. Applications to other large-scale district heating networks are under development.

8. Flexible control of space-heating demand

In DH systems, similarly to other energy networks, the demand of consumer often follow similar patterns, leading to peak consumption at given points in time. Demand-side management (DSM) is a way of better matching production and demand, without requiring heavy investment in storage. In the context of DH networks, DSM could be particularly efficient if space-heating could be controlled: flexibility could be provided to the network, without impacting inhabitants comfort thanks to the inherent thermal inertia in buildings.

Our team has been conducting research in this area with an innovative approach, allowing DH operators to perform DSM at the level of substations, without requiring them to operate inside buildings. In particular, the PhD work of Nadine Aoun [T4] has provided a strategy for modeling [10] and identifying a building model [11,12] only with data available at substations. In particular, no measurement inside buildings is required. It has also been shown that such an identified building model is accurate enough to design an efficient controller able to minimize energy costs while guaranteeing thermal comfort inside the building [13]. This line of work has been protected by two patents [14,15], and is currently being implemented in a demonstrator building in the city of Grenoble in the context of the City-Zen project [P1]. □

Fig. 4: View of the PCM HS demonstrator [P3]– before PCM filling.

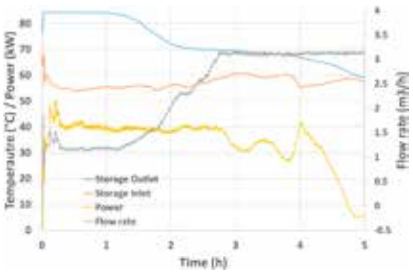

Fig. 5: Operational conditions observed during a 40 kW discharge test with the PCM HS demonstrator [P3].

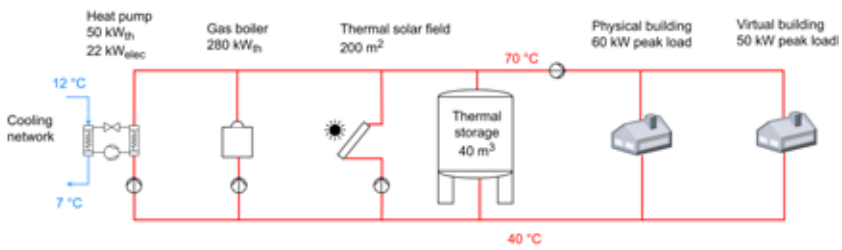

Fig. 6: CEA-LITEN district heating network at INES (Chambéry neibourghoud).

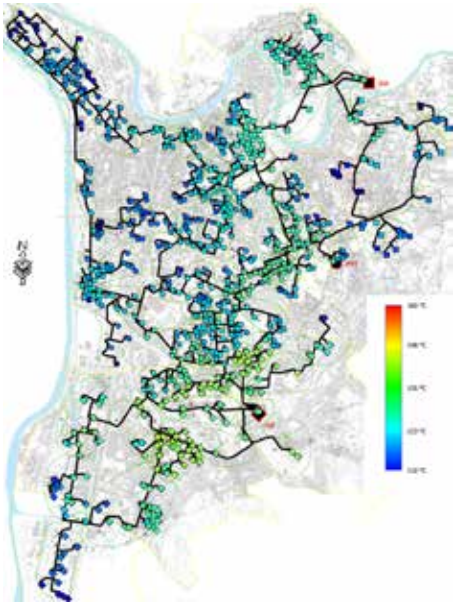

Fig. 7: Screenshot of the optimal temperature control application, based on the Pegase framework, for the Grenoble DH network.

Papers

[1] C. Paulus et al., *Monitoring results for the two first solar plants on district heating network in France: Balma Gramont and Juvignac,* SDH International Conference, Billund, Sept. 2016.

[2] G. Faure et al., *Modelling Faulty Behaviours of large solar thermal systems,* 5th International Solar District Heating Conference, Graz (Austria), 11-12 April 2018.

[3] G. Faure et al., *A methodology to analyse fault effect on large solar thermal system behavior,* 31st International Conference on Efficiency, Cost, Optimization, Simulation and Environmental Impact of Energy System - ECOS 2018, Guimarães (Portugal), 17-22 June 2018.

[4] L. Giraud et al., *Presentation, Validation and Application of the DistrictHeating Modelica Library,* 11th International Modelica Conference ,Versailles, France, 21-23 Sept. 2015.

[5] N. Lamaison et al., *A multi-criteria analysis of bidirectional solar district heating substation architecture,* SWC/SHC, Abu Dhabi, 2017.

[6] N. Lamaison et al., *Modelling and Simulations of solar two-way substation,* Solar District Heating SDH, Graz (Austria), 2018

[7] R. Bavière et al., *Optimal Temperature Control of Large Scale District Heating Networks,* 16th International Symposium on District Heating and Cooling - DHC2018, Hamburg, 9–12 Sept. 2018.

[8] M. Vallée et al., *An efficient co-simulation and control approach to tackle complex multi-domain energetic systems: concepts and applications of the PEGASE platform,* in Proc. of ECOS 2019 - 32nd Int. Conf. on Efficiency, Cost, Optimization, Simulation and Environmental Impact of Energy Systems –ECOS 2019, Wroclaw (Poland), 23-28 June 2019.

[9] L. Giraud, *A global control method of district heating systems based on production and distribution optimization*, 4th International DHC + Student Awards, Frankfurt, 19-21 April 2016.

[10] N. Aoun et al., *Sensitivity analysis of internal heat gains and furniture thermal inertia on demand in district heating systems,* Smart Energy Systems and 4th Generation District Heating, Copenhagen, 12-13 Sept. 2017.

[11] N. Aoun et al., *Load shifting of space-heating demand in district heating systems based on a reduced-order building model identifiable at substation level*, 4th International Conference on Smart Energy Systems and 4th Generation District Heating, Aalborg, 13-14 Nov. 2018.

[12] N. Aoun et al., *Development and assessment of a reduced-order building model designed for model predictive control of space-heating demand in district heating systems,* in Proc. of 32nd Int. Conf. on Efficiency, Cost, Optimization, Simulation and Environmental Impact of Energy Systems - ECOS 2019, Wroclaw (Poland) 23-28 June 2019.

[13] N. Aoun et al., *Modelling and flexible control of building space-heating demand in district heating systems,* submitted to Energy.

[14] M. Vallée and R. Bavière, "*Procédé de détermination de la capacité de délestage d'un bâtiment exploitant l'inertie thermique, procédé de délestage associé et système mettant en œuvre lesdits procédés*", Patent EN1663218, Dec. 2016.

[15] M. Vallée and R. Bavière, *"Procédé de contrôle d'une puissance thermique à injecter dans un système de chauffage et système de chauffage mettant en œuvre ce proceed",* Patent EN1860428, Nov. 2018.

PhD Thesis

[T1] "Étude de défauts critiques des installations solaire thermique de grande dimension : définition, modélisation et diagnostic", Gaelle Faure, Univ. Grenoble Alpes, 2018.

[T2] "Modélisation thermique de la cristallisation des alcools de sucre pour le stockage par Matériau à Changement de Phase". Louis Piquard, PhD, Univ. Lyon 1, on going.

[T3] "Modélisation dynamique et gestion avancée de réseaux de chaleur", Loïc Giraud, PhD, Univ. Grenoble Alpes, 2016.

[T4] "Modelling and flexible control of space heating demand in District Heating networks", Nadine AOUN, PhD, on going.

Projects

[P1] H2020 "Pentagon project", http://www.pentagon-project.eu/, dec 2016 – dec 2019

[P2] H2020 "Thermoss project", https://thermoss.eu/ , jan 2017 - jun 2020

[P3] FP7 "City-Zen Project", http://www.cityzen-smartcity.eu/fr/home-fr/, mar 2014 – Nov 2019

VALIDATION OF A VERSATILE MODEL OF THERMOCLINE THERMAL ENERGY STORAGE

Energy storage is one of the most promising ways to enhance the penetration of intermittent energy sources in power grids while ensuring electricity supply, as well as ensuring better thermal efficiency of many industrial processes. Dual media thermocline thermal storage, based on the use of inexpensive solid material as storage media, is considered to be a very promising way to store thermal energy. However, to achieve that, deep understanding of the internal behaviour of such storage and precise evaluation of its performances are needed. These two issues have been studied both experimentally and numerically.

Despite its advantages, dual-media thermocline thermal energy storage was considered to be too much "unpredictable and uncontrollable", which negates any potential benefits and use. Before any development, deployment and integration of such storage, it was necessary to assess our capability to control and predict the performances of dual-media thermocline. A 3 m^3 prototype of dual-media thermocline (rock and oil) has been built and tested at CEA-LITEN. The extensive testing procedure (hundreds of experimental tests and thousands of hours of operation) leads us to a deep understanding of the behaviour of dual-media thermocline. At the same time, a simplified numerical model was developed to simulate the experimental results. A specific focus was given to the enhancement of the numerical simulation of dual-media thermocline in the frame of a PhD work defended in 2018. The model has been compared to internal experimental results as well as to many experimental results available in the literature.

The work mentioned here has highlighted the dimensionless behaviour of dual-media thermocline, i.e. kind of general behaviour and trends, irrespective of the operating conditions and storage characteristics This is clearly illustrated in Figure 1 with dimensionless experimental results obtained by CEA and by CNRS teams [1]: despite the differences in temperature, in the solid medium and so on, performing similar tests on both setups leads to dimensionless similar results. Greatest development lies in a versatile numerical model [2] applicable to all kind of dual-media thermocline, i.e. for liquid and gaseous heat transfer fluid, from low to very high operating temperature (20 °c up to 1000 °C), for small to large scale prototype (less than 1 m^3 up to thousands of m^3) and so on. As illustrated in Figure 2, this model has been validated on very large and different ranges of operating parameters. Thus, it can be used now with a high degree of confidence. In Figure 2, geometries of the thermal storage setups are represented using a single scale to illustrate the large range of dimensions encountered and used for the model validation. Further work will deal with the lack of data on scale-1 demonstrators and out-of-design values as it is the case in the experimental field of dual-media thermocline. □

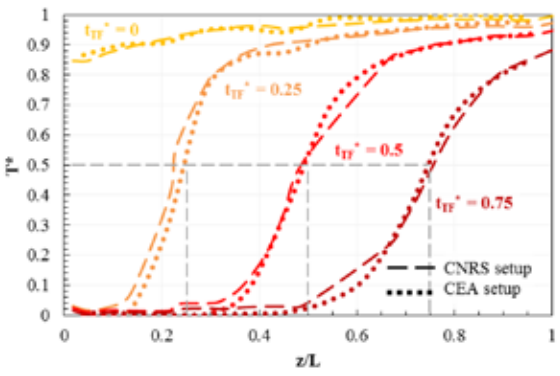

Fig. 1: Dimensionless behaviour of dual-media thermocline obtained on CEA and CNRS setups. T*, z* and t_{TF}* are respectively dimensionless parameters for temperature, axial coordinate in flow direction and relative thermal front velocities.

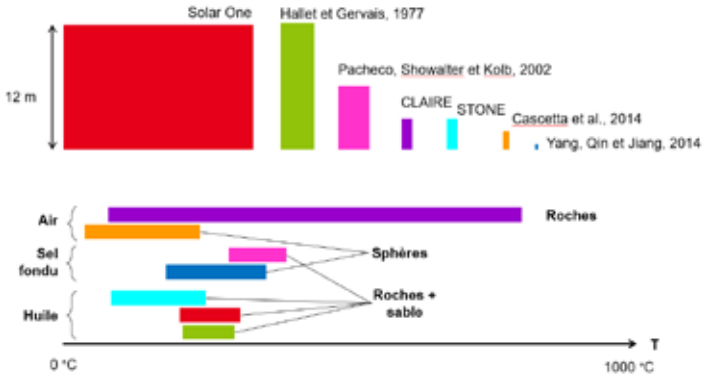

Fig. 2: Validation ranges of the versatile numerical model for dual-media thermocline.

[1] T. Esence et al., AIP Conference Proceedings, vol. 2033, (2018) 090006.
[2] T. Esence et al., Renewable Energy , vol. 133, (2019) 190204.

TEAM Arnaud BRUCH, Raphaël COUTURIER, Thibaut ESENCE
PARTNERS PROMES (Perpignan)
CONTACT arnaud.bruch@cea.fr

THERMODYNAMIC COMBINED CYCLE FOR COOLING AND ELECTRICITY PRODUCTIONS

The TRICYCLE project aims at studying and developing a thermodynamic heat recovery cycle for combined production of cooling and electricity (5 kW of cold and 1 kW of electricity) from a low-temperature (80 °C to 160 °C) heat source, which can be industrial heat, heat networks or non-concentrated solar thermal.

On the one hand, we develop numerical models of a combined cycle for cooling and power production. It consists of an expander integrated into a water-ammonia absorption cycle. In comparison to the serial architecture, the parallel architecture is more versatile for co-production [1]. The first objective focuses on the performance of a scroll-type expander for varying water/ammonia fraction of the expanded fluid and its input temperature in the scroll. For such purpose, the steady-state flow equations of the cycle model are solved. Besides, a dynamic model is introduced for the same cycle. This model is based on Modelica language using TIL suite library (www.tlk-thermo.com/index.php). Dynamic simulations are run to foresee the response of the expander and global cycle performances in transient conditions such as start, stop or change of operating point. On the other hand, three experimental devices available in the laboratory supported the numerical study: two Organic Rankine Cycles to qualify different components producing power, and an absorption chiller to manage cooling production. This last prototype will now welcome new components to complete the prototype of the TRICYCLE machine: a tailor made expander and a new generator. The final cycle is illustrated in Fig. 1.

The rectification of the water/ammonia fraction is an essential process in water/ammonia absorption chillers to enhance the performance of the cooling production. While running static simulations of the TRICYCLE cycle, we were also able to test the effect of the rectification on the power production. Even with pure ammonia having a better expansion potential than water/ammonia, the simulations show that the rectification tends to decrease the power production performance due to the reduction of the flow rate the rectification involves. The combination of the static cycle model with a genetic algorithm allowed us to perform a dual optimization of cooling and power productions operating either separately or simultaneously. The graph on Fig. 2 illustrates the expected production capacity for the different production modes. In addition, the dynamics analysis performed with high-level numerical tools highlighted the high sensitivity of the system inertia to the volume of the heat exchangers. From those numerical results supported with experimental characterizations, we designed an expander able to produce work with ammonia as operating fluid. Measurements on the complete TRICYCLE prototype will enable us to a better understanding of the functioning of the machine as well as to validate the simulation results. More complex architectures are also under investigation; the better are to be patented. □

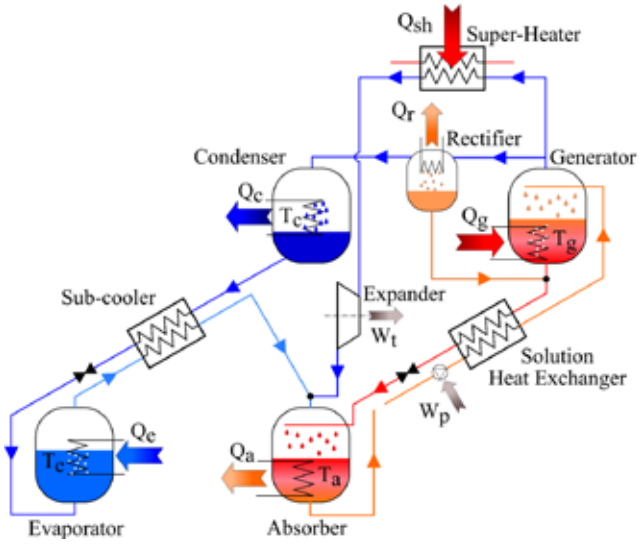

Fig. 1: TRICYCLE cycle.

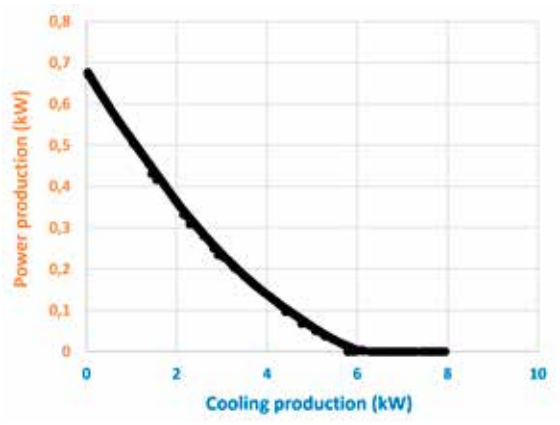

Fig. 2: Dual optimization of power and cooling production.

[1] L. C. Mendoza, Appl. Therm. Eng., vol. 72, (2014) 258–265.

TEAM Amélie MAISSE, Bertrand CHANDEZ, Brigitte GONZALEZ, François BOUDEHENN, Jérôme BENTIVOGLIO, Hai Trieu PHAN, Nicolas TAUVERON, Nicolas VOELTZEL, Mathilde WIRTZ, Quentin BLONDEL
PARTNERS LOCIE (Bourget-du-Lac)
CONTACT haitrieu.phan@cea.fr

DYNAMIC MODELING OF BUILDINGS TO SIMULATE THE INTERCONNECTION WITH ENERGY GRIDS

The interconnection between buildings and energy grids is currently shifting: the former are becoming energy consumer and producer when the latter are more and more powered by intermittent sources. This situation needs new design and control strategies for a global optimization. This can only be done with appropriate tools like suitable buildings models for this context.

So far, hypothesis about the buildings/grids interconnections were simplified: infinite sources or load profiles. A dynamic interaction must now be taken into account. The main issues are as follows:

- Scientists and engineers work with different software tools. It would be burdensome to translate every existing model for every existing software. The proposed solution is to turn existing building models into interoperable models.
- Increasing models complexity will increase computing times. The impact of models complexity on results and computing times must be evaluated in order to find the appropriate compromise for each possible case study.

We are working on a library gathering reference interoperable buildings and thermal systems models that can be easily used for studies of interconnection with energy grids. The connection between the experimental heat network and the four experimental houses at INES campus will then be simulated using the models from this library.

The library, called « BASTET », was created. The Fonctional Mock-up Interface (FMI) standard has been chosen to offer an interoperable version of each reference model of the library. This standard defines a common interface which enables to encapsulate a dynamic model as a "black box". This way, a Functional Mock-up Unit (FMU) of each reference model can be operated by any co-simulation software. First trials of co-simulations with well-known model were carried out. The objective is to have a first evaluation of the impact of using FMUs on simulation results and computing times. A reference dynamic model of a Solar Combisystem supplying Domestic Hot Water and Space Heating to a Single Family House has been split into several FMUs and simulations were run on different co-simulation tools. The main observations are that results are generally close to the reference case when using FMUs but simulation times can soar, according to the number and type of FMUs involved and the co-simulation tool used (Fig. 1). FMUs should thus be used sparingly. The next steps are the modeling of the experimental houses district with FMUs from the BASTET library and finally the connection with the experimental heat network model, developed with another library from the "district heating" team of the LITEN (Fig. 2). □

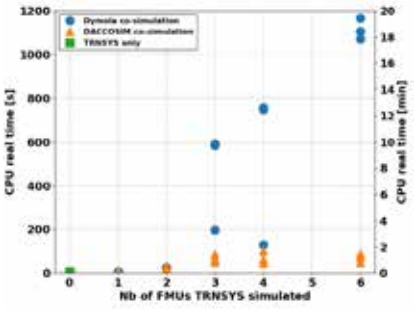

Fig. 1: Example of the impact of the number of FMUs and the co-simulation tool used on the computing time

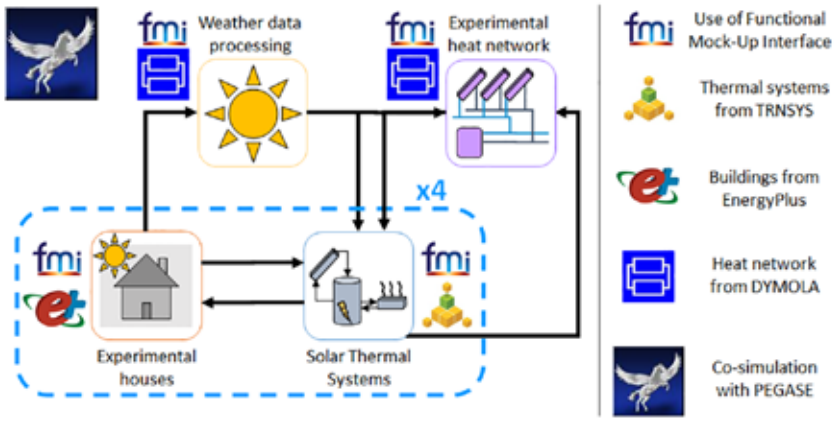

Fig. 2: Diagram of the final target model and the different software tools involved

TEAM Roland BAVIERE, Pauline BRISCHOUX, Antoine LECONTE
PARTNERS LOCIE (Bourget-du-Lac), G2ELAB (Grenoble)
CONTACT antoine.leconte@cea.fr

DYNAMIC PREDICTION OF A BUILDING INTEGRATED PHOTOVOLTAIC SYSTEM THERMAL BEHAVIOR

For Net Zero Energy Building (NZEB) design, Building Integrated Photovoltaic systems (BIPV) predictive thermal models require great accuracy to ensure an energy demand balance. Nevertheless, existing models need time-consuming refined discretization levels for each specific system. We developed and validated a dynamic model independent of detailed knowledge of system geometry.

BIPV systems aim to replace standard construction materials (tiles, claddings...). They are widely considered to respond to most of NZEB energy needs and optimal energy performance. Thus, a great accuracy of systems predictive thermal models is necessary considering also their interaction with building. Indeed, existing simplified models give reasonable estimation of photovoltaic modules performance. Nevertheless, they are inadequate to represent building integration effects (module heating, airflow...). Moreover, accuracy of detailed models depends upon a time-consuming high level of discretisation of each system geometry that is often unknown [1]. We developed a dynamic two-dimensional thermal model, including photovoltaic modules, their integration structure and the roof insulation layer [2]. A nodal approach and relevant hypotheses to shortlist main heat exchanges allowed reducing simulation time, discretization level and dependency to configuration. We first validated this model on some weeks with a test bench of a partially integrated rooftop BIPV installation in France. Then, to optimize heat transfer coefficients, CEA compared the calculated heat dissipation of the system with the ones obtained using a Nominal Operating Cell Temperature (NOCT) model and measured data. Finally, a test bench of a fully integrated rooftop installation permitted to assess the model flexibility for different configurations.

The validation of the model and of the heat dissipation (equivalent thermal resistance and heating) calculated for the partially integrated BIPV system has confirmed the choice of correlations. Compared to the NOCT model, our model results and the measured ones are close (figure 1). Then, the model validation with a fully integrated system has demonstrated its utility for different architectures. The discretization could be limited to only ten finite volumes. Its mean bias error of 2.71 °C for module temperature is satisfactory (figure 2). Therefore, the model could be useful for design studies requiring temperatures prediction based on few BIPV geometry information. It could also be important for future regulations and business models such as self-consumption. Future work will consider other installations (façade, sun shading elements...) and coupling to an electrical model. Preliminary results of energy production indicate an accuracy of 4.7% using a simplified electrical model. □

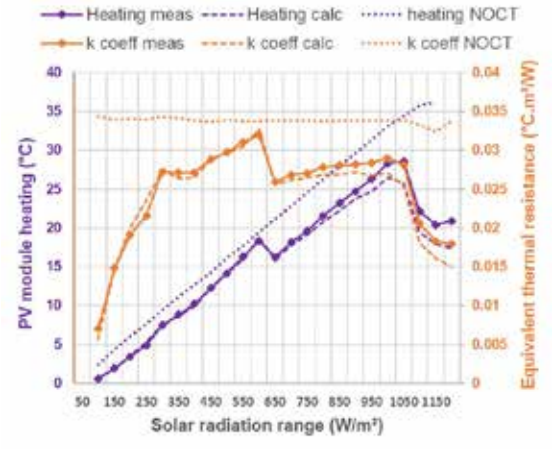

Fig. 1: Measured (solid lines) and calculated (dashed lines) aggregated heating and equivalent thermal resistance using CEA model and a NOCT model (50 W/m² range in incident radiation).

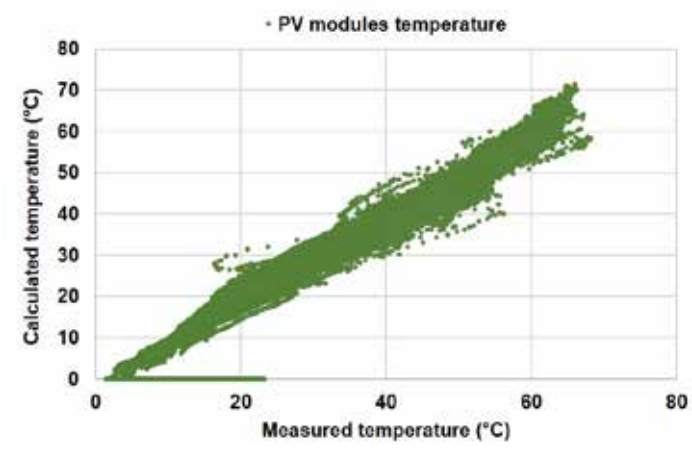

Fig. 2: Calculated PV modules temperature according to measured temperatures on a month for the fully integrated BIPV system.

[1] Y. B. Assoa, et al., Solar Energy, vol.155, (2017) 1289–1299
[2] Y. B. Assoa, et al., Applied Energy, vol. 214, (2018) 73–82

TEAM Ya Brigitte ASSOA, Nicolas NEGRI, François SAUZEDDE
PARTNERS CSTB (Saint-Martin d'Hères), LOCIE (Bourget-du-Lac), TransEnergy, Cythelia Energy
CONTACT ya-brigitte.assoa@cea.fr

STUDY OF THE DEGRADATION OF CATALYSTS FOR CO_2 METHANATION

Power-to-gas technologies, combining hydrogen produced by water electrolysis with carbon dioxide to produce substitute natural gas, can support the increased penetration of renewable electricity sources. The JUPITER 1000 project aims to build and operate a Power to Gas pilot plant (1 MW). In this project, we qualify and study efficient and resistant catalysts for methanation reactors.

The reaction of hydrogen and CO_2 to produce methane (Substitute Natural Gas) requires the use of catalyst. However, in practice, a gradual degradation of the performance of this catalyst is generally observed and is attributed to the high temperatures (350-700 °C) resulting from the heat produced by the reaction. The objective of the study is to determine the degradation mechanisms of a nickel on alumina catalyst to be able to specify a catalyst formulation adapted to the application, and to predict its lifetime. In particular, it is essential to know how the conditions (temperature, duration, partial pressure of H_2O and H_2) of catalyst use affect the evolution of its structure (active surface, particle size), and how this structure is related to the kinetics. In the frame of the JUPITER 1000 project and the research work of a PhD student, Isabelle Champon, two complementary approaches are implemented:

- A technological approach, through the development of aging test facilities equipped with single channel reactors that represent the behavior of a real multi-tubular reactor. The interactions between the reactive channel and the catalyst are studied by the mean of temperature and gas composition measurements.
- A scientific approach through the determination of kinetic laws on a fresh catalyst, the characterization of the structure and the activity of catalysts aged under controlled non-reactive hydrothermal conditions, and the introduction of a law of degradation in the kinetic model.

Three commercial catalysts have been tested under reactive conditions using the aging test facilities during 1000 hours. It appeared that the method of manufacture and the stability of the ceramic support of the catalyst are key points in the search for stability of the performances. The short-term aging of the catalyst selected for the Jupiter 1000 pilot plant has been qualified under stationary conditions. Focusing on this catalyst, in a first step, the kinetics of the 3 main reactions have been determined by analytical isothermal reaction tests carried out on a fresh catalyst [1]. In a second step, the alteration of the kinetics has been quantified on samples aged under controlled conditions of temperature, water pressure and hydrogen, which proved to be the main parameters. A law of variation of the activity of the catalyst has been established and implemented in a previously developed dynamic 2D reactor model [2]. This implementation allowed us to reproduce the performance decrease and the evolution of the temperature profile observed experimentally along a reactor channel (Fig. 1). The results of this study will give us the ability to specify efficient catalysts adapted to the specific constraints of CO_2 methanation, and to design reactors that promote catalyst life-time. □

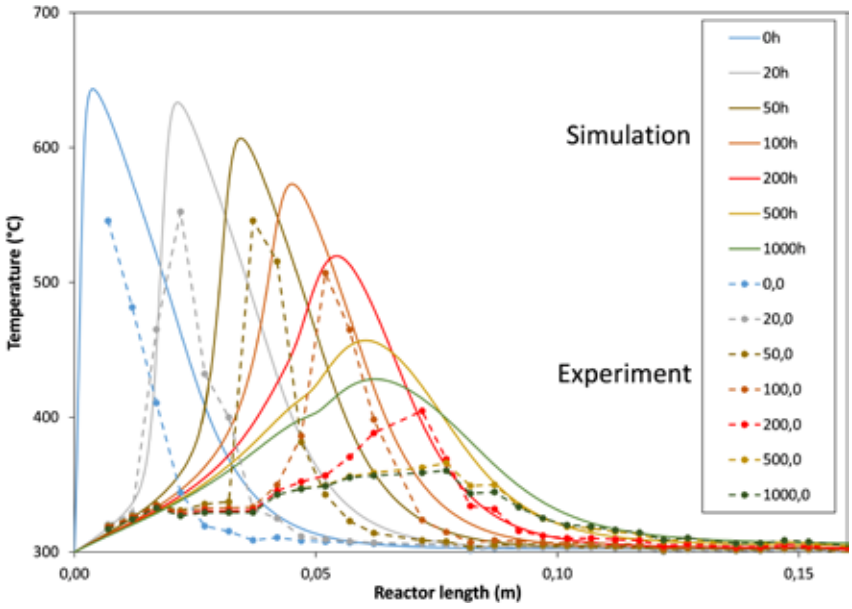

Fig. 1: Evolution of the temperature profile along a reactor channel due to the catalyst aging.

[1] I. Champon et al., J. CO_2 Util., vol. 34 (2019) 256–265.
[2] R. Try et al., AIChE J., vol. 64 (2018) 468–480.

TEAM Alain BENGAOUER, Albin CHAISE, Isabelle CHAMPON, Alban CHAPPAZ, Julien CIGNA, Geneviève GEFFRAYE, Michel JOUVE, Isabelle MORO, Benoit SOMMACAL
PARTNERS ICPEES (Strasbourg), ATMOSTAT; GRTgaz; ADEME
CONTACT albin.chaise@cea.fr

EXPERIMENTAL AND NUMERICAL PERFORMANCE EVALUATION OF CO_2 METHANATION REACTORS

Power-to-gas technologies, combining hydrogen produced by water electrolysis with carbon dioxide to produce substitute natural gas, can support the increased penetration of renewable electricity sources. Smaller scale and more compact and cost effective methanation reactors, operating under unsteady operation due to fluctuating availability are required. We are involved in the design, manufacturing and qualification of methanation reactors at laboratory and pilot scale.

The temperature control within a methanation reactor is a key point as temperature must be limited according to the thermodynamics on an exothermic reaction to ensure a high CO_2 conversion and methane selectivity, and to prevent catalyst thermal deactivation, but must be high enough to provide a high catalyst productivity. At the laboratory scale, an experimental performance comparison of three catalytic methanation reactor concepts, a fixed-bed reactor, a millistructured reactor (Fig.1), and a metallic foam reactor has been performed with the same nickel/alumina catalyst. The response of each reactor was analyzed in light performance criteria, representing the methane yield, space time yield (product of the yield by the Gas Hour Space Velocity GHSV), and the maximum temperature elevation [1]. For the millistructured reactor, a multidimensional heterogeneous and dynamic model has been developed based on mass, energy and momentum balances in the gas phase and mass and energy balances in the catalyst phase. The dynamic behavior of this reactor is simulated for transient variations in inlet gas temperature, cooling temperature, gas inlet flow rate and outlet pressure [2-3].

The operating conditions (Temperature, Pressure, GHSV, Yield) retained for comparison are respectively (225 °C, 0.4 MPa, 2630 h^{-1}, 0.83) for the annular fixed bed reactor, (280 °C, 0.25 MPa, 15 800 h^{-1}, 0.82) for the millistuctured reactor and (325 °C, 1.5 MPa, 2700 h^{-1}, 0.65) for the metallic foam reactor. The millistructured reactor channel showed better performances than the other reactor channels for the space time yield criteria due to a high volume productivity but shows a significant temperature elevation. On the other hand, the metallic foam reactor shows a very good heat management and a limited load of catalyst, but shows a poor productivity. Both the concepts can be scaled-up to the pilot and demonstration size by using cost effective manufacturing routes and catalysts. Dynamic simulations of the millistructured reactor channel shows that wrong-way behaviors can occur for abrupt temperature changes. Conversely, temperature ramp changes enable to attenuate and even fade the wrong-way behavior. Traveling hot spots appear only when the change of an operating condition shifts the reactor from an ignited steady state to a non-ignited one (Fig.2). Experimental evidences of these traveling hot spots have been obtained, confirming these numerical results. Operating conditions avoiding these traveling hot spots potentially detrimental to the catalysts are proposed [3]. □

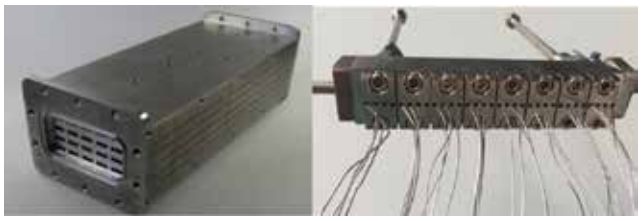

Fig. 1: the multi-tubular (right) and the single channel (left) fixed-bed reactor-exchangers.

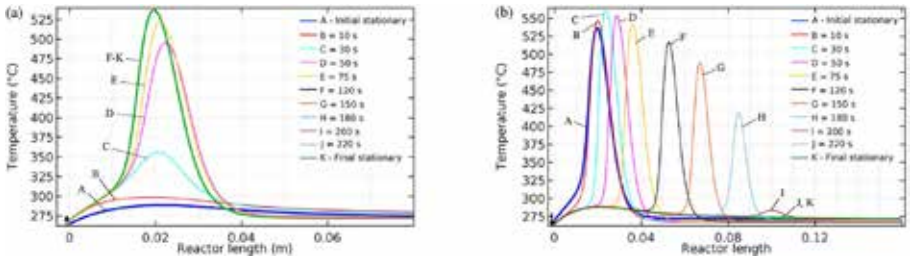

Fig. 2: Axial reactor temperature profiles with respect to time at 0.4 MPa: **(a)** Tc positive step from 265 °C to 270 °C; **(b)** Tc negative step from 270 °C to 265 °C.

[1] A. Bengaouer et al., J. Chem. Eng., vol. 96, (2018) 1937-1945.
[2] R. Try et al., AIChE, vol. 64, (2018) 468-480.
[3] R. Try, PhD Thesis, University of Lyon, 2018.

TEAM Alain BENGAOUER, Albin CHAISE, Isabelle CHAMPON, Alban CHAPPAZ, Julien CIGNA, Geneviève GEFFRAYE, Michel JOUVE, Isabelle MORO, Benoit SOMMACAL, Rasmey TRY
PARTNERS ICPEES (Strasbourg), LAGEP (Lyon), ATMOSTAT
CONTACT alain.bengaouer@cea.fr

FIRST STEP TO ACCOUNT FOR UNCERTAIN PARAMETERS IN MULTI-ENERGY SYSTEM DESIGN

Techno-economic optimization of remote microgrids using renewable power sources require dynamic simulation tool to account for the variability of use conditions. A two-step global sensitivity analysis implemented between simulation and uncertainty software shows the first exhaustive quantification of the impact of uncertain techno-economic parameters on the resulting cost of energy.

Techno-economic analysis of remote microgrids using renewable power sources require dynamic simulation to account for (i) the variability of sources and demands, (ii) the resultant necessity of storage and (iii) the presence of multiple energy carriers. Simulation tools can model the operation of such remote power systems on a time horizon and compute resulting performance indicators, namely the Levelized Cost of Energy produced (LEC) and the load satisfaction through the Unmet Load indicator (UL). Design optimization minimizes both indicators by fitting system sizing parameters like renewable energy conversion and storage capacities on a unique Pareto Front. This information, however, is incomplete and misleading for the choice of optimal design as most techno-economic parameters are uncertain, as well as time series of sources and demands. Two approaches can avoid system oversizing and non-optimal LEC resulting from parametric sensitivity analysis performed on reduced parameter sets: the two-stage global sensitivity analysis (GSA) assessing sensitivity of an optimal design to uncertain techno-economic parameters, and the robust optimization (RO) yielding an optimal design accounting for these uncertainties. The following focuses on GSA, a theoretical framework to quantify uncertainties of parameters, propagate them and perform sensitivity analysis to determine most influent parameters using Morris and Sobol methods.

Coupling Odyssey, a simulation tool for remote power system developed at CEA-Liten, with Uranie, an uncertainty analysis platform developed at CEA-DEN, has enabled to set up the GSA method on an illustrative case. The remote power system modelled by Odyssey consists in a photovoltaic production, battery storage and hydrogen supply chain. Odyssey controls the system to meet the electrical demand during one year by control strategies to start or stop the electrolysis and fuel cell components, when the battery state-of-charge (SOC) reaches defined threshold. Figure 1 shows the strong impact of uncertain techno-economic parameters on the performance indicators (LEC and UL) for four selected design points of the initial unique blue Pareto Front. Moreover, the sensitivity analysis identifies the most responsible uncertain parameters for these dispersions in Figure 2. Next step will deal with RO approach to try improving the robustness of the optimal design by including uncertainties within the optimization process to get a so-called robust design. □

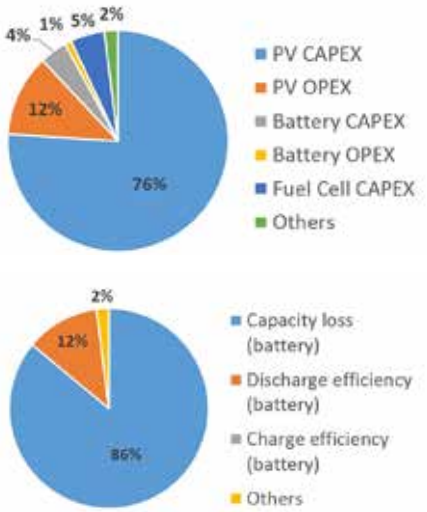

Fig. 2: Identification of the most influencing uncertain parameter for the design case 0; (a) Impact on Levelized Cost of Energy (b) Impact on Unmet Load

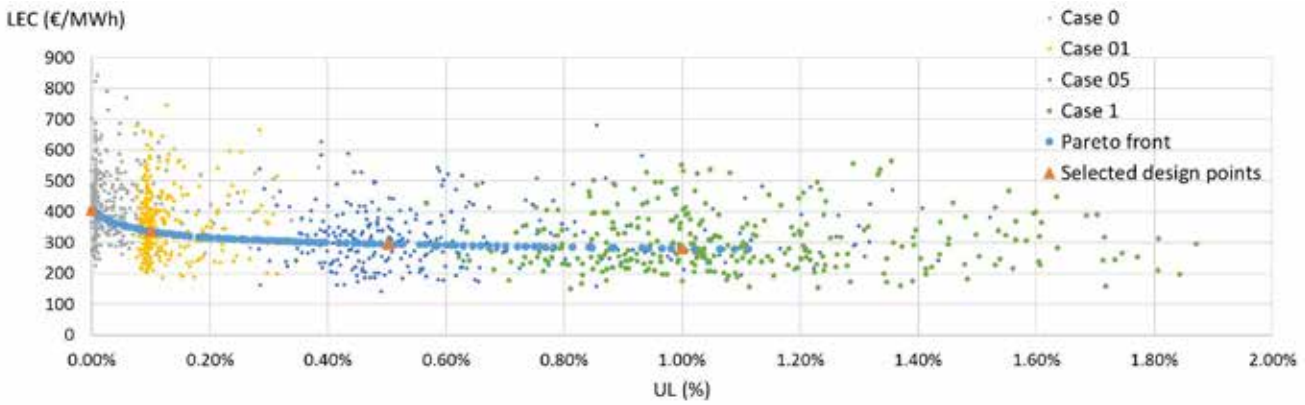

Fig. 1: Pareto front of optimal designs – Impact of uncertainty propagation for 4 selected designs.

[1] A. Nadal et al., Safety and Reliability - Safe Societies in a Changing World - Proceedings of the 28th International European Safety and Reliability Conf. ESREL 2018, Haugen et al. (Eds), (2018) 2627-2634.

TEAM Cyril BOURASSEAU, Amélia NADAL, Alain RUBY
PARTNERS G2Elab (Grenoble), GIPSA-lab (Grenoble)
CONTACT alain.ruby@cea.fr

SCIENTIFIC OUTPUTS

PHD DEFENSE AT LITEN

Matter & Materials

Gaella FRAJER
Syntheses, shaping and study of the frequency dependence of (NiZnCuCo) Fe2O4 ferrite magnetic properties, Univ. Grenoble Alpes
(01/01/2018)

Matthieu MAUNAY
Diffusion bonded heat exchanger: simulation of deformations and interface mechanical strength prediction, Univ. Grenoble Alpes
(06/04/2018)

Sophie CAILLIET
Ceramic object in stabilized zirconia by stereolithography for medical application, Univ. Grenoble Alpes
(15/10/2018)

Lorie DAVID
Hot filament-assisted chemical vapor deposition of carbon nanotube forests: growth kinetics and electrical performances, Claude Bernard Univ. at Lyon (22/10/2018)

Djadidi TOYBOU
Silver nanowires with controlled dimensions: synthesis, toxicity and manufacturing of transparent electrodes, Univ. Grenoble Alpes
(29/11/2018)

Vincent CHEVALIER
Purification of the air of the aeronautical cabins: elaboration of innovative adsorbents and understanding of their behaviors at sub-ppm concentrations of volatile organic compounds, Univ. Grenoble Alpes
(07/12/2018)

Amandine ARNOULD
Characterization of nanoparticles in sensitive media: application to organic and metallic nanoparticles, Univ. Grenoble Alpes
(20/12/2018)

Clara HADDAD
Manufacturing, electrical characterization and reliability of printed OTFTs on plastic substrate, Univ. Grenoble Alpes (20/12/2018)

Pierre LHERITIER
Study of PVDF derivatives for actuation purpose, Univ. Grenoble Alpes (09/10/2018)

Renewable energy

Mouhannad DBEISS
Mission profile-based accelerated ageing tests of SiC MOSFET and Si IGBT power modules in DC/AC photovoltaic inverters, Univ. Grenoble Alpes
(14/03/2018)

Sacha JUILLARD
Optimization of the interfaces of encapsulated OPV devices, Univ. Grenoble Alpes
(05/04/2018)

Ramzi SOUIDI
Studies of the physical and chemical properties of the surface of the silicon substrate after cutting in applications to solar cells, Univ. Grenoble Alpes
(26/06/2018)

Arthur LANTREIBECQ
Determination of the origin and nature of crystalline defects in solar silicon, Paul Sabatier Univ. at Toulouse
(20/09/2018)

Viet Huong NGUYEN
Development of transparent electrodes by vacuum-free and low cost deposition methods for photovoltaic applications, Univ. Grenoble Alpes
(08/10/2018)

Coralie AVENE
Durability of mirrors for concentrating solar power: study of aging modes, Clermont Auvergne Univ.
(16/10/2018)

Gaelle FAURE
Study of large solar thermal system critical faults: definition, modelling and diagnosis, Univ. Grenoble Alpes
(25/10/2018)

Arnaud RITOU
Development, manufacturing and characterization of ultra-high efficiency concentrated photovoltaic modules based on micro-concentrators, Univ. Grenoble Alpes
(22/11/2018)

Aziz SUZON MD-ABDUL
Pathways towards efficiency improvement of kesterite based solar cell, Univ. Grenoble Alpes
(03/12/2018)

Giri Wahyu ALAM
Influence of seeding and growth conditions on grain selection, defects, and properties of high-performance multi-crystalline silicon (HPmc-Si), Aix-Marseille Univ. (13/12/2018)

Energy storage and conversion

Guillaume LEFEVRE
Synthesis and electrochemical study of silicate materials for Li-ion batteries, Univ. Grenoble Alpes
(23/02/2018)

Alice ROBBA
Lithium-ion/sulfur batteries development and understanding of the working mechanism, Univ. Grenoble Alpes
(17/07/2018)

Xavier FLEURY
Correlation between degradation of internal components and operational safety of Li-ion batteries, Univ. Grenoble Alpes (26/10/2018)

Vincent CADIOU
Development of organic electrode materials for anionic battery, Nantes univ. (29/11/2018)

Baptiste VERDIN
Study of large surface area PEM WE electrodes: homogeneity of current distribution and innovative catalysts integration, Paris Saclay Univ.
(21/03/2018)

Bolahaga RANDRIANARIZAFY
Multi-physics modeling of startup and shutdown of a PEM fuel cell and study of the carbon support degradation: mitigation strategies and design optimization, Univ. Grenoble Alpes
(13/12/2018)

Maria GONZALEZ-MARTINEZ
Woody and agricultural biomass torrefaction: experimental study and modelling of solid conversion and volatile species release based on biomass extracted macromolecular components, Toulouse INP
(12/10/2018)

Clément VANNESTE-IBARCQ
Study of biomass powder flows in the gasification process, Toulouse INP
(15/11/2018)

Energy efficiency

Natalia SALAMON
Development of thermal energy harvesting systems, Univ. Grenoble Alpes (24/01/2018)

Lauren FARCOT
Design and analysis of a thermochemical heat storage process with separated reactor, Univ. Grenoble Alpes (09/03/2018)

Rasmey TRY
Experimental study and dynamic simulation of a catalytic reactor for the hydrogenation of CO2 into methane, Claude Bernard Univ. at Lyon
(22/03/2018)

Thomas BUSSER
Study of hydrothermal transfers in wood-based materials and their contributions to the interior environment of buildings, Univ. Grenoble Alpes (08/10/2018)

Kevin ATTONATY
Electricity storage system combining a high efficiency thermodynamic cycle with a high temperature thermal storage, Pau Univ. (25/10/2018)

Nahia SASSINE
Study of the thermo-mechanical behavior of granular media and medium-tank interactions, Univ. Grenoble Alpes (16/11/2018)

ALLARD Stéphane
Long-term development of the grid infrastructure and flexibility options in the electric system, Univ. Grenoble Alpes
(29/11/2018)

Franck MASTRIPPOLITO
Shape optimization of multi-scales and multi-physics problems: application to heat exchangers, INSA Lyon (14/12/2018)

Patricia CARBAJO JIMENEZ
Methodology for optimizing a new concept of hybrid water-air solar thermal system, Univ. Grenoble Alpes
(20/12/2018)

HABILITATED SCIENTISTS

Renewable energy

Sylvain RODAT
Concentration solar energy: Towards continuous energy production and material transformation processes
(07/06/2018)

Energy storage and conversion

Geert HAARLEMMER
Chemical engineering for advanced biofuels
(20/03/2018)

Arnaud MORIN
Towards the understanding of the components of the proton exchange membrane fuel cell... The importance of transport phenomena and other work (12/04/2018)

2018 PUBLICATIONS

Matter & Materials

1. Impact of a van der Waals interface on intrinsic and extrinsic defects in an $MoSe_2$ monolayer
C. J. Alvarez et al., Nanotechnology - DOI: 10.1088/1361-6528/aad66f

2. Oxidation of copper nanowire based transparent electrodes in ambient conditions and their stabilization by encapsulation: Application to transparent film heaters
C. Celle et al., Nanotechnology - DOI: 10.1088/1361-6528/aaa48e

3. Variability study of MWCNT local interconnects considering defects and contact resistances-Part II: Impact of charge transfer doping
R. Chen et al., IEEE Transactions on Electron Devices - DOI: 10.1109/TED.2018.2868424

4. Piezo-potential generation in capacitive flexible sensors based on GaN horizontal wires
A. El Kacimi et al., Nanomaterials - DOI: 10.3390/nano8060426

5. Impact of a model soil microorganism and of its secretome on the fate of silver nanoparticles
E. Eymard-Vernain et al., Environmental Science and Technology - DOI: 10.1021/acs.est.7b04071

6. Self-assembled uv photodetector made by direct epitaxial GaN growth on graphene
T. Journot et al., ACS Applied Materials and Interfaces - DOI: 10.1021/acsami.8b01194

7. Understanding electromigration in Cu-CNT composite interconnects: a multiscale electrothermal simulation study
J. Lee et al., IEEE Transactions on Electron Devices - DOI: 10.1109/TED.2018.2853550

8. In vitro dermal safety assessment of silver nanowires after acute exposure: tissue vs. cell models
S. G. Lehmann et al., Nanomaterials - DOI: 10.3390/nano8040232

9. A physics-based investigation of Pt-salt doped carbon nanotubes for local interconnects
J. Liang et al., Technical Digest – Int. Electron Devices Meeting IEDM - DOI: 10.1109/IEDM.2017.8268502

10. Insights into polythiol-assisted AgNP dissolution induced by bio-relevant molecules
M. Marchioni et al., Environmental Science: Nano - DOI: 10.1039/c8en00340h

11. Aging of silver nanocolloids in sunlight: Particle size has a major influence
S. Motellier et al., Environmental Chemistry - DOI: 10.1071/EN18056»

12. Electrical mapping of silver nanowire networks: a versatile tool for imaging network homogeneity and degradation dynamics during failure
T. Sannicolo et al., ACS Nano - DOI: 10.1021/acsnano.8b01242

13. A nanomaterial release model for waste shredding using a Bayesian belief network
N. Shandilya et al., Journal of Nanoparticle Research - DOI: 10.1007/s11051-018-4137-2

14. Silver nanowire networks for transparent film heaters: Synthesis nanoscale characterization and integration in functional devices
J.-P. Simonato et al., Abstracts of papers of the American chemical society

15. Chitosan-lipid nanoparticles (CS-LNPs): Application to siRNA delivery
O. Tezgel et al., Journal of colloid and interface science - DOI: 10.1016/j.jcis.2017.09.045

16. Challenges and Progress on Carbon Nanotube Integration for BEOL Interconnects
B. Uhlig et al., 2018 IEEE International Interconnect Technology Conference IITC 2018 - DOI: 10.1109/IITC.2018.8430411

17. Progress on carbon nanotube BEOL interconnects
B. Uhlig et al., Proceedings of the 2018 Design Automation and Test in Europe Conference and Exhibition - DOI: 10.23919/DATE.2018.8342144

18. The methodologies and strategies for the development of novel material systems and coatings for applications in extreme environments a critical review
M. Urbina et al., Manufacturing Review - DOI: 10.1051/mfreview/2018006

19. On the front and back side quantum efficiency differences in semi-transparent organic solar cells and photodiodes
B. Bouthinon et al., Journal of Applied Physics - DOI: 10.1063/1.5017030

20. Open-access pilot line to accelerate industrial uptake of hybrid printed electronics
M. Cauwe et al., 12th Smart Systems Integration 2018 - International Conference and Exhibition on Integration Issues of Miniaturized Systems, p. 31 – ISBN: 9781510867710

21. A large-area gravure printed process for P-type organic thin-film transistors on plastic substrates
M. Charbonneau et al., European Solid-State Device Research Conference - DOI: 10.1109/ESSDERC.2018.8486895

22. The formation of polymer-dopant aggregates as a possible origin of limited doping efficiency at high dopant concentration
J. Euvrard et al., Organic Electronics: physics materials applications - DOI: 10.1016/j.orgel.2017.11.020

23. Impact of unintentional oxygen doping on organic photodetectors
J. Euvrard et al., Organic Electronics: physics materials applications - DOI: 10.1016/j.orgel.2017.12.008

24. Toward a better understanding of the doping mechanism involved in Mo(tfd-COCF3)3 doped PBDTTT-c
J. Euvrard et al., Journal of Applied Physics - DOI: 10.1063/1.5029810

25. Lambert W-function based modelling of P-OTFTs and application to low temperature measurements
C. Haddad et al., Organic Electronics: physics materials applications - DOI: 10.1016/j.orgel.2018.06.037

26. A plastic electronic circuit based on low voltage organic thin-film transistors for monitoring the X-Ray checking history of luggage in airports
S. Lai et al., Organic Electronics: physics materials applications - DOI: 10.1016/j.orgel.2018.04.029

27. All-polymer integrated circuit for monitoring the x-ray checking history of luggage
S. Lai et al., Proc. of IEEE International Symposium on Circuits and Systems - DOI: 10.1109/ISCAS.2018.8351691

28. Actuation efficiency of polyvinylidene fluoride-based co- and ter-polymers
P. Lheritier et al., Polymer - DOI: 10.1016/j.polymer.2018.10.003

29. Near-field communication tag development on a paper substrate - Application to cold chain monitoring
A. Pereira et al., Flexible and Printed Electronics - DOI: 10.1088/2058-8585/aaaeca

30. Influence of hydrogen and oxygen impurity content in a natural gas / hydrogen blend on the toughness of an API X70 steel
L. Briottet et al., in Proc. of ASME 2018 Pressure Vessels and Piping Conference – DOI: 10.1115/PVP2018-84658

31. Study of magnetic properties of NiZnCu ferrite synthesized by Pechini method and solid-state reactions
G. Frajer et al., AIP Advances - DOI: 10.1063/1.4994035

32. Fabrication methods for high-performance miniature disks of Terfenol-D for energy harvesting
V. Issindou et al., Sensors and Actuators A: Physical - DOI: 10.1016/j.sna.2018.09.003

33. Prototyping and testing embedded transformer for 100W 1MHz GaN converter
M. Bohnke et al., in IEEE Proc. of 20th European Conference on Power Electronics and Applications (EPE 2018 ECCE Europe), p. 194 – ISBN: 978-90-75815-28-3

34. Hydrogen effect on the fatigue behavior of LBM Inconel 718
S. Puydebois et al., MATEC Web of Conferences - DOI: 10.1051/matecconf/201816502010

35. Anisotropic intergranular damage development and fracture in a 14Cr ferritic ODS steel under high-temperature tension and creep
H. Salmon-Legagneur et al., Materials Science and Engineering A - DOI: 10.1016/j.msea.2018.02.102

36. Dissolution Mechanisms of LiNi1/3Mn1/3Co1/3O2 Positive Electrode Material from Lithium-Ion Batteries in Acid Solution
E. Billy et al., ACS Applied Materials and Interfaces - DOI: 10.1021/acsami.8b01352

Renewable energy

37. Review of accelerated ageing test modelling and its application to solar mirrors
C. Avenel et al., Solar Energy Materials and Solar Cells - DOI: 10.1016/j.solmat.2018.06.024

38. Comprehensive performance assessment of a continuous solar-driven biomass gasifier
S. Chuayboon et al., Fuel Processing Technology - DOI: 10.1016/j.fuproc.2018.10.016

39. Experimental analysis of continuous steam gasification of wood biomass for syngas production in a high-temperature particle-fed solar reactor
S. Chuayboon et al., Chemical Engineering and Processing: Process Intensification - DOI: 10.1016/j.cep.2018.02.004

40. Solar chemical looping gasification of biomass with the ZnO/Zn redox system for syngas and zinc production in a continuously-fed solar reactor
S. Chuayboon et al., Fuel - DOI: 10.1016/j.fuel.2017.11.021

41. Accelerated aging test of solar reflectors according to the new AENOR standard - Results of a round Robin test
A. Fernández-García et al., AIP Conference Proceedings 2033 - DOI: 10.1063/1.5067231

42. Degradation of solar glass mirrors paints at marine outdoor site
M. Guerguer et al., AIP Conference Proceedings 2033 - DOI: 10.1063/1.5067232

43. Exposure conditions effect on soiling of solar glass mirrors
M. Karim et al., AIP Conference Proceedings 2033 - DOI: 10.1063/1.5067234

44. Survey of potential outdoor accelerated ageing systems for the characterization of CSP components' durability
A. Nijaoui et al., Proc. of 9th International Renewable Energy Congress (IREC 2018) - DOI: 10.1109/IREC.2018.8362548

45. Accelerated ageing tests for durability study of solar absorber coatings on metallic substrate for solar thermal energy (STE) application
O. Raccurt et al., AIP Conference Proceedings 2033 - DOI: 10.1063/1.5067239

46. Dynamic simulation of a Fresnel solar power plant prototype with thermocline thermal energy storage
S. Rodat et al., Applied Thermal Engineering - DOI: 10.1016/j.applthermaleng.2018.02.083

47. Development and application of a multi-domain dynamic model for direct steam generation solar power plant
A. Rousset et al., IFAC-PapersOnLine - DOI: 10.1016/j.ifacol.2018.04.008

48. The effect of initial growth interface on the grain structure in HPMC-Si ingot
G. W. Alam et al., Proc. of ICSEEA 2017 Int. Conf. on Sustainable Energy Engineering and Application - DOI: 10.1109/ICSEEA.2017.8267705

49. Bifacial crystalline silicon homojunction cells contacted with highly resistive TCO layers
E. Bruhat et al., AIP Conference Proceedings 1999 - DOI: 10.1063/1.5049267

50. Multiscale modeling and back contact design of bifacial silicon heterojunction solar cells
A. Campa et al., IEEE Journal of Photovoltaics - DOI: 10.1109/JPHOTOV.2017.2775155

51. Homo-heterojunction concept: From simulations to high efficiency solar cell demonstration
T. Carrere et al., Solar Energy Materials and Solar Cells - DOI: 10.1016/j.solmat.2018.03.027

52. Mechanical stirring influence on solute segregation during plane front directional solidification
M. Chatelain et al., International Journal of Thermal Sciences - DOI: 10.1016/j.ijthermalsci.2017.12.024

53. High Efficiency Hetero-Junction: From Pilot Line to Industrial Production
G. Condorelli et al., in Proc. of IEEE 7th World Conference on Photovoltaic Energy Conversion WCPEC 2018 - A Joint Conference of 45th IEEE PVSC 28th PVSEC and 34th EU PVSEC - DOI: 10.1109/PVSC.2018.8548197

54. An eco-design approach to the systemic integration of environmental aspects in the development of innovative photovoltaic solar systems
N. Gazbour et al., ECOS 2018 – Proc. of the 31st Int. Conf. on Efficiency Cost Optimization Simulation and Environmental Impact of Energy Systems - ISBN: 978-972-99596-4-6

55. A path to reduce variability of the environmental footprint results of photovoltaic systems
N. Gazbour et al., Journal of Cleaner Production - DOI: 10.1016/j.jclepro.2018.06.276

56. Stability enhancement of silver nanowire networks with conformal ZnO coatings deposited by atmospheric pressure spatial atomic layer deposition
A. Khan et al., ACS Applied Materials and Interfaces - DOI: 10.1021/acsami.8b03079

57. Efficiency limiting crystal defects in monocrystalline silicon and their characterization in production
F. Korsós et al., Solar Energy Materials and Solar Cells - DOI: 10.1016/j.solmat.2018.06.030

58. Impact of thermal history on defects formation in the last solid fraction of Cz silicon ingots
A. Lanterne et al., AIP Conference Proceedings 1999 - DOI: 10.1063/1.5049331

59. Spatial distribution of structural defects in Cz-seeded directionally solidified silicon ingots: An etch pit study
A. Lantreibecq et al., Journal of Crystal Growth - DOI: 10.1016/j.jcrysgro.2017.11.024

60. Conductivity and surface passivation properties of boron-doped poly-silicon passivated contacts for c-Si solar cells
A. Morisset et al., Physica Status Solidi (A) Applications and Materials Science - DOI: 10.1002/pssa.201800603»

61. Improvement of the conductivity and surface passivation properties of boron-doped poly-silicon on oxide
A. Morisset et al., AIP Conference Proceedings 1999 - DOI: 10.1063/1.5049280

62. Electron tunnelling through grain boundaries in transparent conductive oxides and implications for electrical conductivity: The case of ZnO:Al thin films
V. H. Nguyen et al., Materials Horizons - DOI: 10.1039/c8mh00402a

63. Elimination of oxidation-induced stacking faults in silicon single crystals using the kyropoulos crystal growth method
A. Nouri et al., Physica Status Solidi (A) Applications and Materials Science - DOI: 10.1002/pssa.201700961

64. Cellular dislocations patterns in monolike silicon: Influence of stress time under stress and impurity doping
V. A. Oliveira et al., Journal of Crystal Growth - DOI: 10.1016/j.jcrysgro.2018.03.002

65. Potential niobium base superalloys
F. Saint-Antonin et al., High Temperature Materials and Processes - DOI: 10.1515/htmp-2017-0023

66. Laser-induced BSF: A new approach to simplify IBC-SHJ solar cell fabrication
R. Vasudevan et al., AIP Conference Proceedings 1999(1) - DOI: 10.1063/1.5049287

67. Silicon bottom subcell optimization for wafer-bonded III-V on Si multijunction solar cells
L. Vauche et al., IEEE 7th World Conference on Photovoltaic Energy Conversion WCPEC 2018 - DOI: 10.1109/PVSC.2018.8547745

68. Plasma immersion ion implantation (PIII): New path for optimizing doping profiles of advanced phosphorus emitters
A. Veau et al., AIP Conference Proceedings 1999(1) - DOI: 10.1063/1.5049316

69. Output power simulation for CPV receivers based on experimental spectral matching ratio modelling
M. Benhammane et al., AIP Conference Proceedings 2012(1) - DOI: 10.1063/1.5053532

70. III-V-on-silicon solar cells reaching 33% photoconversion efficiency in two-terminal configuration
R. Cariou et al., Nature Energy - DOI: 10.1038/s41560-018-0125-0

71. Evaluation of III-V/Si multi-junction solar cells potential for space
R. Cariou et al., IEEE 7th World Conference on Photovoltaic Energy Conversion WCPEC 2018 - DOI: 10.1109/PVSC.2018.8547773

72. Influence of optics temperature on 3J solar cells efficiency in an off axis mirror system with secondary optics
R. Couderc et al., AIP Conference Proceedings 2012(1) - DOI: 10.1063/1.5053501

73. Power semiconductor ageing test bench dedicated to photovoltaic applications
M. Dbeiss et al., Proc. Of IEEE Applied Power Electronics Conference and Exposition - APEC - DOI: 10.1109/APEC.2018.8341407

74. Development of lightweight and flexible c-Si photovoltaic modules for the STRATOBUS™
J. Gaume et al., 2018 IEEE 7th World Conference on Photovoltaic Energy Conversion WCPEC 2018 - DOI: 10.1109/PVSC.2018.8548263

75. A cost-controlled highly efficient SiC-based current source inverter dedicated to photovoltaic applications
G. Lefevre et al., 20th European Conference on Power Electronics and Applications EPE 2018 ECCE Europe – ISBN: 978-1-5386-4145-3

76. Improved Matlab Simulink two-diode model of PV module and method of fast large-scale PV system simulation
T. Le et al., 7th International IEEE Conference on Renewable Energy Research and Applications ICRERA 2018 - DOI: 10.1109/ICRERA.2018.8566792

77. Does micro-scaling of CPV modules improve efficiency? A cell-to-module performance analysis
A. Ritou et al., Solar Energy - DOI: 10.1016/j.solener.2018.07.074

78. Comparing strategies for improving efficiencies in vacuum processed Cu2ZnSnSe4 solar cells
L. Grenet et al., Journal of Renewable and Sustainable Energy - DOI: 10.1063/1.5034526

79. Influence of the AlN interlayer thickness on the photovoltaic properties of in-rich AlInN on Si heterojunctions deposited by RF sputtering
S. Valdueza-Felip et al., AIP Advances - DOI: 10.1063/1.5041924

80. Mechanical reliability of flexible encapsulated organic solar cells: characterization and improvement
S. Juillard et al., ACS Applied Materials and Interfaces - DOI: 10.1021/acsami.8b06684

Energy storage and conversion

81. Model of lithium intercalation into graphite by potentiometric analysis with equilibrium and entropy change curves of graphite electrode
D. Allart et al., Journal of the Electrochemical Society - DOI: 10.1149/2.1251802jes

82. Diagnostic of failure mechanisms in Li/S rechargeable batteries using thermal micro-calorimetry technique applied to pouch and cylindrical type cells
C. Barchasz et al., Electrochimica Acta - DOI: 10.1016/j.electacta.2018.09.167

83. Investigation of Li+ cation coordination and transportation by molecular modeling and NMR studies in a LiNTf2-doped ionic liquid-vinylene carbonate mixture
E. Bolimowska et al., Journal of Physical Chemistry B - DOI: 10.1021/acs.jpcb.8b05231

84. Development in the ionic liquid based electrolytes for lithium-ion batteries
E. Bolimowska et al., 2017 IEEE International Conference on Industrial and Information Systems ICIIS 2017 - Proceedings - DOI: 10.1109/ICIINFS.2017.8300394

85. Sulfur-containing molecules grafted on carbon nanotubes as highly cyclable cathodes for lithium/organic batteries
G. Charrier et al., ChemElectroChem - DOI: 10.1002/celc.201700970

86. Lithiation heterogeneities of graphite according to C-rate and mass-loading: A model study
N. Dufour et al., Electrochimica Acta - DOI: 10.1016/j.electacta.2018.03.196

87. Adiponitrile-based electrolytes for high voltage graphite-based Li-ion battery
N. Ehteshami et al., Journal of Power Sources - DOI: 10.1016/j.jpowsour.2018.07.004

88. Fast-charging of lithium-iron-phosphate battery with ohmic-drop compensation method: Ageing study
X. Fleury et al., Journal of Energy Storage - DOI: 10.1016/j.est.2017.12.015

89. Operation of thin-plate positive lead-acid battery electrodes employing titanium current collectors
J. Lannelongue et al., Journal of Energy Storage - DOI: 10.1016/j.est.2018.09.020

90. Gelled electrolyte containing phosphonium ionic liquids for lithium-ion batteries
M. Leclère et al., Nanomaterials - DOI: 10.3390/nano8060435

91. Insights on the Na+ ion storage mechanism in hard carbon: Discrimination between the porosity surface functional groups and defects
C. Matei Ghimbeu et al., Nano Energy - DOI: 10.1016/j.nanoen.2017.12.013

92. EIS and XPS investigation on SEI layer formation during first discharge on graphite electrode with a vinylene carbonate doped imidazolium based ionic liquid electrolyte
J. E. Morales-Ugarte et al., Journal of Physical Chemistry C - DOI: 10.1021/acs.jpcc.8b03636

93. Synthesis of Li and Mn-rich layered oxides as concentration-gradients for lithium-ion batteries
S. Pajot et al., Journal of the Electrochemical Society - DOI: 10.1149/2.0031803jes

94. Submicronic LiNi1/3Mn1/3Co1/3O2 synthesized by co-precipitation for lithium ion batteries - Tailoring a classic process for enhanced energy and power density
D. Peralta et al., Journal of Power Sources - DOI: 10.1016/j.jpowsour.2018.06.075

95. ESTOR: A versatile and wide spectrum database for energy storage technical data
F. Perdu et al., 2018 IEEE International Energy Conference ENERGYCON 2018 - DOI: 10.1109/ENERGYCON.2018.8398816

96. Solvent and salt effect on lithium ion solvation and contact ion pair formation in organic carbonates: A quantum chemical perspective
V. Ponnuchamy et al., Journal of Physical Chemistry C - DOI: 10.1021/acs.jpcc.8b09892

97. Operando analysis of lithium profiles in Li-ion batteries using nuclear microanalysis
S. Surblé et al., Journal of Power Sources - DOI: 10.1016/j.jpowsour.2018.05.027

98. Ex situ solid electrolyte interphase synthesis via radiolysis of Li-ion battery anode-electrolyte system for improved coulombic efficiency
F. Varenne et al., Sustainable Energy and Fuels - DOI: 10.1039/c8se00257f

99. Towards practical sulfolane based electrolytes: Choice of Li salt for graphite electrode operation
T. Zhang et al., Journal of Power Sources - DOI: 10.1016/j.jpowsour.2018.05.077

100. Heterobimetallic sodium rare-earth complexes: «Third-Generation» MOCVD precursors for the deposition of NaREF4 (RE = Y Gd) films
S. Battiato et al., Inorganic Chemistry - DOI: 10.1021/acs.inorgchem.8b02267

101. On the current distribution at the channel – rib scale in polymer-electrolyte fuel cells
N. Belgacem et al., International Journal of Hydrogen Energy - DOI: 10.1016/j.ijhydene.2018.01.097

102. Investigation of degradation heterogeneities in PEMFC stack aged under reformate coupling in situ diagnosis post-mortem ex situ analyses and multi-physic simulations
M. Chandesris et al., Journal of the Electrochemical Society - DOI: 10.1149/2.0321806jes

103. Surface distortion as a unifying concept and descriptor in oxygen reduction reaction electrocatalysis
R. Chattot et al., Nature Materials - DOI: 10.1038/s41563-018-0133-2

104. Sequential catalytic growth of sulfur-doped carbon nanotubes and their use as catalyst support
S. Louisia et al., Catalysis Communications - DOI: 10.1016/j.catcom.2018.02.024

105. Vertically aligned platinum copper nanotubes as PEM fuel cell cathode: Elaboration and fuel cell test
O. Marconot et al., Fuel Cells - DOI: 10.1002/fuce.201700242

106. Multiscale water dynamics in a fuel cell by operando quasi elastic neutron scattering
N. Martinez et al., Journal of Physical Chemistry C - DOI: 10.1021/acs.jpcc.7b11189

107. Lifetime prediction of a polymer electrolyte membrane fuel cell under automotive load cycling using a physically-based catalyst degradation model
M. Mayur et al., Energies - DOI: 10.3390/en11082054

108. Sb-doped SnO_2 aerogels based catalysts for proton exchange membrane fuel cells: Pt deposition routes electrocatalytic activity and durability
G. Ozouf et al., Journal of the Electrochemical Society - DOI: 10.1149/2.0041806jes

109. Fuel cell management system: PEMFC lifetime optimization by model based approach
M. Piffard et al., ECS Transactions - DOI: 10.1149/08613.0025ecst

110. Sliding mode observer for proton exchange membrane fuel cell: automotive application
M. Piffard et al., Journal of Power Sources - DOI: 10.1016/j.jpowsour.2018.03.057

111. Evaluation of parameters accelerating the aging of PEMFCs operating under reformate containing carbon monoxide
I. Profatilova et al., Journal of the Electrochemical Society - DOI: 10.1149/2.0281806jes

112. Impact of electrochemical pre-treatment step on accelerated ageing of membrane under OCV protocol in polymer electrolyte membrane fuel cell
I. Profatilova et al., ECS Transactions - DOI: 10.1149/08301.0111ecst

113. A locally resolved investigation on direct methanol fuel cell uneven components fading: Steady state and degradation local analysis
C. Rabissi et al., Journal of Power Sources - DOI: 10.1016/j.jpowsour.2018.07.034

114. A locally resolved investigation on direct methanol fuel cell uneven components fading: Local cathode catalyst layer tuning for homogeneous operation and reduced degradation rate
C. Rabissi et al., Journal of Power Sources - DOI: 10.1016/j.jpowsour.2018.09.094

115. Design optimization of rib/channel patterns in a PEMFC through performance heterogeneities modelling
B. Randrianarizafy et al., International Journal of Hydrogen Energy - DOI: 10.1016/j.ijhydene.2018.03.036

116. Optimization and tunability of 2d graphene and 1d carbon nanotube electrocatalysts structure for PEM fuel cells
E. Remy et al., Catalysts - DOI: 10.3390/catal8090377

117. Impact of humidification by cathode exhaust gases recirculation on a PEMFC system for automotive applications
S. Rodosik et al., International Journal of Hydrogen Energy - DOI: 10.1016/j.ijhydene.2018.11.139

118. Investigation of activity and stability of carbon supported oxynitrides with ultra-low Pt concentration as ORR catalyst for PEM fuel cells
L. Wang et al., Journal of Electroanalytical Chemistry - DOI: 10.1016/j.jelechem.2017.10.067

119. Impact of nickel agglomeration on solid oxide cell operated in fuel cell and electrolysis modes
M. Hubert et al., Journal of Power Sources - DOI: 10.1016/j.jpowsour.2018.06.097

120. Efficient correction of wavefront inhomogeneities in X-ray holographic nanotomography by random sample displacement
M. Hubert et al., Applied Physics Letters - DOI: 10.1063/1.5026462

121. Online total harmonic distortion analysis for solid oxide fuel cell stack monitoring in system applications
L. Malafronte et al., Fuel Cells - DOI: 10.1002/fuce.201700230

122. Experimental validation of a $La_{0.6}Sr_{0.4}Co_{0.2}Fe_{0.8}O_3$-δ electrode model operated in electrolysis mode: Understanding the reaction pathway under anodic polarization
F. Monaco et al., Solid State Ionics - DOI: 10.1016/j.ssi.2018.02.012

123. Stochastic geometrical modeling of solid oxide cells electrodes validated on 3D reconstructions
H. Moussaoui et al., Computational Materials Science - DOI: 10.1016/j.commatsci.2017.11.015

124. Differential analysis of SOFC current-voltage characteristics
Z. Stoynov et al., Applied Energy - DOI: 10.1016/j.apenergy.2018.06.138

125. Corrigendum to '3D phase mapping of solid oxide fuel cell YSZ/Ni cermet at the nanoscale by holographic X-ray nanotomography'
J. Villanova et al., Journal of Power Sources - DOI: 10.1016/j.jpowsour.2018.02.043

Energy efficiency

126. Performance evaluation of fixed-bed millistructured and metallic foam reactor channels for CO_2 methanation
A. Bengaouer et al., Canadian Journal of Chemical Engineering - DOI: 10.1002/cjce.23140

127. Innovative 3D-manufacture of structured copper supports post-coated with catalytic material for CO_2 methanation
S. Danaci et al., Chemical Engineering and Processing - Process Intensification - DOI: 10.1016/j.cep.2018.03.023

128. Statu quo on CO_2 methanation: A review
J. Ducamp et al., Comptes Rendus Chimie - DOI: 10.1016/j.crci.2017.07.005

129. Dynamic modeling and simulations of the behavior of a fixed-bed reactor-exchanger used for CO_2 methanation
R. Try et al., AIChE Journal - DOI: 10.1002/aic.15874

130. Optimal Energy Management for an On-Grid Microgrid by Using Branch and Bound Method
L. N. An et al., Proc. Of 2018 IEEE International Conference on Environment and Electrical Engineering and 2018 IEEE Industrial and Commercial Power Systems Europe (EEEIC/I and CPS Europe 2018) - DOI: 10.1109/EEEIC.2018.8493753

131. Dynamic programming for optimal energy management of hybrid wind-PV-diesel-battery
L. N. An et al., Energies - DOI: 10.3390/en11113045

132. A protective relaying scheme for a microgrid with high penetration of PV systems
T. T. Hoang et al., Proc. of 2018 IEEE International Conference on Environment and Electrical Engineering and 2018 IEEE Industrial and Commercial Power Systems Europe (EEEIC/I and CPS Europe 2018) - DOI: 10.1109/EEEIC.2018.8493867

133. Diagnosis and prognosis of complex energy storage systems: Tools development and feedback on four installed systems
F. Karoui et al., Energy Procedia - DOI: 10.1016/j.egypro.2018.11.066

134. CIM compliant multiplatform approach for cyber-physical energy system assessment
M. T. Le et al., 2017 IEEE Innovative Smart Grid Technologies - Asia: Smart Grid for Smart Community ISGT-Asia 2017 - DOI: 10.1109/ISGT-Asia.2017.8378389

135. Environmental impact indicators for the electricity mix and network development planning towards 2050 – A POLES and EUTGRID model
J.-N. Louis et al., Energy - DOI: 10.1016/j.energy.2018.08.093

136. Systems level validation of a distributed frequency control algorithm
T.-L. Nguyen et al., Proc. of 2018 IEEE International Conference on Environment and Electrical Engineering and 2018 IEEE Industrial and Commercial Power Systems Europe (EEEIC/I and CPS Europe 2018) - DOI: 10.1109/EEEIC.2018.8493909

137. Multi-agent system with plug and play feature for distributed secondary control in microgrid—controller and power hardware-in-the-loop implementation
T.-L. Nguyen et al., Energies - DOI: 10.3390/en11123253

138. FMI compliant approach to investigate the impact of communication to islanded microgrid secondary control
T.-L. Nguyen et al., 2017 IEEE Innovative Smart Grid Technologies - Asia: Smart Grid for Smart Community (ISGT-Asia 2017) - DOI: 10.1109/ISGT-Asia.2017.8378397

139. Using power-hardware-in-the-loop experiments together with co-simulation for the holistic validation of cyber-physical energy systems
V.H. Nguyen et al., Proc. of 2017 IEEE PES Innovative Smart Grid Technologies Conference Europe (ISGT-Europe 2017) –- DOI: 10.1109/ISGTEurope.2017.8260122

140. On the applicability of distributed ledger architectures to peer-to-peer energy trading framework
V.H. Nguyen et al., Proc. of 2018 IEEE International Conference on Environment and Electrical Engineering and 2018 IEEE Industrial and Commercial Power Systems Europe (EEEIC/I and CPS Europe 2018) - DOI: 10.1109/EEEIC.2018.8494446

141. Cross-infrastructure holistic experiment design for cyber-physical energy system validation
V.H. Nguyen et al., Int. Conf. on Innovative Smart Grid Technologies (ISGT Asia 2018) - DOI: 10.1109/ISGT-Asia.2018.8467943

142. Benefits of demand side management strategies for an island supplied by marine renewable energies
A. Roy et al., 7th Int. IEEE Conf. on Renewable Energy Research and Applications (ICRERA 2018) - DOI: 10.1109/ICRERA.2018.8566784

143. Electrical power supply of remote maritime areas: A review of hybrid systems based on marine renewable energies
A. Roy et al., Energies - DOI: 10.3390/en11071904

144. An integrated pan-European research infrastructure for validating smart grid systems
T. I. Strasser et al., Elektrotechnik und Informationstechnik - DOI: 10.1007/s00502-018-0667-7

145. Integration of PV systems into grid: From impact analysis to solutions
Q.-T. Tran et al., Proc. of 2018 IEEE International Conference on Environment and Electrical Engineering and 2018 IEEE Industrial and Commercial Power Systems Europe (EEEIC/I and CPS Europe 2018) - DOI: 10.1109/EEEIC.2018.8494400

146. Modelling and experimental validation of a 46 kW PEM high pressure water electrolyzer
M. Espinosa-López et al., Renewable Energy - DOI: 10.1016/j.renene.2017.11.081

147. Use of hydrogen in off-grid locations a techno-economic assessment
L. Gracia et al., Energies - DOI: 10.3390/en11113141

148. Uncertainty sensitivity assessment on the optimization of the design and operation of complex energy systems: A comprehensive approach
A. Nadal et al., Proc. of the 28th International European Safety and Reliability Conference ESREL 2018 – ISBN: 9781351174664

149. Dynamic prediction of a building integrated photovoltaic system thermal behaviour
Y. B. Assoa et al., Applied Energy - DOI: 10.1016/j.apenergy.2018.01.078

150. Numerical parametric study of the thermal and electrical performance of a BIPV/T hybrid collector for drying applications
Y. B. Assoa et al., Renewable Energy - DOI: 10.1016/j.renene.2018.05.102

151. Towards new metrics for the characterisation of the dynamic performance of adaptive façade systems
L. Bianco et al., Journal of Facade Design and Engineering - DOI: 10.7480/jfde.2018.3.2564

152. Comparison of model numerical predictions of heat and moisture transfer in porous media with experimental observations at material and wall scales: An analysis of recent trends
T. Busser et al., Drying Technology - DOI: 10.1080/07373937.2018.1502195

153. Dynamic experimental method for identification of hygric parameters of a hygroscopic material
T. Busser et al., Building and Environment - DOI: 10.1016/j.buildenv.2018.01.002

154. Experimental and dimensional study of the draining process in drainback solar thermal systems
P. Carbajo Jiménez et al., Solar Energy - DOI: 10.1016/j.solener.2018.07.075

155. Demand control ventilation with hygro passive sensors: impact of sensor's characteristics
X. Faure et al., International Journal of Ventilation - DOI: 10.1080/14733315.2018.1518056

156. Low-emissivity coating coupled with aerogel-based plaster for walls' internal surface application in buildings: Energy saving potential based on thermal comfort assessment
M. Ibrahim et al., Journal of Building Engineering - DOI: 10.1016/j.jobe.2018.04.008

157. Improved model for calculating instantaneous efficiency of flat-plate solar thermal collector
O. Ibrahim et al., Journal of Heat Transfer - DOI: 10.1115/1.4038827

158. Macro flat-plate solar thermal collector with rectangular channels
O. Ibrahim et al., Journal of Solar Energy Engineering Transactions of the ASME - DOI: 10.1115/1.4040535

159. Performances and modelling of a circular moving bed thermochemical reactor for seasonal storage
J. Wyttenbach et al., Applied Energy - DOI: 10.1016/j.apenergy.2018.09.008

160. Design simulation and experimental study of a directly-irradiated solar chemical reactor for hydrogen and syngas production from continuous solar-driven wood biomass gasification
Q. Bellouard et al., International Journal of Hydrogen Energy - DOI: 10.1016/j.ijhydene.2018.04.147

161. The influence of char preparation and biomass type on char steam gasification kinetics
T. Dahou et al., Energies - DOI: 10.3390/en11082126

162. Neodymium recovery by chitosan/iron(III) hydroxide ChiFer(III). sorbent material: Batch and column systems
H. Demey et al., Polymers - DOI: 10.3390/polym10020204

163. Thermo-economic analysis and multi-objective optimisation of lignocellulosic biomass conversion to Fischer-Tropsch fuels
E. Peduet al.,i et al., Sustainable Energy and Fuels - DOI: 10.1039/c7se00468k

164. Do lignin-carbohydrates complexes (LCC) survive to acid chlorite delignification?
D. da Silva Perez et al., Abstracts of Papers of the American Chemical Society

165. A novel high-temperature solar chemical reactor for syngas production from solar-driven thermochemical gasification of wood biomass
S. Rodat et al., AIP Conference Proceedings 2033(1) - DOI: 10.1063/1.5067146

166. Biochars from various biomass types as precursors for hard carbon anodes in sodium-ion batteries
C. D. M. Saavedra Rios et al., Biomass and Bioenergy - DOI: 10.1016/j.biombioe.2018.07.001»

167. The design of dust barriers to reduce collector mirror soiling in CSP plants
C. Sansom et al., AIP Conference Proceedings 2033 - DOI: 10.1063/1.5067033

168. The effect of pyrolysis heating rate on the steam gasification reactivity of char from woodchips
S. Septien et al., Energy - DOI: 10.1016/j.energy.2017.09.114

169. First-principles quantitative prediction of the lattice thermal conductivity in random semiconductor alloys: The role of force-constant disorder
M. Arrigoni et al., Physical Review B - DOI: 10.1103/PhysRevB.98.115205

170. Topologically nontrivial phase in the hexagonal antiperovskites A3BiB (A=BaSr; B=PN)
C. K. Barman et al., Physical Review B - DOI: 10.1103/PhysRevB.98.245149

171. Coupling of PZT thin films with bimetallic strip heat engines for thermal energy harvesting
J. Boughaleb et al., Sensors (Switzerland) - DOI: 10.3390/s18061859

172. Predictive design and experimental realization of InAs/GaAs superlattices with tailored thermal conductivity
J. Carrete et al., Journal of Physical Chemistry C - DOI: 10.1021/acs.jpcc.7b11133

173. Novel Approaches to spectral properties of correlated electron materials: From generalized Kohn–Sham theory to screened exchange dynamical mean field theory
P. Delange et al., Journal of the Physical Society of Japan - DOI: 10.7566/JPSJ.87.041003

174. Resonant phonon scattering in semiconductors
B. Dongre et al., Journal of Materials Chemistry C - DOI: 10.1039/c8tc00820e

175. Ab initio lattice thermal conductivity of bulk and thin-film α-Al_2O_3
B. Dongre et al., MRS Communications - DOI: 10.1557/mrc.2018.161

176. AFLOW-ML: A RESTful API for machine-learning predictions of materials properties
E. Gossett et al., Computational Materials Science - DOI: 10.1016/j.commatsci.2018.03.075

177. Phonon transport unveils the prevalent point defects in GaN
A. Katre et al., Physical Review Materials - DOI: 10.1103/PhysRevMaterials.2.050602

178. Cystamine-configured lead halide based 2D hybrid molecular crystals: Synthesis and photoluminescence systematics
S. Krishnamurthy et al., APL Materials - DOI: 10.1063/1.5042268

179. Materials screening for the discovery of new half-heuslers: Machine learning versus ab initio methods
F. Legrain et al., Journal of Physical Chemistry B - DOI: 10.1021/acs.jpcb.7b05296

180. Vibrational properties of metastable polymorph structures by machine learning
F. Legrain et al., Journal of Chemical Information and Modeling - DOI: 10.1021/acs.jcim.8b00279

181. Nature of the charge carriers in $LaAlO_3$-$SrTiO_3$ oxide heterostructures probed using hard X-ray photoelectron spectroscopy
S. Mukherjee et al., EPL - DOI: 10.1209/0295-5075/123/47003

182. Influence of point defects on the thermal conductivity in FeSi
R. Stern et al., Physical Review B - DOI: 10.1103/PhysRevB.97.195201

183. Heat conduction measurements in ballistic 1D phonon waveguides indicate breakdown of the thermal conductance quantization
A. Tavakoli et al., Nature Communications - DOI: 10.1038/s41467-018-06791-0

184. Thermal transport through Ge-rich Ge/Si superlattices grown on Ge (0 0 1)
L. Thumfart et al., Journal of Physics D: Applied Physics - DOI: 10.1088/1361-6463/aa98c5

185. Quasiballistic heat removal from small sources studied from first principles
B. Vermeersch and N. Mingo, Physical Review B - DOI: 10.1103/PhysRevB.97.045205

186. Full-field thermal imaging of quasiballistic crosstalk reduction in nanoscale devices
A. Ziabari et al., Nature Communications - DOI: 10.1038/s41467-017-02652-4

187. Thermodynamic and economic evaluation of an innovative electricity storage system based on thermal energy storage
K. Attonaty et al., ECCOS 2018 Proc of the 31st Int. Conf. on Efficiency Cost Optimization Simulation and Environmental Impact of Energy Systems - ISBN: 978-972-99596-4-6

188. Optimal temperature control of large scale district heating networks
R. Bavière and M. Vallée, Energy Procedia - DOI: 10.1016/j.egypro.2018.08.170

189. Nucleation triggering methods in supercooled phase change materials (PCM) a review
N. Beaupere et al., Thermochimica Acta - DOI: 10.1016/j.tca.2018.10.009

190. Solidification monitoring of supercooled phase change materials
N. Beaupere et al., Refrigeration Science and Technology - DOI: 10.18462/iir.pcm.2018.0022

191. Performance assessment of a multi-source heat production system with storage for district heating
M. N .Descamps et al., Energy Procedia - DOI: 10.1016/j.egypro.2018.08.203

192. Experimental investigation of the solid filler influence in thermocline storage systems through the comparison of two different setups
T. Essence et al., AIP Conference Proceedings 2033(1) - DOI: 10.1063/1.5067100»

193. Extended modeling of packed-bed sensible heat storage systems
T. Essence et al., AIP Conference Proceedings 2033(1) – DOI: 10.1063/1.5067101

194. Numerical investigations of a continuous thermochemical heat storage reactor
L. Farcot et al., Journal of Energy Storage - DOI: 10.1016/j.est.2018.08.020

195. A methodology to analyse fault effect on large solar thermal system behaviour
G. Faure et al., ECOS 2018 – Proc. of the 31st Int. Conf. on Efficiency Cost Optimization Simulation and Environmental Impact of Energy Systems - ISBN: 978-972-99596-4-6

196. An innovative practical battery thermal management system based on phase change materials: Numerical and experimental investigations
A. Lazrak et al., Applied Thermal Engineering - DOI: 10.1016/j.applthermaleng.2017.08.172

197. Supercritical carbon dioxide brayton cycle for hybridization of a small modular reactor and a concentrated solar power plant with thermal energy storage
Q. T. Pham et al., Proceedings of the 2018 International Congress on Advances in Nuclear Power Plants ICAPP 2018 - ISBN: 978-1-5108-6120-6

198. Numerical analysis of granular bed behavior in thermocline storage tank and bed/wall interactions
N. Sassine et al., AIP Conference Proceedings 2033 - DOI: 10.1063/1.5067120

199. Thermal stress numerical study in granular packed bed storage tank
N. Sassine et al., Granular Matter - DOI: 10.1007/s10035-018-0817-y

200. Interest of ammonia-water absorption chiller to enhance closed cycle gas turbine performance during peak demand. Comparison with centrifugal chiller
N. Tauveron et al., Refrigeration Science and Technology - DOI: 10.18462/iir.gl.2018.1214

201. Replacing incandescent lamps with an LED panel for hydrogen production by photofermentation: Visible and NIR wavelength requirements
V. Turon et al., International Journal of Hydrogen Energy - DOI: 10.1016/j.ijhydene.2018.03.019

202. Gravity assisted recovery of liquid xenon at large mass flow rates
L. Virone et al., Nuclear Instruments and Methods in Physics Research Section A: Accelerators Spectrometers Detectors and Associated Equipment - DOI: 10.1016/j.nima.2018.02.097

Editorial: CEA Liten / Graphic design: DEUXPONTS Manufacture d'Histoires

AWARDS

YESS Award 2018 (First prize) - Young Energy Storage Scientist Award of the French network on electrochemical energy storage (RS2E)
"To understand and overcome the ionic conduction mechanism of the new "hot" lithium solid-state batteries material: The solid polymer electrolyte from the start-up Ionic Material"
Laurent BERNARD, *PhD student*

Best FCH-JU Project Innovation 2018 (Nomination)
"Game-changing technology for higher performance, lower cost fuel cells" in the frame of FCH-JU COBRA project
Fabrice MICOUD, *COBRA Project leader*

Europe Star Trophy - 5th HORIZON 2020 Forum, 2018
"Development of AlmaBTE, the first public software for simulating heat exchange in multi-scale systems, which predicts heat flows in complex structured materials"
Natalio MINGO, *ALMA Project leader*

Best Poster Award – GECat Congress 2018 – French Chemical society
"Understanding of the deactivation mechanisms of a CO_2 methanation catalyst in a fixed bed millistructured reactor"
Isabelle CHAMPON, *PhD student*

PhD Thesis Award – ComUE Université Grenoble Alpes 2018
"Transparent electrodes based on percussive networks of silver nanowires: Physical properties and applications"
Thomas SANNICOLO, *PhD student*

Graduate Student Award – E-MRS Spring Meeting 2018 – Symposium I
"Conductivity and Surface Passivation Properties of B-doped Poly-Silicon Passivated Contacts for Crystalline Si Solar Cells"
Audrey MORISSET, *PhD student*

Best Presentation Award 2018 – Energies & Researches School
"Development of "tunnel" oxides and TCOs (Transparent Conductive Oxides) for passivation of contacts on homojunction industrialisable PV silicon cells"
Elise BRUHAT, *PhD student*

Best Paper Award DMKD 2018 – International Conference on Data Mining and Knowledge Discovery
"Circular background decreases misunderstanding of multidimensional scaling results for naive readers"
Sylvain LESPINATS, *Energy grids scientist*

CONTACTS

MATTER AND MATERIALS

Laurent BRIOTTET
Scientific Advisor for the
Mechanics and assembly processes
laurent.briottet@cea.fr

Gérard DELETTE
Scientific Advisor for the
Nanomaterials for energy
gerard.delette@cea.fr

Gérard GEBEL
Scientific Advisor for the
Advanced characterization
gerard.gebel@cea.fr

Natalio MINGO
Scientific Advisor for the
Nanomaterials for energy
natalio.mingo@cea.fr

Amélie REVAUX
Scientific Advisor for the
Organic electronics
amelie.revaux@cea.fr

Jean-Pierre SIMONATO
Scientific Advisor for the
Nanomaterials for energy
jean-pierre.simonato@cea.fr

RENEWABLE ENERGY

Béatrice DREVET
Scientific Advisor for the
PV solar cells
beatrice.drevet@cea.fr

Nicolas GUILLET
Scientific Advisor for the
Stationary Energy storage
nicolas.guillet@cea.fr

ENERGY STORAGE AND CONVERSION

Philippe AZAIS
Scientific Advisor for the
Electrochemistry, Batteries & Supercapacities
philippe.azais@cea.fr

Sébastien ROSINI
Scientific Advisor for the
Fuel cells
sebastien.rosini@cea.fr

Julie MOUGIN
Scientific Advisor for the
Hydrogen chain
julie.mougin@cea.fr

ENERGY EFFICIENCY

Laurent GARNIER
Scientific Advisor for the
Energetic system integration & Hybridisation
sebastien.rosini@cea.fr

Murielle MARCHAND
Scientific Advisor for the
Bio-resources
murielle.marchand@cea.fr

Jean-François FOURMIGUÉ
Scientific Advisor for the
Thermal storage and transfer
jean-francois.fourmigue@cea.fr

Philippe THONY
Scientific Advisor for the
Building energy efficiency
philippe.thony@cea.fr

Tuan Quoc TRAN
Scientific Advisor for the
Smart Grid
QuocTuan.TRAN@cea.fr

liten
cea tech

Scientific report 2018

The French Alternative Energies
and Atomic Energy Commission
Commissariat à l'énergie atomique
et aux énergies alternatives
17 avenue des Martyrs | 38054 Grenoble
Cedex 9 | France

INSTITUT CARNOT
Energies du futur